PR12-13-004

# Symmetry Tests of Rare Eta Decays to All-Neutral Final States: The JLab Eta Factory (JEF) Experiment

May 5, 2013


(The GlueX Collaboration and Other Participants)

M. Dugger,[1] B. Ritchie,[1] E. Anassontzis,[2] P. Ioannou,[2] C. Kourkoumeli,[2] G. Voulgaris,[2] N. Jarvis,[3] W. Levine,[3] P. Mattione,[3] C. A. Meyer,[3] R. Schumacher,[3] P. Collins,[4] F. Klein,[4] D. Sober,[4] D. Doughty,[5] A. Barnes,[6] R. Jones,[6] J. McIntyre,[6] F. Mokaya,[6] B. Pratt,[6] I. Senderovich,[6] W. Boeglin,[7] L. Guo,[7] P. Khetarpal,[7] E. Pooser,[7] J. Reinhold,[7] H. Al Ghoul,[8] V. Crede,[8] P. Eugenio,[8] A. Ostrovidov,[8] N. Sparks,[8] A. Tsaris,[8] D. Ireland,[9] K. Livingston,[9] D. Bennett,[10] J. Bennett,[10] J. Frye,[10] J. Leckey,[10] R. Mitchell,[10] K. Moriya,[10] A. Szczepaniak,[10] R. Miskimen,[11] M. Williams,[12] P. Ambrozewicz,[13] S. Danagoulian,[13,*] A. Gasparian,[13] R. Pedroni,[13] T. Black,[14] L. Gan (Spokesperson),[14] S. Denisov,[15] G. Huber,[16] S. Katsaganis,[16] D. Kolybaba,[16] G. Lolos,[16] Z. Papandreou,[16] A. Semenov,[16] I. Semenova,[16] M. Tahani,[16] W. Brooks,[17] S. Kuleshov,[17] A. Toro,[17] F. Barbosa,[18] E. Chudakov,[18] H. Egiyan,[18] M. Ito,[18] D. Lawrence,[18] L. Pentchev,[18] Y. Qiang,[18] E. S. Smith,[18] A. Somov (Co-Spokesperson),[18] S. Taylor,[18] T. Whitlatch,[18] E. Wolin,[18] B. Zihlmann,[18] V. Berdnikov,[19] A.Pognosov,[19] G. Nigmatkulov,[19] D Romanov,[19] S. Somov,[19] I. Tolstukhin,[19] J. Benesch,[18,*] J. Goity,[18,*] D. Mack (Co-Spokesperson),[18,*] X. Chen (Co-Spokesperson),[20,*] P. Zhang,[20,*] J. He,[20,*] D. Chen,[20,*] H. Yang,[20,*] R. Wang,[20,*] D. Armstrong,[21,*] W. Deconinck,[21,*] W. Briscoe,[22,*] A. Opper,[22,*] N. Semicevic,[23,*] S. Wells,[23,*] J. Dunne,[24,*] D. Dutta,[24,*] P. King,[25,*] J. Roche,[25,*] K.E. Myers,[26,*] M. Dalton,[27,*] A. Asratyan,[28,*] A. Dolgolenko,[28,*] V. Goryachev,[28,*] I. Larin,[28,*] V. Matveev,[28,*] V. Tarasov,[28,*] A. Sitnikov,[28,*] V. Vishnyakov,[28,*] S. Gevorkyan,[29,*] L. Roca,[30,*] S. Fang,[31,*] H. Lui,[31,*] X.Z. Bai,[32,*] H.X. He,[32,*] J. Feng,[32,*] S.Y. Hu,[32,*] S. Y. Jian,[32,*] X.M. Li,[32,*] C. Shan,[32,*] H.H. Xia,[32,*] L. Ye,[32,*] J. Yuan,[32,*] J. Zhou,[32,*] S.H. Zhou,[32,*] B. Hu,[33,*] Y. Zhang,[33,*] and L. Ma[33,*]

[1] *Arizona State University, Tempe, Arizona 85287, USA*

[2] *University of Athens, GR-10680 Athens, Greece*

[3] *Carnegie Mellon University, Pittsburgh, Pennsylvania 15213, USA*

[4] *Catholic University of America, Washington, D.C. 20064, USA*

[5] *Christopher Newport University, Newport News, Virginia 23606, USA*

[6] *University of Connecticut, Storrs, Connecticut 06269, USA*

[7] *Florida International University, Miami, Florida 33199, USA*

[8] *Florida State University, Tallahassee, Florida 32306, USA*

[9] *University of Glasgow, Glasgow G12 8QQ, United Kingdom*

[10] *Indiana University, Bloomington, Indiana 47405, USA*

[11] *University of Massachusetts, Amherst, Massachusetts 01003, USA*

[12] *Massachusetts Institute of Technology, Cambridge, Massachusetts 02139, USA*

[13] *North Carolina A&T State University, Greensboro, North Carolina 27411, USA*

[14] *University of North Carolina, Wilmington, North Carolina 28403, USA*

[15] *Institute for High Energy Physics, Protvino, Russia*

[16] *University of Regina, Regina, SK S4S 0A2, Canada*

[17] *Universidad Técnica Federico Santa María, Casilla 110-V Valparaíso, Chile*

[18] *Thomas Jefferson National Accelerator Facility, Newport News, Virginia 23606, USA*

[19] *National Research Nuclear University MEPhI, Moscow, Russia*

[20] *Institute of Modern Physics, Lanzhou, P.R.China*

[21] *College of William and Mary, Williamsburg, VA*

[22] *The George Washington University, Washington, DC, USA*

[23] *Louisiana Tech University, Ruston, LA, USA*

[24] *Mississippi State University, Mississippi State, MS, USA*

[25] *Ohio University, Athens, OH, USA*

[26] *Rutgers University, Piscataway, NJ*

[27] *University of Virginia, Charlottsville, VA*

[28] *Institute for Theoretical and Experimental Physics, Moscow, Russia*

[29] *Joint Institute for Nuclear Research, Dubna, Russia*

[30] *Universidad de Murcia, E-30071 Murcia, Spain*

[31] *Institute of High Energy Physics, Beijing, P.R. China*

[32] *Chinese Institute of Atomic Energy, Beijing, P.R.China*

[33] *Lanzhou university, Lanzhou, P.R.China*

*Other participant

# Executive Summary

Rare decays of the neutral and long lived $\eta$ meson provide a unique, flavor-conserving laboratory to search for new sources of C, P, or CP violation while testing predictions of chiral perturbation theory at high order. Because G parity conservation prevents the $\eta$ from rapidly decaying to pions by the isospin-conserving strong interaction, the branching ratios for various rare and forbidden $\eta$ decays are potentially 5 orders of magnitude more sensitive to new interactions than the decays for comparable hadrons. Our three priority physics channels are: $\eta \to 2\pi^0$, which is effectively forbidden by P and CP invariance; $\eta \to 3\gamma$, which is effectively forbidden by charge conjugation invariance C; and the rare decay $\eta \to \pi^0 2\gamma$ where large contributions begin only at $O(p^6)$ in chiral perturbation theory. Our measurements in the Standard Model forbidden channels will reduce the branching ratio upper limits by 1-1.5 orders of magnitude, improving constraints on anomalous interactions at the *amplitude* level by factors of 3-6. For the allowed channel $\eta \to \pi^0 2\gamma$, the branching ratio will be determined to approximately 4%, several times below the uncertainties of published data. The differential decay width $d\Gamma/dM_{2\gamma}$ will be determined with errors averaging 9% for each of 7 bins, providing important dynamical information to stringently constrain the $O(p^6)$ terms in chiral perturbation theory. In parallel, the large new dataset of $\eta \to 3\pi^0$ we obtain will not only constrain backgrounds for the rare decay channels, but may yield an important new extraction of the $m_d - m_u$ quark mass with different systematics than published results.

No new inventions are required but the technology will be state-of-the-art. Hall D's high energy, tagged photon facility with its planned 30 cm $LH_2$ target will yield a competitive rate of exclusively produced $\eta$'s from forward $\gamma + p \to \eta + p$ with good acceptance. However, reducing backgrounds by two orders of magnitude compared to older experiments is an important reason why the proposed experiment will yield 1-1.5 orders of magnitude improvement in rare $\eta$ decays to all-neutral final states. This will be achieved by significantly boosting the $\eta$'s and measuring the decay photons in a high-granularity, high-resolution lead tungstate calorimeter with flash ADC readout on every crystal.

Boosted $\eta$'s not only provide freedom from low detector thresholds and low energy backgrounds, but also cause $\eta \to 3\pi^0$ decays with lost photons to fall out of the $\eta \to 4\gamma$ signal window. The invariant mass resolution with lead tungstate is over a factor of 2 better than with lead glass. The small crystal size and 6m target-to-calorimeter distance greatly reduce a potentially important background from $\eta \to 3\pi^0$ with shower merging. Good resolution plus measurement of the recoil proton for larger $\eta$ angles will control the background from continuum $\gamma + p \to 2\pi^0 + p$. Timing information for each calorimeter module from the flash ADC readout will play a critical role in reducing accidental background from pile-up showers.

**Contents**

## I. PHYSICS MOTIVATION AND OVERVIEW

The broad goal of our proposed experimental program is to measure various $\eta$ rare decays to study confinement QCD and search for new physics beyond the Standard Model (SM). Specifically, we will provide precision data on the highly suppressed $\eta \to \pi^0\gamma\gamma$ channel to constrain the $\mathcal{O}(p^6)$ terms of chiral perturbation theory (ChPT), while searching for new sources of C, P and CP symmetry violation in $\eta \to \pi^0\pi^0$ and $\eta \to 3\gamma$. The current proposal focuses on $\eta$ rare decay channels leading to 3 or $4\gamma$ final states which have traditionally suffered from large backgrounds. We propose measuring the SM allowed $\eta \to \pi^0\gamma\gamma$ branching ratio with $\sim 4\%$ precision and its differential decay width $d\Gamma/dM_{2\gamma}$. In doing so, we will improve the upper limits on the SM forbidden channels by 1-1.5 orders of magnitude.

These seemingly disparate physics goals are quite complementary: the background studies overlap, a sensitive measurement in one channel implies high sensitivity in the others, and the allowed $\eta \to \pi^0\gamma\gamma$ decay allows us to not only monitor data quality on a daily basis but to reduce uncertainties in the backgrounds for the SM forbidden channels $\eta \to \pi^0\pi^0$ and $\eta \to 3\gamma$. As a by-product, the Dalitz plot of the second largest decay channel, $\eta \to 3\pi^0$, one of the major sources of background in our rare decays, will be measured with high statistics and precision. Although rare decays of the $\eta$ are an active field of research at other laboratories, we anticipate that the background will be reduced by about two orders of magnitude relative to any other on-going rare $\eta$ decay program. This is achieved by using Hall D's high energy, high intensity, tagged photon beam and the GlueX apparatus combined with the proposed high-resolution, high-granularity calorimeter with flash ADC readout on every crystal.

**This is a resubmission of a proposal to PAC39. Our slides with responses to issues and recommendations of PAC39 are attached to the end of this pdf file.**

### A. The $\eta$ meson and Symmetry Tests

Two of the major challenges in contemporary physics are: (1) QCD confinement, and (2) the search for physics beyond the Standard Model. Due to color confinement, traditional perturbation theory breaks down at low energies. A quantitative understanding of the strong interaction in this region remains one of the greatest intellectual challenges. Two independent theoretical approaches have been developed in this area: one is Chiral Perturbation Theory (ChPT) based on the chiral symmetry of QCD in the quark massless limit (the chiral limit); the second is numerical simulation of QCD on a lattice. In recent years, significant progress [1] has been achieved using both approaches. A technique considering next-to-next-to-leading order of the chiral expansion and computing up to two-loop diagrams has been developed [2], providing useful guidance for lattice QCD extrapolations to the physical quark mass region. In the meantime, progress in lattice QCD calculations has made it possible to calculate the low energy constants in the chiral Lagrangian. Recently the Jlab lattice QCD group fully demonstrated their capability to access the light meson decays on the lattice by applying the Lehmann-Symanzik-Zimmermann reduction formula [3]. A recent lattice QCD calculation by N.H. Christ *et al.* [4] predicted the $\eta - \eta'$ mixing angle to be $\theta = -14.1 \pm 2.8^{\circ}$. Their extrapolation to the physical light quark mass gives masses of $\eta$ and $\eta'$ that are consistent with the physical masses of those mesons. These new developments lead to the expectation that a breakthrough will occur in our understanding of the confinement region of QCD in the foreseeable future. The low-energy theorems for various hadronic processes based only on the chiral invariance of the underlying QCD Lagrangian are highly developed and well tested in the domain of pionic and kaonic reactions [5]. **It is important and also urgent to extend this success into the eta sector[6].** The proposed measurements on the $\eta$ branching ratios (listed in Table I), along with the PrimEx measurement of the $\Gamma(\eta \to \gamma\gamma)$ decay width which will ultimately be used to normalize all branching ratios to neutral final states, represent a comprehensive experimental program in the physics of $\eta$ neutral decays.

The Standard Model of particle physics has been overwhelmingly successful in describing phenomena in nuclear and particle physics. However, there are strong indications that Standard Model is

incomplete: it needs 17 input parameters and it does not explain the origin of the three fermion families or why their masses are widely different. Furthermore, the SM does not explain the dominance of matter over anti-matter, the nature of dark matter needed to explain the rotation curves of the galaxies, or the nature of dark energy which causes the accelerated expansion of the universe. Searching for physics beyond the SM has become one of the top priorities for twenty-first century physics. The search embraces astrophysics, collider experiments, and precision tests at low energies. Enormous investments have been made in flavor-changing decays in K and B mesons, as well as weak decays of the pion and muon, with no uncontroversial evidence found for new physics. However, the sector of flavor-conserving, non-weak decays has not been as thoroughly exploited due to experimental challenges. This presents an opportunity for JLab's Hall D. We propose searching for new physics through tests of fundamental symmetries such as charge conjugation C, parity P, and time reversal T, as well as CP and CPT.

One distinguishing feature of the $\eta$ meson which makes it a unique probe for symmetry tests is directly related to its birth. In the chiral limit, the condensation of quark-antiquark pairs in the QCD vacuum spontaneously breaks $SU_L(3) \times SU_R(3)$ symmetry down to the flavor $SU(3)$ symmetry. As a result, there are eight massless Goldstone Bosons corresponding to the eight spontaneously broken symmetry generators. These Goldstone Bosons are identified with the octet of pseudoscalar mesons ($\pi^0$, $\pi^\pm$, $K^\pm$, $K^0$, $\bar{K}^0$, and $\eta$). In reality, the quark masses are non-zero (albeit small), thus breaking the chiral symmetry explicitly and giving rise to masses for the Goldstone Bosons following the mechanism discovered by Gell-Mann, Oakes and Renner [8]. As the most massive member in the octet pseudoscalar meson family, the $\eta$ is more sensitive to QCD symmetry breaking. On the other hand, the $\eta$ is an eigenstate of P, C, CP, and G: $I^G J^{PC} = 0^+0^{-+}$, which makes it a unique probe to test discrete symmetries.

Another distinguishing feature of the $\eta$ is that all its strong and electromagnetic decays are forbidden to lowest order due to P, C, CP, G-parity and angular momentum conservation [9]. This enhances the relative importance of higher order or otherwise rare processes. The width of the $\eta$ ($\Gamma_\eta$ = 1.3 KeV) is about five orders of magnitude smaller than the $\rho$ meson ($\Gamma_\rho$ = 149 MeV), for example. All other things being equal, this makes measurements of branching ratios or upper limits of various

| Mode | Branching Ratio | Symmetry Highlight | Role in Proposal |
|---|---|---|---|
| $\pi^0 2\gamma$ | $(2.7 \pm 0.5) \times 10^{-4}$ | $\chi$PTh, $\mathcal{O}(p^6)$ | priority |
| $\pi^0\pi^0$ | $< 3.5 \times 10^{-4}$ | CP, P | priority |
| $3\gamma$ | $< 1.6 \times 10^{-5}$ | C | priority |
| $4\pi^0$ | $< 6.9 \times 10^{-7}$ | CP, P | ancillary |
| $4\gamma$ | $< 2.8 \times 10^{-4}$ | suppressed ($< 10^{-11}$) | ancillary |
| $\pi^0\gamma$ | $< 9 \times 10^{-5}$ | C, L | ancillary |
| $2\pi^0\gamma$ | $< 5 \times 10^{-4}$ | C | ancillary |
| $3\pi^0\gamma$ | $< 6 \times 10^{-5}$ | C | ancillary |
| $3\pi^0$ | $(32.57 \pm 0.23)\%$ | $m_d - m_u$ | ancillary |
| $2\gamma$ | $(39.31 \pm 0.20)\%$ | anomaly, $\eta$-$\eta'$ mixing | by PR12-10-011 |

TABLE I: Some $\eta$ rare decays to all-neutral final states, their role in this proposal, plus a few closely related channels [15]. The PDG branching ratio for $\pi^0 2\gamma$ is the average of several widely inconsistent measurements as suggested below in Figure 2. The theoretical upper limit for the $\eta \to 4\gamma$ decay is estimated from a $\pi^0$ calculation [42]. Two largest neutral decays $\eta \to 3\pi^0$ and $\eta \to 2\gamma$ are listed here also. The $3\pi^0$ channel will be measured to help control the background in the rare decay channels. The decay width of $\eta \to 2\gamma$ will be measured in a separate experiment via the Primakoff effect (PR12-10-011) which has been approved by PAC35. (The decay widths of all other neutral channels will ultimately be normalized to $\eta \to 2\gamma$.) All branching ratio upper limits in this proposal are quoted at 90% confidence level.

rare and forbidden $\eta$ decays about 5 orders of magnitude more sensitive to new interactions. The potential of a broad program of $\eta$ rare decay studies has been discussed by Kullander *et al.* [10] and Nefkens and Price [9]. The status has evolved since those articles were written due to results from KLOE and BES plus newer initiatives in Europe such as the Crystal Ball at MAMI [11] and WASA at COSY [12].

Table I summarizes various $\eta$ rare decays to all-neutral final states of relevance to this proposal.[1] Our flagship channels will be the all-neutral final states with 3 or 4 $\gamma$'s: $\eta \to \pi^0\gamma\gamma$ to constrain higher order ChPT and to test future lattice QCD predictions, and $\eta \to 2\pi^0$ and $3\gamma$ to investigate P

[1] Based on the C and P conservation selection rules given in Appendix A, all neutral final states with up to four $\pi^0$'s and/or up to four $\gamma$'s are listed in Table VIII.

and CP, and C violation, respectively. We also anticipate that significant improvements in several ancillary channels will result as well, particularly those that had large backgrounds in previous experiments such as $\eta \to 4\gamma$ and $\eta \to 2\pi^0\gamma$. In parallel, the large new dataset of $\eta \to 3\pi^0$ (BR=32.57%) we obtain will not only constrain backgrounds for the rare decay channels, but may yield an important new extraction of the quark mass difference $m_d - m_u$ with different systematics than published results. Finally, we note that the rare $\eta$ decay program can potentially be extended to charged decay channels to provide constraints on $\eta \to e^+e^-$ and the dark matter sector: e.g., a "dark photon"(neutral vector U-boson) may be accessible via the reaction $\eta \to \gamma U$ followed by $U \to e^+e^-$ [7].

### B. The rare decay $\eta \to \pi^0\gamma\gamma$

The decay $\eta \to \pi^0\gamma\gamma$ is sufficiently suppressed that, while it has been relatively straightforward to observe a non-zero signal, measurements accurate enough to challenge chiral perturbation theory have proven elusive. In addition to its own significant scientific merit, this channel serves as a stepping stone to optimize the experimental design for other decay channels effectively forbidden in the SM with a similar number of final state $\gamma$'s.

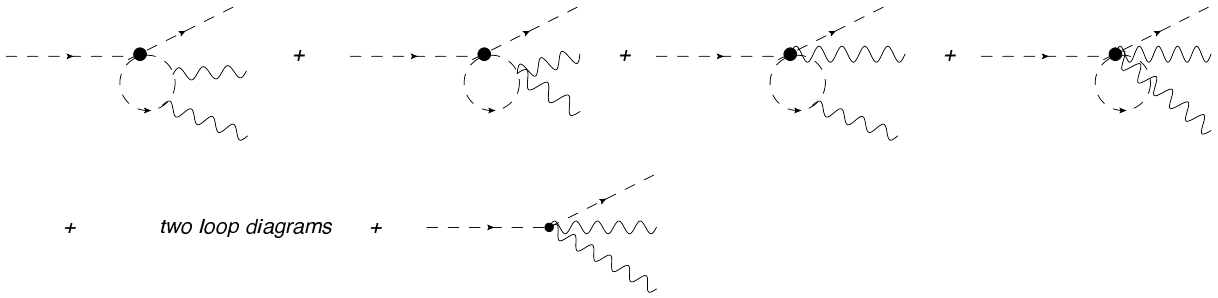


FIG. 1: Feynman diagrams in ChPT contributing to the $\eta \to \pi^0\gamma\gamma$ decay. The one loop diagrams are of order $p^4$. At the order of $p^6$, there are two loop contributions and counter-terms depicted by the last diagram.

This "doubly radiative" $\eta$ decay has a dramatic history spanning more than four decades [16] and has attracted much attention from both theorists and experimentalists. In chiral perturbation

theory (the related Feynman diagrams are shown in Figure 1), the tree level amplitudes vanish at both $\mathcal{O}(p^2)$ and $\mathcal{O}(p^4)$, and the first non-vanishing contribution comes from $\mathcal{O}(p^4)$ *loop* terms [17]. However, loops involving kaons are largely suppressed due to the large kaon mass while pion loops are suppressed due to G parity. The first *sizable* contribution comes at $\mathcal{O}(p^6)$; hence this channel provides a unique probe to test the $\mathcal{O}(p^6)$ term of ChPT. Because the $\mathcal{O}(p^6)$ coefficients in the chiral Lagrangian are not all known, these effects cannot be calculated in a model independent way.[19] This situation has improved significantly due to new work by Oset *et al.* [18], who carefully studied the different sources of uncertainty. In their approach, the contributions of the $a_0(980)$, $f_0(980)$ and $\sigma(600)$ resonances were reliably included by using the unitary extension of ChPT. Using updated inputs from PDG 2007 for the radiative decays of vector mesons, Oset *et al.* updated the central value of $\Gamma(\eta \to \pi^0\gamma\gamma)$ from 0.42 eV to 0.33 eV with a factor of two reduction in the uncertainty compared to the result calculated with the data from PDG 2002. The predicted result in [18] is $\Gamma = 0.33 \pm 0.08$ eV for the $\eta \to \pi^0\gamma\gamma$ decay width, shown as a yellow band in Fig. 2. In addition, this work also demonstrates how the shape of the two-photon invariant mass spectrum, $d\Gamma/dM_{2\gamma}$, probes the underlying dynamics [18] (see Fig 3). Because this spectrum provides much more information than the simple branching ratio, the first precise measurement proposed in this experiment, shown in Figure 3, would be critical to understand the dynamics of ChPT at $\mathcal{O}(p^6)$ level.

### 1. *Status of $\eta \to \pi^0\gamma\gamma$ measurements*

About two dozen experiments have been performed to measure this decay width since 1966. The first significant result was published by the GAMS-2000 collaboration [20] in 1984 yielding $\Gamma(\eta \to \pi^0\gamma\gamma) = 0.84 \pm 0.18$ eV, more than two times larger than the ChPT prediction as shown in Figure 2. By contrast, more recent results from the Crystal Ball and KLOE collaborations are significantly lower. The Crystal Ball results are consistent with the prediction by Oset [18]; however, the result from KLOE differs from the Crystal Ball result by a factor of 3.

The discrepancies are almost certainly due to large backgrounds in the older experiments, including

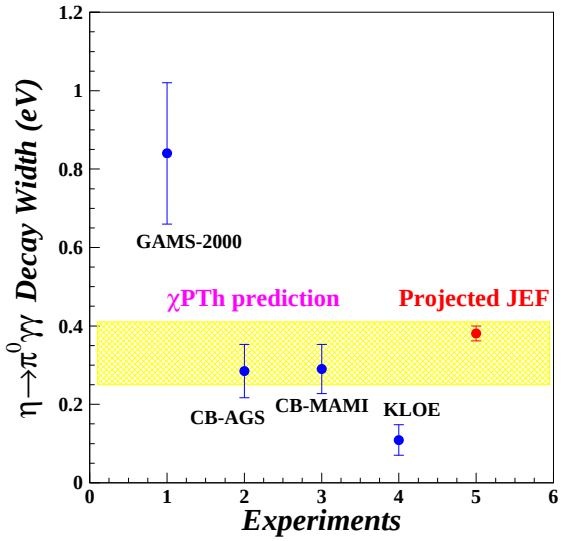


FIG. 2: Experimental results on the decay width of $\eta \to \pi^0\gamma\gamma$. From left to right, the blue points are from GAMS-2000 [20], the Crystal Ball collaboration at the AGS [21][22], the Crystal Ball collaboration at MAMI [23], and KLOE [24]. The yellow band is the most recent unitary ChPT calculation by Oset *et al.* with quoted theoretical uncertainty [18]. The expected precision from our proposed experiment (in red), is arbitrarily plotted at the un-weighted average of previous experimental results. (The projected PrimEx uncertainty of 3.2% on the $\eta \to 2\gamma$ decay width is assumed.)

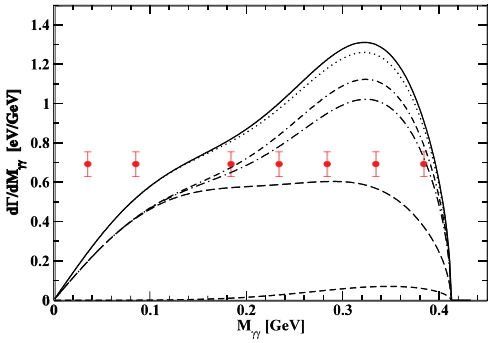


FIG. 3: Predicted two-photon invariant mass distribution from $\eta \to \pi^0 2\gamma$ [18]. From bottom to top: the short-dashed line is for chiral loops, the long-dashed line is tree-level VMD, the dashed-dotted line is the coherent sum of the previous two, the double dashed-dotted line is the same but with VMD loops added, the solid line is the same but with the anomalous terms added. The dotted line is the same as the solid line but substituting the $K^+K^- \to \eta\pi^0$ amplitude by its lowest order. The red dots with error bars indicate our projected sensitivity.

a class of backgrounds that can peak beneath the signal. A new experiment with a significantly improved reduction in backgrounds would provide greatly reduced statistical and systematic errors leading to a definitive result for the $\pi^0 2\gamma$ decay width. More importantly, the two-photon invariant mass spectrum, $d\Gamma/dM_{2\gamma}$, will provide key guidance for understanding the underlying dynamics as suggested by many theorists. At the same time, this improved capability is expected to allow us

to reduce the upper limits for several all-neutral CP and C forbidden decays by up to 1.5 orders of magnitude.

### C. Anomalous Decays $\eta \to 2\pi^0, 3\gamma$, etc.

#### 1. *The Figure of Merit for $\eta$ Rare Decay Experiments*

A tentative signal for an anomalous rare $\eta$ decay would appear as an excess at the $\eta$ mass that is statistically unlikely (10% probability or lower). To a useful approximation, the branching ratio (BR) upper limits in published work can be estimated by

$$BR < 2\frac{\sqrt{N_{bkg}}}{N_\eta \times Acceptance} \tag{1}$$

where $N_{bkg}$ is the number of background events in the signal window, and the factor of 2 corresponds to roughly 90% CL.[2] However, the above equation gives a misleading impression of the figure of merit since the number of background and signal events are linearly proportional if pile-up does not dominate. If we define the background fraction $f_{bkg} \equiv N_{bkg}/(N_\eta \times Acceptance)$, then the estimated BR upper limit expression becomes

$$BR < 2\frac{\sqrt{f_{bkg} \times N_\eta \times Acceptance}}{N_\eta \times Acceptance} = 2\sqrt{\frac{f_{bkg}}{N_\eta \times Acceptance}} \tag{2}$$

from which it is clearer that the figure of merit the experimenter needs to maximize is $N_\eta \times Acceptance/f_{bkg}$.

Equation 2 highlights the level of experimental effort needed to reduce the BR upper limits by one order of magnitude in any rare decay experiment with non-negligible background: one has to increase $N_\eta \times Acceptance$ by *2* orders of magnitude, or decrease $f_{bkg}$ by *2* orders of magnitude, or some combination of both. This means that a single order of magnitude reduction in the BR upper limit for a rare $\eta$ decay channel would normally only be expected once per generation. Yet for the

[2] Strictly speaking, 95% CL. We use this equation only to estimate the sensitivity of this proposal. For published experiments, only the published BR's are quoted or plotted.

anomalous channels described in the following sections, we expect to improve the upper limits by 1-1.5 orders of magnitude. That corresponds to a factor of 3 to 6 improvement at the *amplitude* level as we show in the next paragraph.

Assume that an anomalous decay yield arises from a contact interaction proportional to $(g/\Lambda)^2$ with coupling constant $g$ and mass scale $\Lambda$. Relative to the highly suppressed, isospin violating strong interaction amplitude $A_{IV\,strong}$, the BR upper limit constrains $\left|\frac{g}{\Lambda}\right|$ to be

$$\left|\frac{g}{\Lambda}/A_{IV\,strong}\right| < \sqrt{2 \times BR} \tag{3}$$

where the factor of 2 comes from changing the BR normalization from the total decay width to the decay width of all $\eta \to 3\pi$ channels, and process-dependent phase space factors have been neglected. Using the above equation and the BR sensitivity estimates from Section VIII B, our measurements will constrain the *amplitude* for a new CP violating interaction to less than 0.4% of the highly suppressed, isospin violating strong interaction. The corresponding constraint on a new C violating amplitude will be less than 0.2%.[3]

### *2. The CP violating decay* $\boldsymbol{\eta \to \pi^0\pi^0}$

Another interesting four-photon final state reaction is $\eta \to \pi^0\pi^0$, which would violate P while conserving C and thus violate CP. (See Appendix A.1 for discussion of selection rules in $\eta \to N\pi^0$.) The discovery of a 0.2% CP violation in 1964 came as a great surprise, and the origin remains one of the most mysterious phenomena in elementary particle physics. In the Standard Model, CP symmetry is broken by a single complex phase in the Cabibbo-Kobayashi-Maskawa quark matrix (CKM) that gives the W-boson couplings to an up-type antiquark and a down-type quark, known as the Kobayashi-Maskawa (KM) mechanism. For flavor-conserving processes, CP violation is minute because it requires a two-step change of flavor – a first step to an intermediate flavor state and a second to return to the initial flavor state [26]. As a result, SM sources for CP violation in flavor-

[3] Examples of more rigorous normalization schemes to express constraints on new amplitudes are given in reference [9] for the CP violating channel $\eta \to 4\pi^0$ and the C violating channel $\eta \to 2\pi^0\gamma$.

conserving reactions like $\eta \to \pi^0\pi^0$ are expected to lead to an unobservably small branching ratio, at the level of $2 \times 10^{-27}$ [26]. This makes the $\eta$ an ideal candidate – effectively SM "background" free – to search for new sources of symmetry violations.

The decay $\eta \to 2\pi$ is among the few possible flavor-conserving tests listed in the Review of Particle Physics to search for non-conventional CP violation [28]. Studying this decay channel could potentially shed light on a long-standing puzzle of QCD, the so-called "strong CP problem". Beyond the standard KM CP-violating mechanism described above, QCD itself provides another potential source of CP violation: following a general tenet of quantum field theory, the QCD Lagrangian does not rule out a so called "$\theta_{QCD}$" term [31]-[35]:

$$\mathcal{L}_\theta = \theta_{QCD} \frac{{g_s}^2}{32\pi^2} F \cdot \tilde{F} \tag{4}$$

where $\theta_{QCD}$ is an arbitrary coefficient called the QCD vacuum angle, and $F$ and $\tilde{F}$ are the gluon field strength tensor of a non-Abelian gauge group and its dual. This term violates P, T and CP. Due to the chiral anomaly (the same "triangle" anomaly which gives $\eta_0$ non-zero mass in the chiral limit), the axial $U_A(1)$ symmetry is explicitly broken:

$$\partial_\mu J^5_\mu = \partial_\mu \sum_q \bar{q}_L \gamma_\mu q_L = \frac{{g_s}^2}{32\pi^2} F \cdot \tilde{F} \neq 0 \tag{5}$$

Therefore, for $\theta_{QCD} \neq 0$, neither parity nor time reversal invariance are fully conserved by QCD. When electroweak dynamics in the standard model are included, the anomaly induces an additional term from the electroweak sector when the quark fields are rotated to diagonalize the corresponding flavor matrices G. The coefficient in the equation (4) becomes

$$\bar{\theta} = \theta_{QCD} + arg\ det \left( G^{(U)} G^{(D)} \right). \tag{6}$$

Since in general the G matrices are complex, the second term can add a non-zero contribution to $\bar{\theta}$ when they are rotated to yield real masses [35]. Since the "$\theta_{QCD}$" term is diagonal in flavors, its effects can only manifest in flavor-conserving phenomena: either in the static properties of particles, such as the electric dipole moment (EDM) of the neutron, or through dynamical processes, such as $\eta \to \pi\pi$.

The current experimental limit for the EDM of the neutron, $d_n \leq 2.9 \times 10^{-26}$ $e$·cm [36], leads to a value of $\bar{\theta} \sim 10^{-10\pm1}$ (see the discussion in [34, 35] for details). The unnaturally small size for $\bar{\theta}$ is called the **"strong CP problem"**. A small value for the neutron EDM could be due to a subtle cancellation between tree and loop contributions (see for example [39]), thus allowing the possibility that $\bar{\theta} > 10^{-10}$. In models where CP symmetry is realized in a spontaneous fashion, $\bar{\theta}$ is a finite and calculable quantity that has no apparent reason to be smaller than $10^{-4}$ [34, 35]. In that scenario, the $\eta \to 2\pi^0$ branching ratio could be on the level of $10^{-6}$, which may fall within the sensitivity of the proposed measurement.

Our motivation for searching for CP violation in $\eta \to 2\pi^0$ is model independent. Since Baryogenesis requires a new source of CP violation, we must fully exploit the few tests of CP that nature has allowed us, both flavor violating and flavor conserving. It is possible that the new source of CP violation is beyond any known mechanism which has been discussed in the literature, just like its initial discovery that was unanticipated. Evading neutron EDM constraints could also take a dynamical form if for example the $s\bar{s}$ content of the $\eta$ turned out to be a new CP violation source.

*Status of $\eta \to 2\pi^0$ tests of CP violation and their figures of merit*

The current experimental limit of $3.5{\times}10^{-4}$ for the branching ratio for $\eta \to 2\pi^0$ was set by the GAMS-4$\pi$ collaboration in 2007 using $\pi^- + p \to \eta + n$ with pion momenta of 32.5 GeV/c [47]. Backgrounds, attributed to copious continuum $2\pi^0$ production, were unusually high. Despite a significant increase in the number of $\eta$'s compared to older experiments, the GAMS-4$\pi$ result was only slightly better than the limit $4.3{\times}10^{-4}$ [45] achieved two decades earlier by the $\phi$ factory-based CMD-2 collaboration. A more recent 2011 result from the BESIII $J/\psi$ factory was actually less sensitive at $6.9{\times}10^{-4}$ [46]. The limit on the *charged* channel $\eta \to \pi^+\pi^-$ from KLOE, $1.3{\times}10^{-5}$ [48], is currently the best result for any $\pi\pi$ decay branch but is somewhat higher than our projection for $\pi^0\pi^0$. Under the assumption of isospin symmetry, and accounting for identical particles in the neutral channel, this would imply an upper limit of $6.5 \times 10^{-6}$ for $\eta \to \pi^0\pi^0$. Our direct measurement of $\eta \to \pi^0\pi^0$ will improve on this implied limit by about 25%. Charged decays of the $\eta$ are beyond the scope of the proposal but will certainly be investigated by the collaboration.

Figure 4 shows the BR upper limits for several experiments along with the effective number of $\eta$'s in their experiments as well as their background fractions. These measurements have been limited both by backgrounds and the number of effective $\eta$ decays. As we'll show in Section VIII B, this proposal presents an opportunity to reduce the upper limit of $\eta \to 2\pi^0$ BR by 1.5 orders of magnitude.

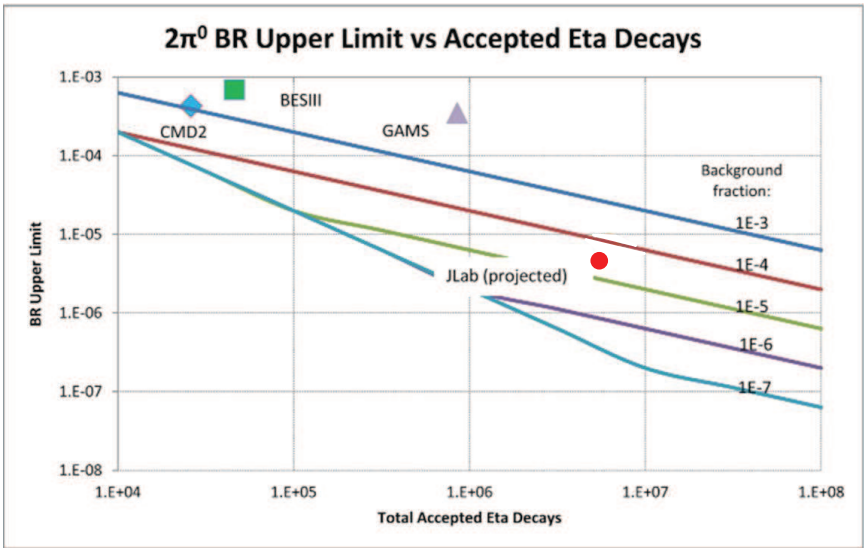


FIG. 4: The branching ratio upper limits and figures of merit for $\eta \to 2\pi^0$ measurements by GAMS [47], CMD-2 [45], and BES-III [46] plus a projection for the JLab Eta Factory.

### *3. The C non-invariant decay* $\boldsymbol{\eta \to 3\gamma}$

Relatively few systems are suitable for tests of the non-invariance of the charge conjugation operation C because one requires a particle of good C (or self-conjugate composite system) whose decay into a state of well-defined but opposite C is blocked *only* by C invariance [44]. Experimental precision is limited by the need to first produce these unusual systems then search for the relevant

decay branches with high efficiency while keeping backgrounds low. A classic example of a purely leptonic self-conjugate system is $e^+e^-(ortho) \to 2\gamma$. Comparisons of Hydrogen and anti-Hydrogen properties have more recently allowed tests of C in atomic systems. The present proposal intends to improve limits for non-weak decays of hadrons using $\eta \to 3\gamma$.

The C operator reverses the sign of all additive quantum numbers of a particle but leaves its spin unchanged. Thus it turns a left-handed neutrino into a left-handed antineutrino. According to the experimental results, however, all neutrinos are left-handed and all antineutrinos are right-handed. Therefore C conjugation is maximally violated in the weak interaction (usually accompanied by P violation so that CP is conserved). The SM does not give an explanation for this, and instead takes it as a input by assuming that all basic fermions come as left-handed doublets and right-handed singlets. This blatant asymmetry makes a strong argument for better experimental tests of the validity of C invariance. On the other hand, both C and P are generally assumed to be exact symmetries in the strong and electromagnetic interactions despite the fact that the experimental bounds have not reached the level of 0.1% by amplitude. In addition to $\eta \to 3\gamma$, we will search for another three photon final state forbidden by charge-conjugation invariance, $\eta \to \pi^0\gamma$. (See Appendix A for discussion of selection rules in $\eta \to 3\gamma$ and $\eta \to \pi^0\gamma$.) However, since the latter is also forbidden by the conservation of angular momentum and gauge invariance (respected by most but not all SM extensions), we assume it will serve as an experimental control.

Before one can search for new sources of C violation, one must have an estimate for the SM background. The only known source of C violation is the weak interaction. Dicus [49] estimated the ratio $\Gamma(\pi^0 \to 3\gamma)/\Gamma(\pi^0 \to 2\gamma) = 10^{-31}$ by applying dimensional arguments to the SM parity violating interaction including Bose symmetry. A similar estimate can be done for the $\eta \to 3\gamma$ process by substituting the $\eta$ mass for the $\pi^0$ mass yielding $\Gamma(\eta \to 3\gamma)/\Gamma(\eta \to 2\gamma) = 10^{-24}$ . Despite the enormous enhancement in this branching ratio for the $\eta$, and considerable uncertainty in the original estimate[4], the SM background for $\eta \to 3\gamma$ is effectively zero. Thus any non-zero result for $\eta \to 3\gamma$ would require a new source of C violation.

[4] The uncertainty was $\pm 6$ orders of magnitude due in part to the somewhat arbitrary choice of effective quark mass in the loop.

*Status of $\eta \to 3\gamma$ tests of C non-invariance and their figures of merit*

In the $\eta \to 3\gamma$ regime, the most precise upper limit of $1.6{\times}10^{-5}$ was set by the KLOE detector at the Frascati $\phi$-factory $DA\Phi NE$ [51]. That experiment produced $1.8{\times}10^{7}$ $\eta$'s in 2001-2 by the $e^{+}{+}e^{-} \to \phi \to \gamma{+}\eta$ process (BR 1.3%). Photons were detected in a lead/scintillating fiber sampling calorimeter. With an estimated acceptance of 20% for $\eta \to 3\gamma$, there were effectively $3.6{\times}10^{6}$ $\eta$'s produced, similar to the effective $\eta$ production from half a year of JLab Eta Factory (JEF) operation. The unique KLOE background in the $3\gamma$ final state was dominated by $e^{+}{+}e^{-} \to \omega\gamma \to \pi^{0}\gamma{+}\gamma \to 4\gamma$ where one of the $\gamma$'s tagged an $\eta$ that did not exist. The signal window contained no significant excess above a background of 1513 counts (0.042% of the accepted $\eta$'s).

The Crystal Ball experiment at BNL AGS set a somewhat weaker upper limit on the existence of the $\eta \to 3\gamma$ process of $4{\times}10^{-5}$ [52]. However, it is important to discuss it because the backgrounds they encountered are more relevant to JEF than those from a $\phi$ factory. Photons were detected in an array of NaI(Tl) crystals. There was an ADC for each crystal, but only one TDC per group of 9 crystals. That experiment produced $2.8{\times}10^{7}$ $\eta$'s via the $\pi^{-} + p \to \eta + n$ reaction at threshold. With an estimated acceptance of 10% for $\eta \to 3\gamma$, there were effectively $2.9{\times}10^{6}$ $\eta$'s produced (similar to KLOE). The dominant background was from $\pi^{-} + p \to 2\pi^{0} + n$ continuum production, followed by the merging or loss of a low energy photon. Other (much smaller) backgrounds in the Crystal Ball experiment arose from the merging of showers from the large branch $\eta \to 3\pi^{0} \to 6\gamma$ or splitting of a photon from the large branch $\eta \to 2\gamma$. A unique background in this experiment was $\pi^{-} + p \to \pi^{0} + n \to 2\gamma + n$ where the $n$ was detected in coincidence with the photons, but which was easily suppressed to a negligible level by cuts. There were about 875 background events in the signal box giving a background fraction of $2.2 \times 10^{-4}$.

Figure 5 shows the BR upper limits for several experiments along with the effective number of $\eta$'s in their experiments as well as their background fractions. These measurements have been limited mostly by background rather than by the number of effective $\eta$ decays. We expect to do about one order of magnitude better.

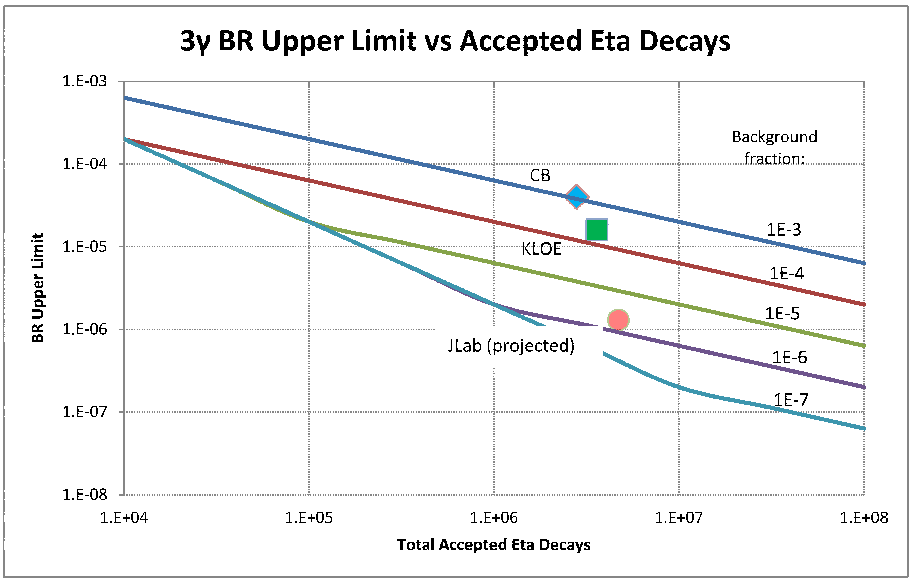


FIG. 5: The branching ratio upper limits and figures of merit for $\eta \to 3\gamma$ measurements by KLOE [51] and the Crystal Ball at BNL [52] plus a projection for the JLab Eta Factory.

### D. The allowed $\eta \to 3\pi^0$ decay

A high statistics data set of $\eta \to 3\pi^0$ (BR=32.57%) would not only help us understand the background in the rare decay channels but also would contain rich physics in its own right. The decay of $\eta$ into three pions occurs primarily due to the $d-u$ quark mass difference which violates isospin invariance, and is widely considered to be one of the best ways to determine the $d-u$ quark mass difference [5][9]. An interesting parameter to investigate is the slope $\alpha$ in the Dalitz parameter $z$ distribution, which is defined as:

$$z = 6\sum_{i=1}^{3} \frac{(E_i - m_\eta/3)^2}{(m_\eta - m_{\pi^0})^2}, \tag{7}$$

where $E_i$ is the energy of the $i$th pion in the $\eta$ rest frame. The variable $z$ varies from $z = 0$, when all three $\pi^0$'s have the same energy $E_i = m_\eta/3$, to $z = 1$, when one of the $\pi^0$'s is at rest. In lowest order, this distribution should be uniform because the final state particles are identical; however, the $\pi$-$\pi$ final state interaction and its strong energy dependence cause a tiny non-uniformity. There are several new experimental results published in the recent years from KLOE, Crystal Ball and

WASA collaborations [53]-[56]. We anticipate that our statistics will be comparable to the existing data sets. Due to the high energy boost in our $\eta$ production, we are able to extend the measurement to a larger $z$ region where one $\pi^0$ has a small energy. The fit range caused the largest systematic uncertainty for the slope parameter $\alpha$ determination in the recent KLOE result [53]. The expansion in the kinematical range of $z$ will help to reduce this uncertainty.

### E. Rare $\eta$ Decay Competition Around the World

Given the promise offered by a rare $\eta$ decay program to our understanding of the SM and beyond, several groups at other facilities have done recent work on this subject.

An example of a recently completed program is the KLOE-I collaboration at the Frascati $\phi$ factory. They accumulated large $\eta$ datasets using $\phi$ production in $e^+e^-$ collision at the center of mass energy of 1.02 GeV. By detecting a mono-energetic photon from the decay of the $\phi$, they tagged $\eta$ production with backgrounds at the part per thousand level. The KLOE-I program was very competitive for final states involving charged particles such as $\eta \to \pi^+\pi^-$ or $\eta \to \pi^+\pi^- e^+ e^-$. We have not studied the backgrounds for these charged particle reactions in JEF, but improvements by an order of magnitude over KLOE-I would be difficult. After luminosity and detector upgrades. the program is now continuing in the form of KLOE-II.[60] Even if KLOE-II succeeds in increasing production to $1{\times}10^8$ $\eta$'s, their lack of significantly boosted $\eta$'s and lack of high quality calorimetry means they cannot reach the sensitivity of JEF for high background, all neutral final states like $\eta \to \pi^0 2\gamma$, $2\pi^0$, and $3\gamma$. While they are the most likely source of significantly improved $\pi^0 2\gamma$ data before JEF results become available, the projected KLOE-2 error bars being circulated appear to ignore the effect of the large background.

After completing a rich experimental program on the $\eta$ physics at Brookhaven National Laboratory where they enjoyed extremely high $\eta$ production rates from $\pi^- + p \to \eta + n$ (as well as high backgrounds), the Crystal Ball collaboration moved their photon spectrometer to the Mainz Microtron facility in 2002. Using a bremsstrahlung photon beam from a 1.5 GeV electron beam, they are

continuing a rare $\eta$ decay program using the same reaction as us, $\gamma p \to \eta p$. Their $\eta$ production rates are reportedly over an order of magnitude higher than that expected in JEF, but the backgrounds in the $\pi^0 2\gamma$ channel are only moderately better than what was obtained with the CB at the AGS. (See Figure 7 for the AGS version.) With respect to $\eta$ decays, they appear to be focusing on precise measurements of relatively large branching ratio channels.[61] They have made cutting edge measurements of the $\eta$ mass as well as the Dalitz distribution slope parameter in $\eta \to 3\pi^0$ (BR = 33%).

Another large acceptance photon detector that has gained a new life by emigration is the Wide Angle Shower Apparatus (WASA). Originally located at Uppsala, Sweden, it is now at the COoler SYnchrotron (COSY) facility in Germany [59]. A 1.0 GeV proton produces $\eta$'s via the $p + d \to^3 He + \eta$ reaction. The clear niche of WASA whether at CELSIUS or at COSY has been $\eta$ decays to final states with $e^+e^-$ pairs. This is because it has an extremely clever cryogenic pellet target that avoids the problem of $\eta \to 2\gamma$ (BR 39%) followed by pair production in a thick target.

The BES-III collaboration [46] at the Beijing Electron Positron Collider got into the $\eta$ rare decay business using $J/\psi \to \gamma\eta$. Possibly because of the large $J/\psi$ mass and the small branching ratio to $\gamma\eta$, they did not obtain a competitive result for the difficult but important $\eta \to 2\pi^0$ channel, although they dramatically lowered the BR upper limits for $\eta', \eta_c \to \pi^+\pi^-$ decays.

What all these groups have in common is that $\eta$'s are produced nearly at rest in the laboratory and then detected in a nominally $4\pi$ detector. As discussed above, this leads to fierce backgrounds in rare decays to $4\gamma$ final states due to $\eta \to 3\pi^0$ with missing or merged photons. Using the high energy $\eta$ production and high-resolution, high-granularity $PbWO_4$ $\gamma$ detector in this proposal, we will be able to reduce the background by orders of magnitude compared to our competitors, while maintaining a healthy $\eta$ production rate. Our niche is $\eta$ rare decays to all-neutral final states, particularly channels with 3 or 4 photons in the final state.

## II. CONTROLLING BACKGROUNDS IN RARE DECAYS USING $\pi^0 2\gamma$ FOR ILLUSTRATION

As in any rare decay experiment, the major challenge is to suppress backgrounds while maintaining high efficiency for the reaction of interest. All our priority rare $\eta$ decay channels require the detection of 3 or 4 photons. Several key features of our proposal which suppress backgrounds while maintaining a high $\eta$ production rate are:

(1) the 12 GeV high intensity tagged photon beam in Hall D to produce $\eta$ mesons on a liquid hydrogen target through the $\gamma p \to \eta p$ reaction,

(2) a forward high-resolution, high-granularity $PbWO_4$ calorimeter (FCAL-II) to detect multiple photons from $\eta$ decays to reduce the $\eta \to 3\pi^0$ background (the scintillation in $PbWO_4$ has a shorter decay time ($\sim$ 20 ns) by about one order of magnitude than NaI(Tl) which helps control pile-up),

(3) measurement of the recoil $p$ with the GlueX detector to establish coplanarity of the proton and $\eta$ from the $\gamma + p \to \eta + p$ production process (and so reduce backgrounds from resonance cascades as well as accidental coincidences), and

(4) using flash ADCs on every crystal for nsec-scale coincidence timing of showers and pile-up rejection.

In the following sections, we employ the allowed channel $\eta \to \pi^0\gamma\gamma$ to highlight the unique experimental challenges of such experiments and explain how our proposal addresses them. Our simulation shows that the electromagnetic background plays no significant role in either the online trigger rate or in the offline accidental background (see Appendix C for detail). In the following discussion, we focus on the hadronic background only.

Two options of the calorimeters are considered in the simulation. One is the the standard GlueX lead glass forward calorimeter (FCAL) with a round front face of 240 cm in diameter, and the other is the proposed $PbWO_4$ crystal calorimeter with an active area of $118 \times 118$ cm$^2$ (FCAL-II). The cell size is 4.0cm x 4.0cm for FCAL and 2.05cm x 2.05cm for FCAL-II. The details of FCAL-II will

be described in section IV.

### A. The $\eta \to 3\pi^0$ Background

Previous $\eta \to \pi^0\gamma\gamma$ experiments [20][22][24] found the dominant background to be from $\eta \to 3\pi^0$ which has a branching ratio three orders of magnitude larger than the desired $\eta \to \pi^0\gamma\gamma$ decay. Obviously, for a $6\gamma$ decay to be a background to a $4\gamma$ process, two photons must effectively go uncounted while the event nevertheless passes the cuts used to define a good signal. There are three contributing cases [20]: (1) two soft photons can fall out of the geometrical acceptance or below threshold of the detector, or (2) four photons can merge into what appears to be two showers, or (3) a combination of soft photon losses and photon mergings.

The first mechanism (the loss of photons) affects the majority of published $\eta$ rare decay experiments because their $\eta$'s had small or modest boost. In that case, decays frequently produce low energy $\gamma$'s whose omission allows the the $\eta \to 3\pi^0$ background to pass missing energy or $\eta$ invariant mass cuts. The second mechanism, the merging of photons, is a problem when individual crystals subtend too large a solid angle, a feature of the legacy Crystal Ball calorimeter which was not optimized for $\eta$ decay experiments. Both mechanisms can be greatly suppressed by increasing the energy of the $\eta$ mesons while maintaining sufficient granularity in the calorimeter.

The advantage of using highly boosted $\eta$'s can be seen by comparing spectra from two older experiments as shown in Figure 6 and Figure 7. The invariant mass spectrum from GAMS (Figure 5) shows a narrow peak from $\eta \to \pi^0\gamma\gamma$ which is 7x larger than a smoothly falling background. [20] In that experiment, the $\eta$'s were produced by a high energy $\pi^-$ beam (30 GeV/c) in the charge exchange reaction $\pi^- p \to \eta n$. The decay photons from $\eta$ decays in flight were detected in the forward direction by a calorimeter consisting of a 48 x 32 array of lead glass modules. Because of the boost, when a photon is lost, the effect on the $\eta$ mass reconstruction is relatively large thus the background from missing photons in $\eta \to 3\pi^0$ events is generally shifted out of the $\eta$ signal window.

In the Crystal Ball [22] and KLOE[24] experiments at the AGS and DA$\Phi$NE, respectively, the $\eta$'s were produced with very little boost so the energy of the decay $\gamma$'s was $\sim$50–500 MeV. Under these

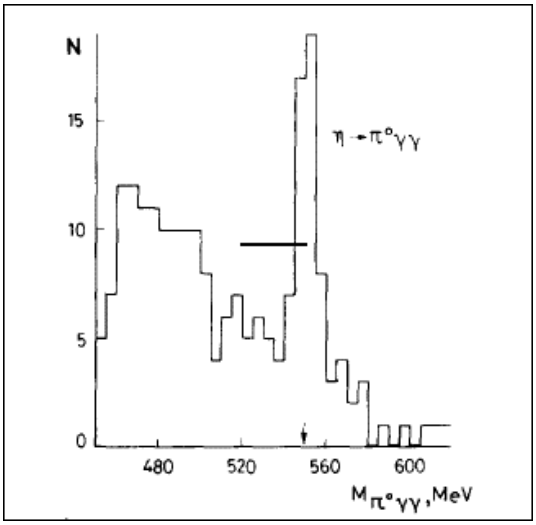


FIG. 6: Invariant mass spectrum for the $\pi^0\gamma\gamma$ reaction measured by the GAMS collaboration [20] using high energy $\eta$'s produced by $\pi^- + p \to \eta + n$.

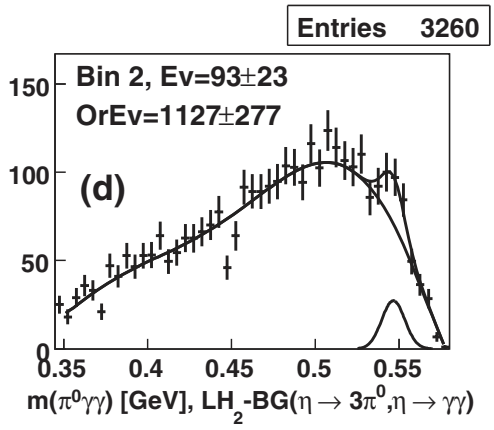


FIG. 7: Invariant mass spectrum for the $\pi^0\gamma\gamma$ system measured by the Crystal Ball collaboration at the BNL AGS [22] with $\eta$'s produced near threshold via $\pi^- + p \to \eta + n$. Compare to the previous figure.

circumstances, the background from $\eta \to 3\pi^0$ is broadly peaked near the $\eta$ mass peak as can be seen in Figure 7.[5] Not only is the smooth background relatively large, but our simulations show that when photons merge there is a peaking component indistinguishable from the signal. In that case, sideband subtractions alone are unreliable and one must rely on simulations of shower merging probability. Under such background conditions it is already difficult to accurately determine the simple branching ratio. The measurement of an accurate $d\Gamma/dM_{\gamma\gamma}$ spectrum to probe the dynamics of the decay is even more difficult.

As mentioned above, the second important mechanism for $\eta \to 3\pi^0$ to mimic the $\eta \to \pi^0\gamma\gamma$ decay is through overlapping photon clusters. The most practical size for a calorimeter element is set by the Moliere radius which, loosely speaking, describes the radial extent of the shower core.[6] $PbWO_4$ crystals have Moliere radii ($\sim 2$ cm) about two times smaller than the typical material (such as lead glass) used in older generation calorimeters. This benefit is partially offset by kinematic focusing

[5] See also Figure 10 (a) in reference [21].

[6] Larger elements lose position information, while smaller elements increase readout costs with little gain in position information.

from our highly boosted $\eta$'s. However, we win because we have moved FCAL-II far downstream from the target center (6m), hence the decay products are distributed over 3445 crystals, each with transverse dimensions of roughly a Moliere radius. By contrast, the Crystal Ball detector with acceptance of 93% of $4\pi$ has only 672 NaI(Tl) crystals. Another advantage we have is algorithms developed by PrimEx to use measured radial energy profiles to identify pairs of showers separated by only a few cm. To conclude, the JEF configuration tightly manages the potential background from photon merging in the copious $\eta \rightarrow 3\pi^0$ channel. This leaves a small peaking background in the invariant mass spectrum that we will be able to accurately simulate and subtract.

Simulations were made to compare the expected performance of FCAL-II and FCAL. Four photon invariant mass distributions for the signal $\eta \rightarrow \pi^0\gamma\gamma$ and the background $\eta \rightarrow 3\pi^0$ are reconstructed. Figure 8 is FCAL-II and Figure 9 is for FCAL, with both located at 6m from the target. As shown in the figures, the signal to background ratio of FCAL-II is two orders of magnitude better than FCAL. We also studied the situation where the FCAL is moved by 3 m further downstream from the target (the maximum possible distance allowed in Hall D) in order to reduce photon merging and improve the angle resolution. The $4\gamma$ invariant mass distribution is presented in Figure 10. As one can see, the signal to background ratio improved slightly to 0.5, but this is still 1.5 orders of magnitude worse than FCAL-II and not good enough for clear signal separation. This is the main reason for us to suggest upgrading the current FCAL with $PbWO_4$ crystals (FCAL-II). All subsequent plots will assume the FCAL-II configuration.

### B. The $\gamma + p \rightarrow 2\pi^0 + p$ (Continuum) Background

The remaining historically dominant background has been non-resonant multiple $\pi^0$ production. The production of $\gamma p \rightarrow 2\pi^0 p$ has been studied using different beam types and targets at low beam energies [57][58]. In our energy range, the production mechanism of $2\pi^0$'s is itself an interesting topic. This channel is expected to form a smooth background that does not produce a peak in the $\eta$ mass region, therefore it can be measured and subtracted using side-band data.

Before presenting our Monte Carlo simulations, we need to introduce the *elasticity* parameter which is the basis for an important missing-energy cut. In our forward, high energy kinematics, the $\eta$

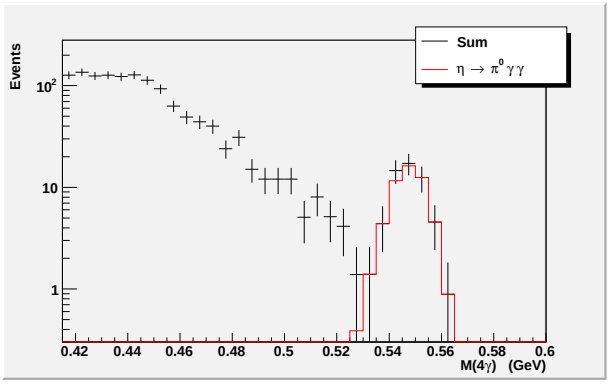


FIG. 8: Monte Carlo simulation of $M_{4\gamma}$ reconstructed in the proposed $PbWO_4$ crystal calorimeter (FCAL-II). The only background considered here is from $\eta \rightarrow 3\pi^0$. The red curve is the signal from $\eta \rightarrow \pi^0\gamma\gamma$. Black points are the signal plus background. The signal to background ratio for $\pm 3\sigma$ around the $\eta$ mass peak is 10:1.

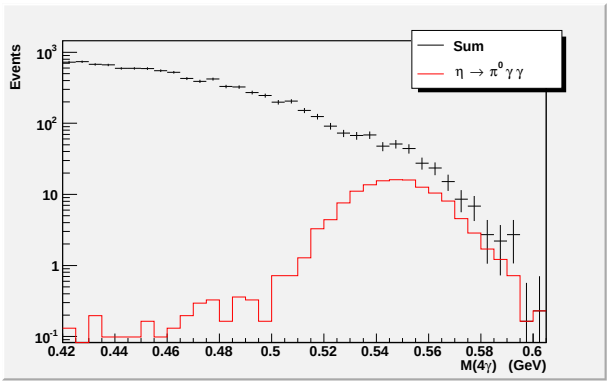


FIG. 9: Same conditions as the previous figure but using a current Hall D forward lead glass calorimeter (FCAL) at 6m. The signal to background ratio is 0.1.

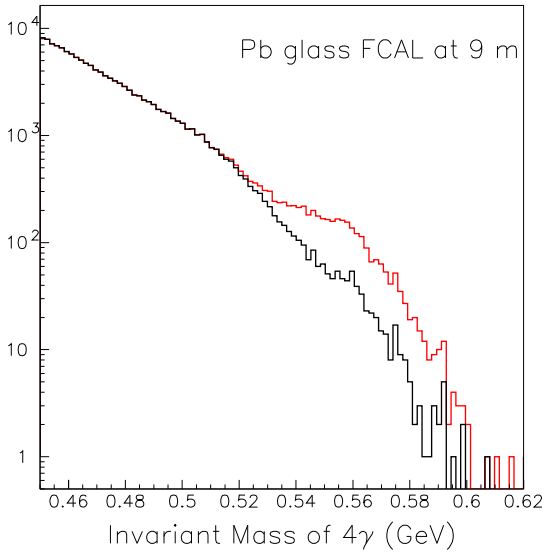


FIG. 10: Monte Carlo simulation of reconstructed $M_{4\gamma}$ assuming the FCAL Pb-glass calorimeter at 9m. The black curve is the background, while the red curve is the signal plus background. The signal to background ratio for $\pm 3\sigma$ around the $\eta$ mass peak is roughly 0.5.

carries almost the full beam energy. This means that the elasticity, defined as

$$EL \equiv \frac{\Sigma E_\gamma}{E_{tagged\gamma}} \tag{8}$$

is approximately 1 for fully contained $\eta$ decays produced by the exclusive $\gamma + p \to \eta + p$ production channel. Requiring that the elasticity be near 1 greatly inhibits nature's ability to mimic a signal from complex backgrounds. Examples of events which could pass an invariant mass cut but fail the elasticity cut include 1) calorimeter pile-up, 2) $\eta$ production by an untagged off-energy photon in random coincidence with a tagged but sterile photon, or 3) continuum $3\pi^0$ production at invariant mass $> m_\eta$ which migrates down into the $\eta$ mass window when two photons are effectively lost.

Three other kinematical variables used for event selection are the invariant mass $M_{4\gamma}$, missing energy $\Delta E$, and the co-planarity $\Delta\phi$. The missing energy here is defined as the energy balance $\Delta E = E(\eta) + E(p) - E(beam) - M(p)$ and contains the recoil proton energy; the $\Delta\phi$ is an azimuthal angle difference between the proton and the reconstructed $\eta$ momenta, $\Delta\phi = \phi(\eta) - \phi(p)$. The event selection windows for these variables correspond to $\pm 3\sigma$ of the corresponding resolutions and are listed in Table II. In the future, in addition to using the $\Delta\phi$ and $\Delta E$ cuts, we will perform a kinematic fit for the reconstructed particles.

| | $M_{4\gamma}$ (GeV) | Elasticity | $\Delta E$ (GeV) | $\Delta\phi$ (deg) |
|---|---|---|---|---|
| FCAL(Pb glass) | [0.500, 0.595] | $\geq 0.92$ | [-0.8 ,0.8] | [-5, 5] |
| FCAL-II (PWO) | [0.526, 0.569] | $\geq 0.95$ | [-0.36,0.36] | [-5, 5][a] |

[a]A smaller range could have been used due to the better PWO resolution.

TABLE II: Event selection ranges used in the analysis.

A Monte Carlo simulation was performed for the $\gamma p \to 2\pi^0 p$ reaction using the PYTHIA event generator incorporating both non-resonant production of the two-pion pairs and production through resonances such as $\gamma + p \to \pi^0 + \Delta^+ \to 2\pi^0 + p$. Figure 11 shows the $4\gamma$ invariant mass distributions for the $\eta \to \pi^0\gamma\gamma$ signal and the three backgrounds ( $\eta \to 3\pi^0$, $\gamma p \to 2\pi^0 p$, and the "other hadronic backgrounds" that will be discussed in the next section). The statistics is normalized to one day

of data taking, while the missing energy and coplanarity cuts that were used are listed in Table II. The projected signal to background ratio is approximately 3:1. The $2\pi^0$ continuum background appears to play a very small role for the $\eta \to \pi^0 2\gamma$ signal channel, however it is an irreducible background for the $\eta \to 2\pi^0$ search whose sensitivity will be discussed later.

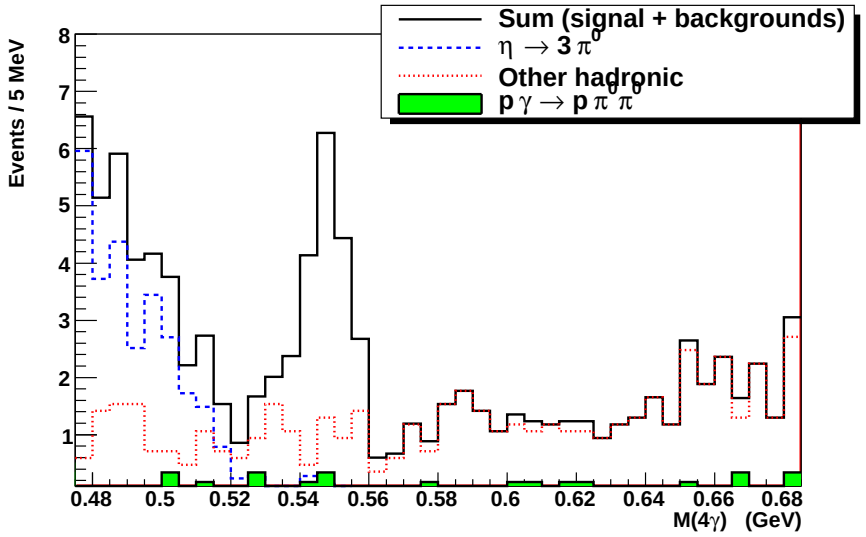


FIG. 11: Invariant mass ($M_{4\gamma}$) for FCAL-II including the signal channel $\eta \to \pi^0\gamma\gamma$ and major background channels. The solid black curve is the sum of signal and background channels. The blue dashed curve is for $\eta \to 3\pi^0$; the solid green area is for $\gamma p \to 2\pi^0 p$, and the red dotted curve is for other hadronic backgrounds predicted by PYTHIA. All rates are normalized using estimated cross sections to 1 beam day. Cuts for FCAL-II listed in Table II have been applied.

### C. Other Hadronic Background

Essentially all remaining hadronic background contributions to the $\eta \to \pi^0\gamma\gamma$ signal channel were studied using a Pythia event generator adapted to GlueX energies. The background was simulated in the photon beam energy range between 9 GeV and 12 GeV. The total photoproduction cross section for this energy range is about 120 $\mu$b, compared to the total $\gamma p \to \eta p$ production cross section of 70 nb. The analysis was carried out in two steps:

First, we identified all possible decay channels that can contribute as a background to the 4 cluster final state using a data sample of 25 million Pythia events. Generated events were passed through the detailed GlueX Geant simulation and were reconstructed using official FCAL and PWO calorimeter cluster reconstruction programs. Since the backgrounds from $\gamma p \to \pi^0\pi^0 p$ and $\gamma p \to p\eta$ (followed by $\eta \to 3\pi^0$ decays) have been discussed in Sections II.A and B, we excluded them from the data sample. We observed that the dominant background originates from multiple photon final states such as $p\ 4\pi^0$, $p3\pi^0\gamma$, $p\ 2\pi^0\ \gamma$, $p\ 2\pi^0\ \gamma\ \gamma$,and $p\ 2\pi^0\ K_L$. Similar to the case of the $p\eta(\eta \to 3\pi^0)$ background described in Section II.A, these channels can lose photons outside the calorimeter acceptance or produce overlapping clusters in the calorimeter, leading to the reconstruction of a four cluster final state.

Subsequently, we generated a MC sample with five times larger statistics for these selected channels. The invariant mass distribution for events reconstructed with the PWO calorimeter (FCAL-II) is presented in Fig. 12 where the sensitivity of the cuts is explored in detail. The majority of the background events are suppressed by the elasticity/missing energy cut(s). These events must have started at higher invariant mass and migrated into the $\eta$ invariant mass window by losing a photon out of the calorimeter acceptance. Also extremely encouraging is the fact that the co-planarity cut is able to suppress the remaining background by an order of magnitude. The contribution of this background to the $4\gamma$ invariance signal window is shown as the red dotted curve in Figure 11.

### D. Backgrounds in $\eta \to 3\gamma$

The backgrounds of relevance to our $\eta \to 3\gamma$ measurement will be qualitatively similar to the non-unique backgrounds at the Crystal Ball [52] (see discussion in section I C.3). The dominant background was from the $2\pi^0$ continuum production. These backgrounds should be greatly reduced at JLab due to our high-granularity calorimeter, which reduces photon merging, and our "boosted $\eta$" kinematics which immensely reduces the phase space for a photon to fall out of the acceptance and remain within our missing energy or invariant mass cuts. We will also detect the recoil proton to ensure it is consistent with the 2-body reaction $\gamma + p \to \eta + p$ rather than 3-body $\gamma + p \to 2\pi^0 + p$.

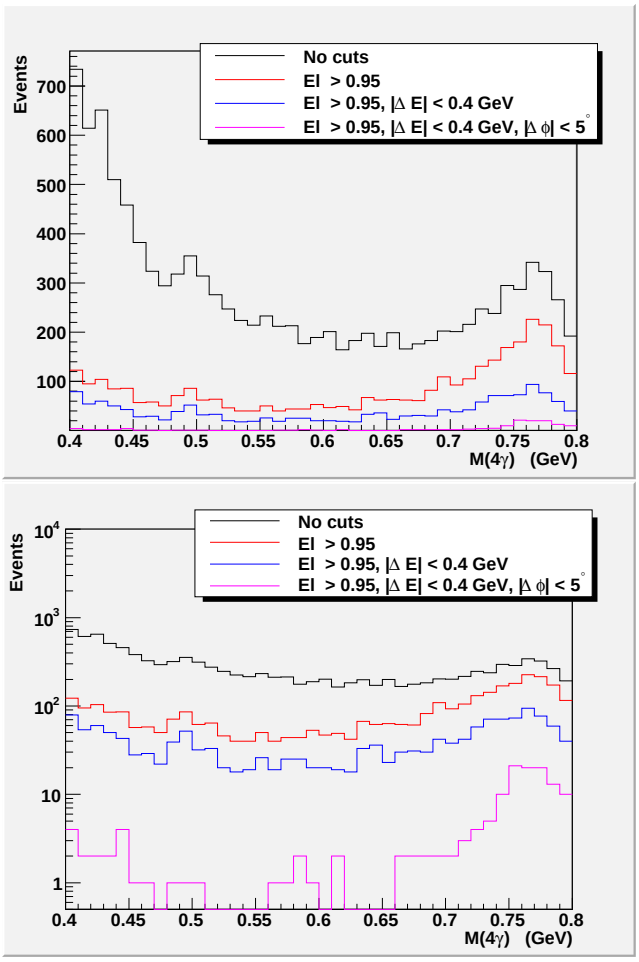


FIG. 12: $4\gamma$ invariant mass distribution for hadronic background events reconstructed with the PWO ($118 \times 118$ cm$^2$) calorimeter. (Top - linear scale; Bottom - log scale) Different curves correspond to various cuts applied during the reconstruction: no cuts (black); elasticity cut (red); elasticity and $\Delta E$ cuts (blue); elasticity, $\Delta E$, and $\Delta\phi$ cuts (purple).

Having a flash ADC per channel will also allow us to flag pile-up in the offline analysis. In addition, there is a continuous $3\gamma$ background from the tail of $\rho$ production through either $\rho \to \eta\gamma$ followed by $\eta \to 2\gamma$ or $\rho \to \pi^0\gamma$ followed by $\pi^0 \to 2\gamma$. Such background can be suppressed by rejecting the events with a photon pair with reconstructed invariant mass equal to the $\eta$ or $\pi^0$ masses.

## III. HALL D BASE EQUIPMENT

We propose to use a 9.0–11.7 GeV incoherent tagged photon beam in Hall D to efficiently produce $\eta$ mesons through the small angle $\gamma + p \rightarrow \eta + p$ reaction. Multiple decay photons from the $\eta$'s will be detected in a new high-resolution and high-granularity $PbWO_4$ calorimeter (FCAL-II) located $\sim$ 6 m downstream of the target. For not-too-small $\eta$ angles, the low energy recoil protons will be detected by the start counter and central drift chamber of the GlueX solenoid detector to help suppress backgrounds. As shown in Figure 13, the experimental apparatus includes: (1) a high energy photon tagger; (2) a pair spectrometer for photon flux monitoring; (3) a 30 cm length liquid hydrogen target; (4) the GlueX solenoid detector; (5) an upgraded forward multichannel electromagnetic calorimeter. The reference design of the experiment is summarized in Table III. Details of each instrument are discussed below.

### A. High Energy Photon Tagger

Hall D is developing and constructing a 12 GeV tagged photon beam line. While details of the design can be found in reference [62], the main features are:

1. Photon energy detection from 70% to 75% of the primary electron beam energy with energy resolution of about 0.5% (r.m.s.) of the primary beam energy. A counting rate of at least $5 \times 10^6$ electrons per second per 0.1% energy bin over this range of photon energies.

2. Additional capability for photon energy detection from 25% to 97% of the primary electron beam energy. Capable of pre-collimated intensities up to 150MHz/GeV for high intensity running, with 50% sampling of 60 MeV energy bins below 9 GeV and full coverage in 30 MeV wide energy bins above 9 GeV photon energy.

TABLE III: Reference design of the JEF experiment.

| **Parameter** | **Value** |
|---|---|
| Solenoidal Field | 2.2 T |
| Photon Beam Energy Range | 9 - 11.7 GeV |
| Beam Current | 400 nA |
| Radiator Thickness (Au) | 2 x $10^{-4}$ $X_0$ |
| 5mm Collimator Transmission | 30% |
| Tagged Photon Rate on Target (9-11.7 GeV) | $\sim$4 x $10^7$ Hz |
| $LH_2$ Target Length | 30 cm (3.46 % R.L.) |
| $LH_2$ Target Thickness | 1.28 x $10^{24}$ protons/cm$^2$ |
| Cross Section for Forward $\gamma p \to \eta p$ | $\sim$70 nb |
| Scintillator in FCAL-II | $PbWO_4$ |
| Outer Active Dimensions of FCAL-II | 118cm x 118cm |
| Beam Hole Dimensions in FCAL-II | 12cm x 12cm |
| Crystal Dimensions | 2.05cm x 2.05cm x 18cm |
| Number of Optically Isolated Crystals | 3445 |
| Acceptance of 118 cm x 118 cm FCAL-II | $\sim$20% (4$\gamma$), $\sim$30% (3$\gamma$) |
| Distance Target Center to FCAL-II Front | $\sim$6 m |
| Exclusive $\eta$ Production Rate | 3.6 Hz (or 3.1 x $10^5$ /day) |
| $LH_2$ Production Request | 100 days |
| Total $\eta$'s Produced in 100 Days | 3.1 x $10^7$ |
| Effective $\eta$'s in 100 Days (Includes Acceptance) | 6.2 x $10^6$(4$\gamma$), 9.3 x $10^6$(3$\gamma$) |
| Total Beam Request | 136 days |

The tagging spectrometer is an Elbek-type spectrometer. The 12 GeV electrons pass through the radiator target where a small fraction undergo bremsstrahlung. The electrons then pass through a focusing quadrupole and are bent by the 6 meter long tagger magnet. The majority of the electrons do not significantly radiate and are bent 13.4° to the electron beam dump. A large

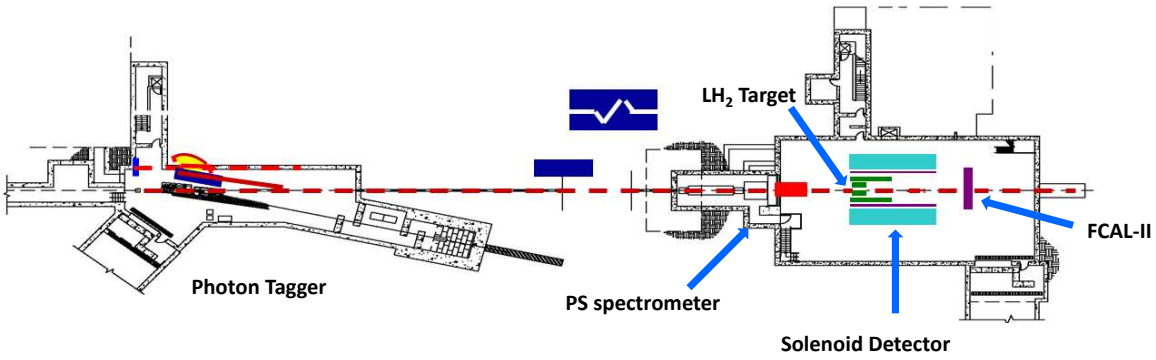


FIG. 13: Top view of the experimental setup for $\eta$ rare decays measurements. This includes: (1) a high energy photon tagger; (2) a pair spectrometer; (3) a solenoid detector with a physics target; (4) a forward $PbWO_4$ crystal calorimeter.

vacuum vessel is integrated into the magnet and extends to the spectrometer focal plane so the only multiple scattering occurs in the radiator and in the exit window, preserving the resolution. The spectrometer detectors are positioned immediately outside the focal plane to determine the momentum of electrons that produce bremsstrahlung photons in the radiator. The photon energy, $E_\gamma$, is determined by the difference between the initial electron beam energy and the energy of the

post-bremsstrahlung electron deflected towards the focal plane.

The detector package is divided into two parts: (1) a set of 190 fixed scintillation counters spanning the photon energy range from 3.0 to 11.7 GeV, and (2), a movable "microscope" of 500 scintillating fibers optimized for coherent photon beam operation spanning the energy range from 8.3 to 9.1 GeV. The fixed array provides access to the full tagged photon spectrum, albeit at a modest energy resolution of $\sim 0.1\%$ and reduced rate capability. These detectors are well suited for running with a broadband incoherent bremsstrahlung source. The microscope provides energy resolution better than 0.07% in order to run in coherent mode at the highest polarization and intensities. Using the microscope, the source is capable of producing collimated photon spectral intensities in excess of $2 \times 10^8$ photons/GeV, although accidental tagging rates will limit normal operation to somewhat less than this.

For the proposed $\eta$ rare decays measurement, we will use an incoherent bremstrahlung photon beam in an energy range from 9.0 GeV to 11.7 GeV. The current design of the fixed scintillation counters in this energy range with 30 MeV wide energy bins is sufficient.

### B. Beam Collimation

A 12 GeV electron beam interacting with a thin radiator produces the photon beam. The characteristic opening angle for bremsstrahlung photons is $m_e/E = 42$ $\mu$rad. After 76 meters of drift in vacuum, the photon beam enters the collimator cave from the left through a thin 250 $\mu$m Kapton window $8''$ (203mm) in diameter and immediately interacts with the primary collimator. The layout of the collimator cave is shown in Figure 14. The primary collimator consists of two main components: an active collimator which measures the centroid of the photon beam and a hybrid tungsten-lead passive collimator. The size of the passive collimator has a couple of options from 3.4 mm to 5.0 mm in diameter. The active collimator is electrically isolated, has an inner aperture of 5 mm, and is precisely mounted in front of the primary collimator. The purpose of the active collimator is to measure the position of the centroid of the photon beam with an accuracy

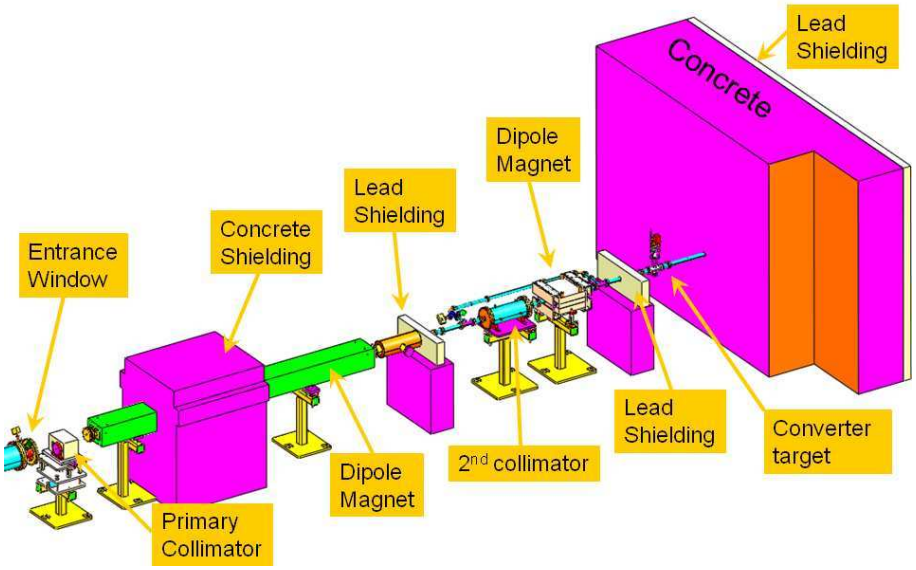


FIG. 14: The layout of the collimator cave.

of 200 $\mu$m. The tungsten passive collimator is surrounded by 8″ of lead for additional shielding. A large flux of background particles are generated in the passive collimator and some lie along the photon beam. A sequence of sweeping magnets after the collimator removes the unwanted charged particles from the photon beam.

A second collimator is located following the lead shielding wall of the first collimator. This collimator is made of stainless steel and is 20″ long and 8″ in diameter. A 1 cm hole is bored along the axis of the collimator and is designed so that the effective aperture can be adjusted to 6, 8, or 10 mm by inserting stainless steel tubes. The purpose of this collimator is to scrape off photons which were produced by small angle scattering on the bore of the primary collimator. A second sweeping magnet is mounted directly after the second collimator. The specification of the tolerance on this alignment during beam operation is a circle of radius 200 microns. The size of the beam spot on target is defined by the primary collimator. We plan to use a 5 mm diameter primary collimator in the proposed experiment.

### C. Pair Spectrometer and Total Absorption Counter

The most important diagnostics for the photon beam flux are the count rates in the tagger's fixed hodoscope array and the microscope. By detecting the electrons that undergo bremsstrahlung, one determines precisely the energy spectrum of the photon beam in front of the collimators. The photon flux on the target however is only a fraction of the tagged photons because of collimation. The absolute photon flux on the target will depend strongly on the exact details of the collimation. For example, a 5 mm diameter primary collimator will pass about 30% of the photons. It is proposed to use pair production, a well understood QED process, as the basis for the relative photon flux determination. An additional calibration measurement is needed to determine the pair spectrometer's absolute efficiency. This is done with dedicated calibration runs at low beam intensity with a total absorption counter (lead glass detector) inserted in the beam after the spectrometer.

The pair spectrometer consists of a thin foil converter ($1 \times 10^{-3}$ radiation length thick) placed in the photon beam following the last collimator (at 0.5 m distance upstream of the front end of the pair spectrometer magnet) to generate electron/positron pairs through pair production. The electrons and positrons produced in the converter are swept away from the photon beam in a strong magnetic field (1.64 T) and are subsequently detected by identical left and right arm detector packages located symmetrically on either side of beam line. The photon energy is then simply the sum of the electron and positron energies. Each detector package covers the electron or position energy from 3 GeV to 6.25 GeV. It consists of a front detector array for fine position resolution and a back scintillating hodoscope array to provide 200 ps time resolution to form the pair production trigger.

The proposed experiment will use the incoherent photon beam at the highest possible energy ($E_\gamma$=9–11.7 GeV). We will measure the branching of various rare decays by normalizing to the $\eta \to \gamma\gamma$ channel. The design specification for the pair spectrometer is to monitor the beam flux at $\sim 1\%$ level, which exceeds the requirements for the proposed experiment.

### D. Target

We propose to use the standard Hall D liquid hydrogen target with 30 cm length, corresponding to approximately 3.46% radiation lengths. Hall D is planning to use a cryogenic target system similar to what has been developed for Hall B [63]. While some details of the Hall D target system are still undefined, the main element of the cryogenic target is a stand alone pulse tube refrigerator. The Hall B g10a target cell, with design similar to that proposed for use in Hall D, is 24 cm in length. The upstream end of the target has an inner diameter of 5.51 cm, tapering down to 4.0 cm inner diameter on the downstream end of the target. The reason for the taper is to allow boil off gas to escape the target. The radius on the endcaps is 4 cm. The target cell is constructed from 5 mil kapton.

During the proposed experiment, target temperatures and pressures will be written into the data stream. Since significant target heating does not occur for a real photon beam, the target density can be deduced from the equation of state and the target pressure-temperature data. However, as we are measuring a branching ratio rather than an absolute cross section, we are insensitive to changes in target density.

### E. The Gluex solenoidal detector

The photon beam used in this experiment will be produced in the tagger hall and travel 76 m, after which the beam will pass through a collimator. The photons then interact in a liquid-hydrogen target. Outside the target, there is a scintillator-based start counter, the central drift chamber (CDC), and the lead scintillating fiber barrel calorimeter (BCAL) all inside a 2.2 T solenoid [67]. Most particles exiting the solenoid in the forward direction will strike a time of flight (TOF) wall. The complete GlueX apparatus is depicted in Figure 15.

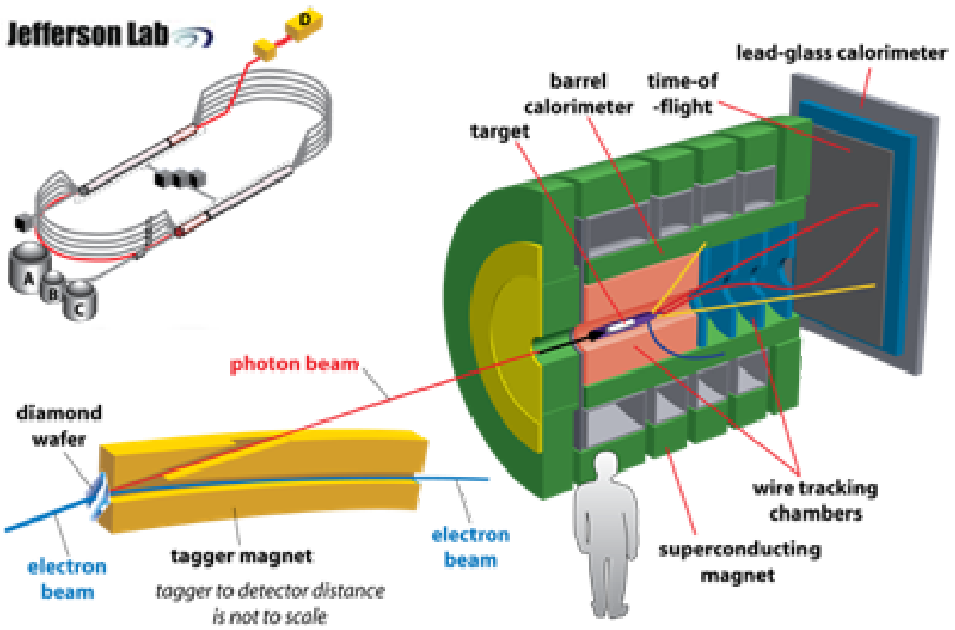


FIG. 15: The cross-sectional view of the complete original GlueX detector. The apparatus is described in detail in Section III E.

### *1. Solenoid*

The solenoid magnet creates a 2.2 T magnetic field at the center of the magnet oriented parallel to the beamline [68]. The magnet is 4.65 m long, has an inner diameter of 1.85 m, and an outer diameter of 3.76 m. The self inductance of the coil is 26.2 H hence at the nominal current of 1500 A the stored energy is 29.5 MJ. The solenoid consists of 4 separate superconducting toroidal coils and cryostats and was recycled from previous experiments.

### *2. Central Drift Chamber (CDC)*

The Central Drift Chamber (CDC) consists of 3500 1.5 m long straw tubes [70]. The straws are oriented in two directions: axial (12) and stereo (16), in order to provide better spatial resolution in the z or longitudinal coordinate. The CDC is a large cylinder surrounding the target and start

counter with an inner radius of 10 cm and an outer radius of 60 cm. The expected position resolution of the CDC is 150 $\mu$m. For the nominal position for the $LH_2$ target, the angular coverage of the CDC is 6° to 165°.

The CDC allows us to detect recoil protons which appears to be important for reducing backgrounds.

### *3. Start Counter*

The start counter is a barrel hodoscope consisting of 30 scintillators surrounding the target that will be used in conjunction with the tagger to measure the beam bucket of the associated event [69]. The detector is a 50 cm long cylinder with a 10 cm cone that tapers toward the beamline on the downstream end of the target. The start counter accepts charged particles at angles between 3° and 134° over the full length of the target. The start counter is self-supporting as to not introduce additional material in the path of the particles.

The start counter will be useful in flagging the presence of extra charged particles, and will provide large pulses with good timing resolution for recoil protons.

### *4. Barrel Calorimeter (BCAL)*

The barrel calorimeter (BCAL) is a lead-scintillating fiber sampling calorimeter that lines the inside of the solenoid. Each individual module consists of layers of corrugated lead sheets, interleaved with planes of 1 mm, round, Kuraray SCSF-78MJ scintillating fibres, bonded to the lead grooves using optical epoxy [71]. The complete detector will consist of 48 identical wedge-shaped modules with each module occupying 7.5° of azimuthal angle. Each module is 3.9 m long and 22.46 cm thick, and once assembled into the final ring shape, the BCAL will have an inner radius of 65 cm and an outer radius of 90 cm. The entire BCAL resides within the 2.2T magnetic field and will be read out by about 4,000 field-insensitive, large-area (1.44 $cm^2$ each) silicon photomultiplier arrays.

### *5. Time of Flight (TOF)*

The time of flight (TOF) detector wall is an array of 2.54 cm thick and 6 cm wide scintillator paddles [72]. The paddles are read out on each end by PMTs, except in the middle where the beamline only allows single ended readout. There will be a horizontally oriented wall and a vertically oriented wall to provide additional location information for a total of 92 paddles. The TOF detector will cover angles of 1° to 11°, providing an overlap with the start counter of angles 3° to 11°. The primary purposes of the TOF detector are to determine charged track multiplicity and provide excellent TOF information with respect to the accelerator RF beam bucket.

## IV. NEW CALORIMETER FCAL-II

The $\eta$ signal is primarily identified by reconstruction of the invariant mass,

$$M_{inv}^2 \equiv p^2 = (\Sigma E_\gamma, \Sigma \overrightarrow{P}_\gamma)^2 \tag{9}$$

from the summed 4-momenta of the decay photons detected in the forward multi-channel calorimeter. The relative error in invariant mass reconstruction is approximately given by the quadrature sum of the relative errors in energy and angle as can be surmised from the formula for reconstruction with two photons

$$M_{inv} = 2\sqrt{E_{\gamma 1} E_{\gamma 2}} \times \sin \alpha/2 \tag{10}$$

where $\alpha$ is the opening angle between the photons. We require percent-level resolution in shower energy reconstruction and, given a typical shower separation of 10's of cm, mm-scale resolution in calorimeter hit position to determine the angle of the photon. Based on PrimEx experience, the calorimeter energy resolution will dominate the invariant mass resolution. The contribution from the target length is quite modest even if the vertex is unknown, but we will detect the recoil proton.

To minimize shower merging and pile-up in the calorimeter, high-granularity and fast decay time are also critical. The scintillator $PbWO_4$ has highly desirable properties for use in an electromagnetic

calorimeter, including a small Molière radius (2.1 cm), short radiation length (7.4 g/cm$^2$), and fast decay time (20 ns). It is also highly radiation resistant and available in large quantities. Based on these features, and the extensive experience of some of us with a smaller lead tungstate calorimeter employed in the PrimEx experiment, we propose to use $PbWO_4$ crystals in an upgraded Hall D Forward Electromagnetic Calorimeter (FCAL-II).

Finalizing the ultimate size of the calorimeter will involve a trade-off between acceptance and cost. For a tagged photon beam of 9.0–11.7 GeV, the average acceptance for 4 photons in the $118 \times 118$ cm$^2$ calorimeter is $\sim$20% while that of the $150 \times 150$ cm$^2$ version is $\sim$40%. (See Figure 19 for the 3 photon acceptance and Figure 20 for the 4 photon acceptance.) In keeping with our philosophy of bridled enthusiasm, all projections in this proposal are based on the smaller, lower acceptance (and lower cost) calorimeter. However, it's worth noting that for less than 60% additional cost, the larger version of the calorimeter would increase the 3-4$\gamma$ acceptance an average of 80% while simultaneously reducing the fraction of $\eta \to 3\pi^0$ events with lost photons.

Our design is basically a larger version of the lead tungstate core of the PrimEx HyCal calorimeter, a 59 element x 59 element matrix of optically-isolated crystals each of size $2.05 \times 2.05 \times 18$ cm$^3$. The crystal transverse dimensions of $2.05 \times 2.05$ cm$^2$ are comparable to the Molière radius of lead tungstate so that shower energy sharing between adjacent crystals can be used to determine the position of the shower with mm-scale accuracy at the energies of interest. The 18 cm thickness (20 radiation lengths) has been shown by PrimEx to be sufficient to achieve the required energy resolution. A central $\sim 12 \times 12$ cm$^2$ hole will be left open to enable the photon beam and small angle electromagnetic background to pass downstream.

Scintillation light from the electromagnetic shower will be detected with Hamamatsu R4125HA photomultiplier tubes coupled to the back of the crystals with optical grease. A fiber optic cable will be glued to the front face of each module for the gain monitoring system. If instrumented as in the PrimEx HyCal, there will be a HV and two signal cables for each base (one for the anode and another for the dynode). The anode signals will each go to a flash ADC as discussed below. The dynode signals will be summed first in groups, and then groups will be summed to form a total calorimeter energy signal for use in the trigger and to provide a hardware timing reference.

Alternatively, the trigger can be built from the Flash ADC data pipeline.

An exciting development in JLab's 12 GeV era is the standardization of most new detector readout systems to flash ADCs. By keeping the cost per channel to less than $300 (and the loaded cost per channel including VME crate, CPU, etc. to less than $400), a single channel of 12 bit, 250 MHz flash ADC (plus fairly cheap memory and processing power) can substitute for an older non-flash ADC, a TDC, and two delay lines. This saves money, space, procurement time, and labor. Sampling is continuous and deadtimeless. When a shower occurs, the 4 nsec samples will be recorded so that the pedestal (zero offset), the energy, and the time can be determined offline. Tests indicate the time resolution is significantly better than 1 nsec[73]. This will allow us to constrain all photons in the event to the same beam burst and so minimize accidental coincidences. Flash ADCs are not merely cost-effective substitutes for older technology, they have been used in rare decay experiments for decades because they allow one to sensitively flag pile-up and even scrutinize interesting events individually when desired. The combination of $PbWO_4$ crystals and a flash ADC on each channel will make FCAL-II truly a cutting edge calorimeter for the 21st century.

Several institutions on this proposal are also major players in the PrimEx collaboration and were heavily involved in the design and construction of the state-of-the-art, high-resolution, $PbWO_4$ crystal and Pb glass Hybrid Calorimeter (HyCal). That detector was used in both the PrimEx-I and PrimEx-II runs. Their experience will be very important for successfully realizing FCAL-II in Hall D. In Appendix section D, we will discuss the performance of the $PbWO_4$ calorimeter in the PrimEx-I and PrimEx-II experiments. The pile-up and photon merging in a cluster reconstruction algorithm are described there as well.

### A. Impact of FCAL-II on Other Hall D Experiments

Upgrading the current FCAL with $PbWO_4$ crystals would also benefit the GlueX spectroscopy program by providing high radiation resistant material near the beamline needed for high beam intensity running ($10^8$ $\gamma$/s) as well as improving the energy and position resolutions for forward

neutral particle reconstruction. Some interesting final states for exotics searches are $3\pi$, $2\pi\omega$, and $2\pi\eta$. Since the $\pi^0$, $\eta$, and $\omega$ widths are rather narrow, and have significant branches to final states yielding photons, clear identifications of these channels will benefit from the improved resolution of the new calorimeter.

An approved experiment, E-10-011, will measure the $\eta$ radiative decay width, $\Gamma(\eta \to 2\gamma)$, via the Primakoff effect in Hall D. The total uncertainty on the radiative width is expected to be decreased from 3% to 2% if the new calorimeter is available (due to a combination of background reduction and improved angle resolution). Since all other decay widths of the $\eta$ are ultimately normalized to $\Gamma(\eta \to 2\gamma)$, this improvement will have a broad impact on $\eta$ physics.

The $\eta'$ radiative width measurement has been identified as one of the physics projects driving the Jlab 12 GeV upgrade in the past decade[79]. Development of this future experiment will definitely benefit from the high resolution, high granularity FCAL-II.

## V. TRIGGER AND DATA ACQUISITION

We will use the standard Hall D trigger and data acquisition system. The trigger will be based on a measurement of the total energy deposition in the FCAL-II calorimeter; events with the total energy less than a threshold value will be rejected.

The trigger rate as a function of the total energy threshold was studied using a Geant detector simulation. Two types of processes were considered: hadronic interactions plus the background originating from the pileup of electromagnetic interactions in the same 100 ns window. The expected trigger rates from hadronic and electromagnetic interactions for a conservative energy threshold of 5 GeV are estimated to be about 1 kHz and 2.5 kHz, respectively. This energy threshold provides 100% trigger efficiency for the signal decays under study produced at beam energies of at least 8 $GeV$.

The GlueX trigger and DAQ architecture is shown in Fig. 16. The trigger logic is imple-

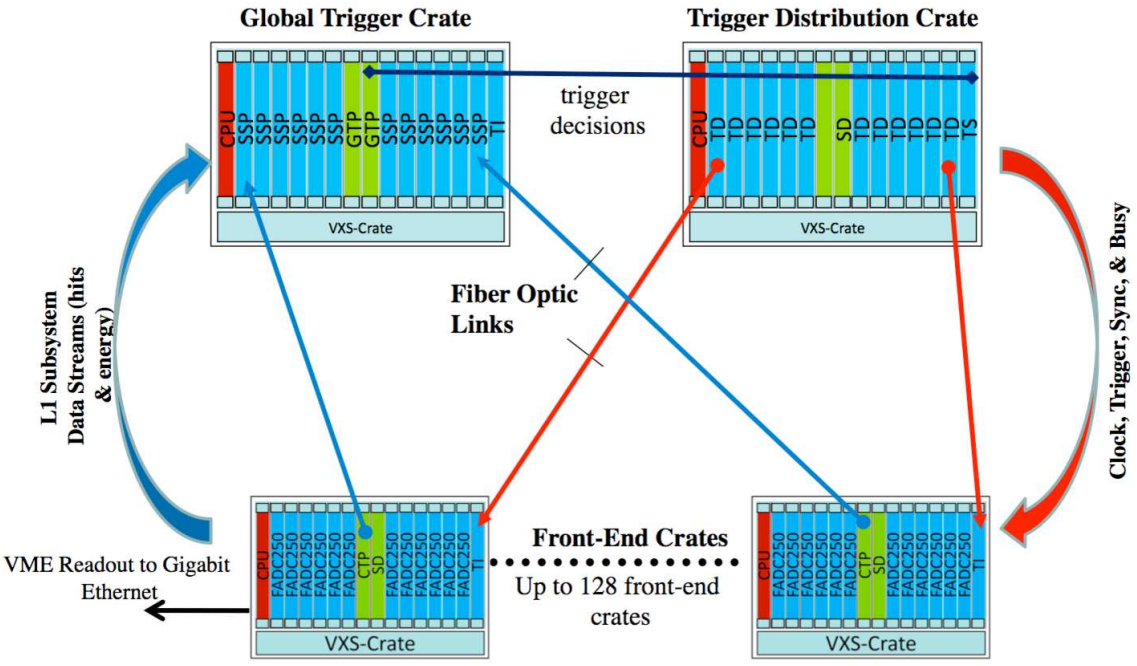


FIG. 16: Schematic of the integrated triggering and DAQ system. Fiber optics continuously stream digitized energy sum information from the CTP (crate trigger processor) module in the front-end crate to the SSP (subsystem processor module) in the Global trigger crate. Trigger decisions can then be made based on total energy sums in FCAL-II.

mented on special purpose programmable electronics boards developed at Jefferson Lab with Field-Programmable Gate Array (FPGA) chips. The electronics is based on pipelined FADC-250 boards running at a 250 MHz clock. The data from the front end calorimeter electronics is digitized and stored in the FADC-250 pipeline waiting for the readout. At the same time, energies from the 16 FADC-250 channels will be summed and forwarded to the Crate Trigger Processors (CTP) board positioned in the switch slot of the VXS crate. The CTP sums energies from all FADCs in the crate and sends the information via optical links to the Sub-System Processors (SSP). The SSP subsequently sums energies from all crates. The Global Trigger Processor (GTP) will make the trigger decision based on the total energy. When the trigger is issued, notification will be sent to the Trigger Interface board of each crate to initiate the event readout.

The algorithm running on the FADC-250 FPGA allows one to determine the time of a hit in the

calorimeter with an accuracy of better than 1 ns by 'fitting' the leading edge of the electronics pulse. The readout information of each hit is coded in two 4 byte words representing the time and the energy integral. For the expected hit multiplicity, the event size is about 0.2 kByte and the data rate is about 800 kByte/sec. As the trigger rate is relatively small, the possibility exists to read out the FADC in the so-called Pulse Integral mode, i.e., read out digitized amplitudes for several FADC 4 ns time stamps around the signal pulse threshold crossing. The mode can allow one to analyze pulses offline. As an example, reading out FADC pulse amplitudes in an 80 ns time window will require 40 bytes of data resulting in a 2 kByte calorimeter event size and a total data rate of 8 MByte/sec. The trigger and the data rates can be handled by the electronics and the DAQ system. Data readout will be performed using the JLab CODA system.

## VI. FCAL-II ACCEPTANCE AND HIGH-LEVEL RECONSTRUCTION

$\eta$ rare decay events will be reconstructed from FCAL-II information, normalizing to $\eta \to \gamma\gamma$ decays measured simultaneously. Since our goal is to measure the branching ratios, knowledge of the absolute luminosity and detection efficiency are important but not as critical as in the PrimEx program where absolute decay widths are determined. Our priorities are isolation of the signal with high efficiency while minimizing the background, specifically, optimizing the figure of merit $N_\eta \times Acceptance/\sqrt{N_{bkg}}$. To achieve this goal, one needs (1) the geometrical acceptance for each $\eta$ decay channel under study, (2) effective cut parameters and their resolutions.[7]

### A. Calorimeter Geometrical Acceptance

Geometrical acceptance for a given $\eta$ decay largely depends on the usual suspects in any solid angle: the distance between the target and FCAL-II, and the effective frontal area of FCAL-II. It decreases with increasing number of photons in the final state since there are more opportunities to lose a photon down the beam hole or (more importantly) around the outer edges of the calorimeter.

[7] For this discussion, we will assume the signal is extracted from a series of cuts rather than a single cut on a likelihood parameter.

Two flagship channels for our experiment are the $4\gamma$ final states, $\eta \to \pi^0\gamma\gamma$ and $\eta \to \pi^0\pi^0$. One of the hard-to-suppress backgrounds for rare $\eta$ decays leading to $4\gamma$'s comes from the apparent merging of photons in the calorimeter from $\eta \to 3\pi^0$. For fixed calorimeter size, as the distance between the target and calorimeter is varied, there is a trade-off between signal and the photon merging background. To optimize this distance, we employ the figure-of-merit (FOM) $FOM \equiv S/\sqrt{B}$ where $S$ is the number of $\eta \to \pi^0\gamma\gamma$ events detected, and $B$ is the number of background events from $\eta \to 3\pi^0$ within a $\pm 3\sigma$ window around the $\eta$ invariant mass. Figure 17 shows this FOM as a function of distance.

*Unless otherwise specified, all acceptances are reported for the reference design of* $118 \times 118$ $cm^2$ *at the "*$4\gamma$*" plateau near 6 m, and for the beam energy range of 9-11.7 GeV.* For $\eta$ decays into $2\gamma$, $3\gamma$, and $4\gamma$ final states, the geometrical acceptances are given by Figures 18, 19, and 20, respectively. The average acceptance is $\sim 45\%$ for $2\gamma$, $\sim 30\%$ for $3\gamma$, and $\sim 20\%$ for $4\gamma$ final states. For the larger, $150 \times 150$ cm$^2$ calorimeter, the acceptance in each case increases by 0.2 which would approximately double the $4\gamma$ acceptance.

### B. Calorimeter Resolutions in Elasticity and Invariant Mass

There are two major kinematical variables for the selection of $\eta$ decay events. The first is the elasticity—the ratio of total energy deposited in FCAL-II to the tagged photon beam energy. Resolution in elasticity depends on the calorimeter energy resolution and, to a lesser extent, the tagger energy resolution. The second variable is the particle's invariant mass reconstructed from the decay of 2 or more photons. In both cases, energy resolution is important, but for the invariant mass the angle resolution is also critical. Since no tracking is possible with photons, the photon angle is determined by the hit position on the calorimeter and the target position. The beam is transported almost entirely in vacuum so the vast majority of high energy calorimeter triggers arise from the target.

Simulations were performed assuming the proposed $PbWO_4$ crystal calorimeter and generating

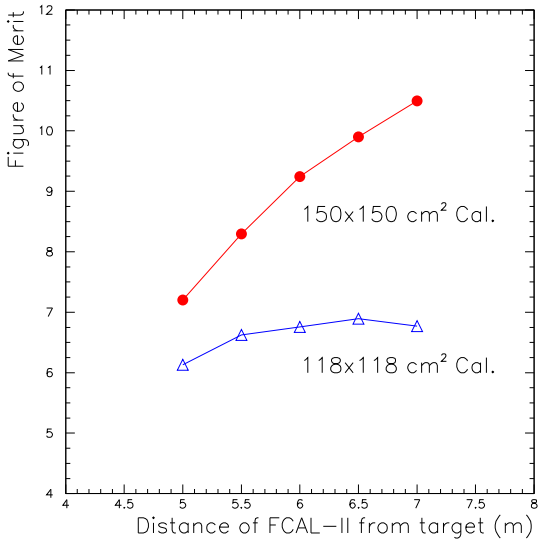


FIG. 17: The figure-of-merit $S/\sqrt{B}$ *versus* the distance between target and FCAL-II, where $S$ is the accepted $\pi^0 2\gamma$ signal and $B$ is the background from photon merging in $\eta \to 3\pi^0$ decays which have a branching ratio 3 orders of magnitude larger. The reference design of $118 \times 118\,\mathrm{cm}^2$ is plateaued near 6m.

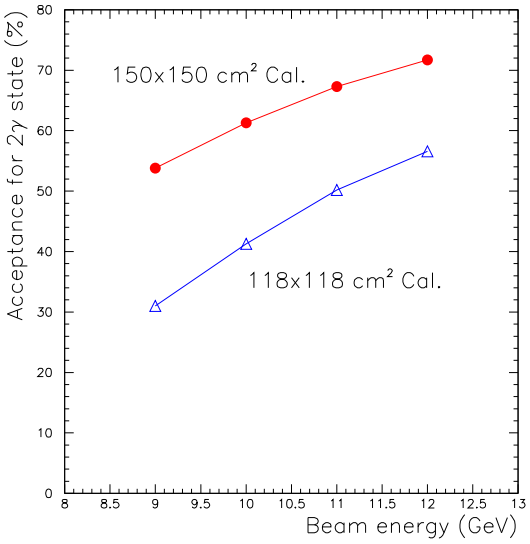


FIG. 18: The geometrical acceptance for $\eta \to \gamma\gamma$ *versus* the beam energy. This is our normalization channel.

$\gamma + p \to \eta + p$ events along the length of a 30 cm $LH_2$ target. Figure 21 shows the resolution in the elasticity variable for fully contained $\eta \to \pi^0 2\gamma$ decays. Resolutions for $2\gamma$ and $3\gamma$ final states are similar. The average peak position is slightly less than 1 due to the missing energy carried away by the proton recoil. Assuming a typical photon energy of 10 GeV, the elasticity resolution of 1.2% corresponds to a missing energy sensitivity of 120 MeV. This cut virtually ensures the forward neutral meson production (be it a $\pi^0$, $\eta$, $\eta$', $\phi$, etc.) was exclusive even without recoil proton detection. It is barely possible for a very soft additional $\pi^0$ to slip past this cut, but the resulting extra photons would have little or no acceptance in FCAL-II while having good acceptance in BCAL, and would be below the energy threshold for shower reconstruction in FCAL-II in any case.

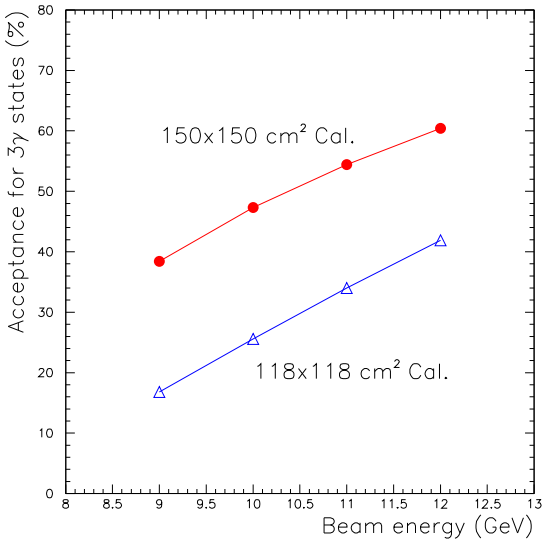


FIG. 19: The geometrical acceptance for the $3\gamma$ states ($\eta \to 3\gamma$ or $\eta \to \pi^0\gamma$) *versus* the beam energy. These are the channels used to search for new sources of C violation.

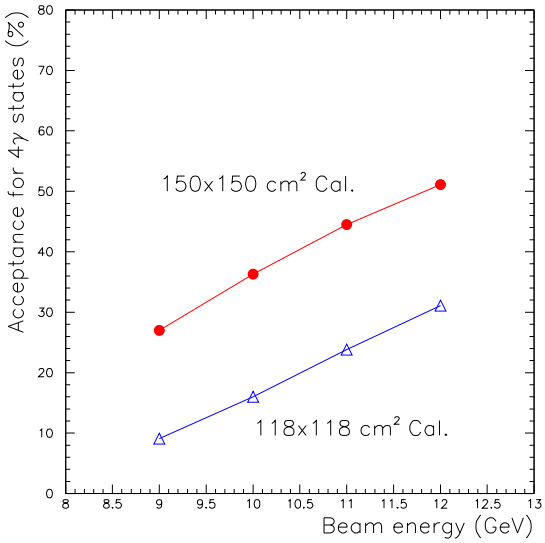


FIG. 20: The geometrical acceptance for the $4\gamma$ states ($\eta \to \pi^0\gamma\gamma$ or $\eta \to \pi^0\pi^0$) *versus* the beam energy. This is the channel used to search for new sources of P and CP violation.

The resolution in invariant mass arises from several factors: (1) the photon beam spot size on the target, (2) the uncertainty of the reaction vertex along the target length if the recoil proton is not detected (as in the simulations presented here), (3) the energy and position resolutions of FCAL-II, and (4) the energy of the photons detected by the calorimeter. The size of the beam spot is directly correlated with the size of the primary collimator in the beam line. For illustration, Figure 22 shows the beam spot $x$ (transverse) projection on the target for a 5 mm diameter primary collimator. In order to simulate the invariant mass resolutions, we have taken into account the beam spot size with a 5 mm diameter primary collimator, a 30 cm thick $LH_2$ target, 6 m distance between the FCAL-II and the target, and a photon beam in the energy range of 9-11.7 GeV. Because the recoil proton was not required in this early simulation, reconstruction assumed all events arose from the target center.

The reconstructed $\eta$ invariant mass resolution for the $\eta \to \pi^0\gamma\gamma$ reactions is shown in Figure 23. Resolutions for $2\gamma$ and $3\gamma$ final states are similar. Despite the high photon energy, the average rms

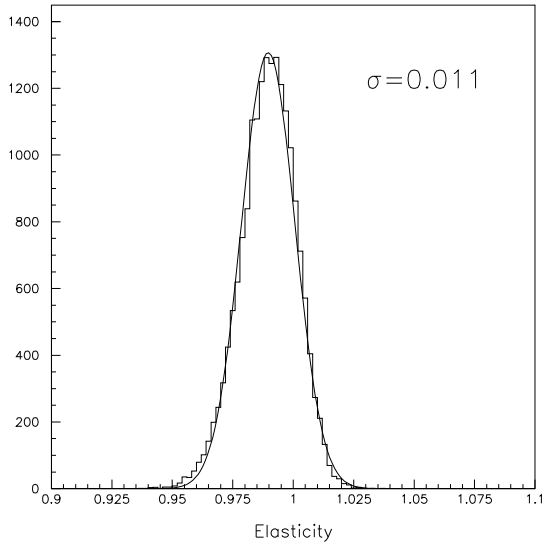


FIG. 21: Elasticity for $\eta \to \pi^0\gamma\gamma$. The resolutions for $\eta \to 2\gamma$ and $\eta \to 3\gamma$ are similar, 1.3% and 1.2%, respectively.

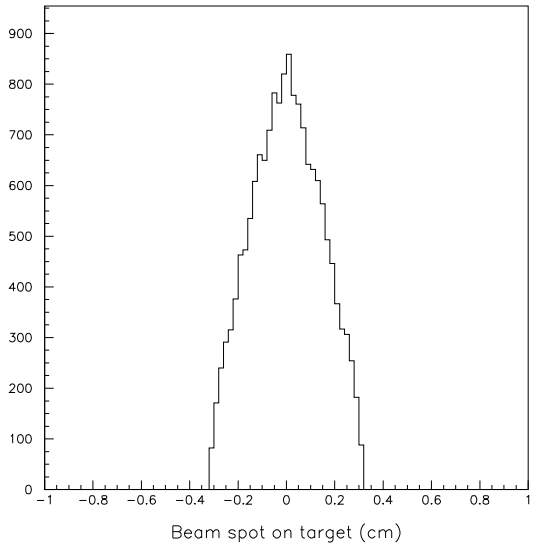


FIG. 22: The $x$ (transverse) distribution of the interaction vertices in the target for a 5 mm diameter primary collimator. The rms width of less than 0.2cm makes a much smaller contribution to the invariant mass resolution than does the calorimeter energy resolution.

resolution of 11 MeV is only 2% of the $\eta$ mass. This is our most important cut to select $\eta$ decay signals while suppressing continuum backgrounds. It will also be used to identify $\pi^0$'s, $\phi$'s, etc., for calibration as well as physics initiatives beyond the scope of this proposal.

Figure 24 shows that the invariant mass resolution of the $\pi^0$ from the $\eta \to \pi^0\gamma\gamma$ reaction is 3.8 MeV. The importance of the $\pi^0$ resolution will be discussed in the next section on event selection. We note that the resolution can be improved an additional 35% using kinematical fits [77][78].

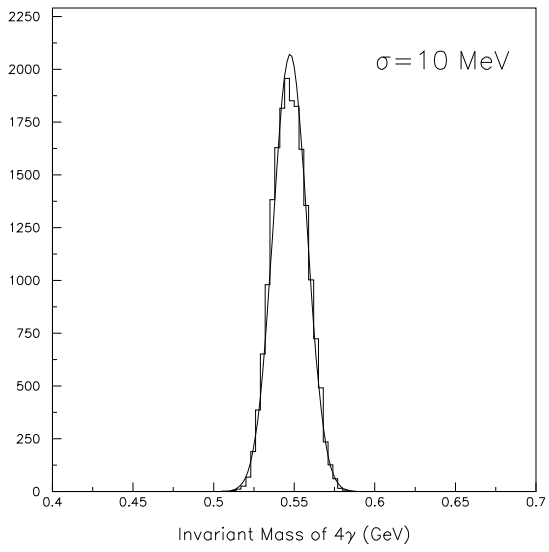


FIG. 23: Reconstructed invariant mass $M_{4\gamma}$ from the $\eta \to \pi^0\gamma\gamma$ reaction. The resolution for $2\gamma$ and $3\gamma$ final states is similar, 12 MeV and 11 MeV, respectively.

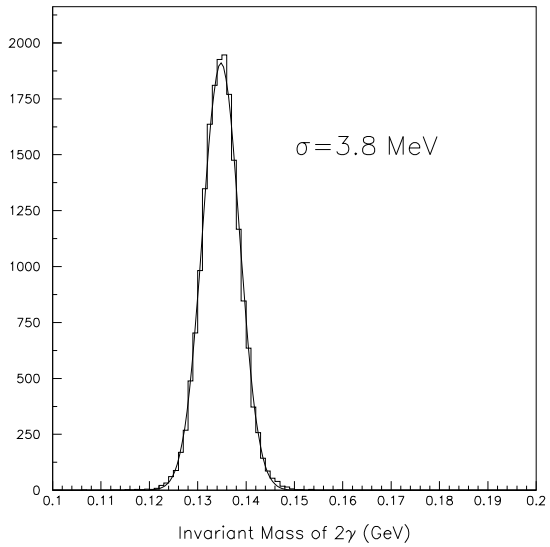


FIG. 24: Reconstructed invariant mass $M_{2\gamma}$ of the $\pi^0$ from the $\eta \to \pi^0\gamma\gamma$ reaction.

### C. Basic Event Selection

Event selection begins at the trigger level. For 9-11.7 GeV photon beam proposed in this proposal, Figure 25 shows the distribution of the energy deposited in FCAL-II from the exclusive reaction $\gamma p \to \eta p$, followed by $\eta \to \pi^0\gamma\gamma$. Plots for $\eta \to 2\gamma$ and $\eta \to 3\gamma$ (not shown) look very similar. Figure 26 shows the total energy spectrum in FCAL-II for one of the major inelastic reactions, $\gamma p \to \eta\pi^0 p$. As one can see, for the beam energy in 9–11.7 GeV range, an FCAL-II threshold of about 8 GeV would safely select all signal events while suppressing triggers from inclusive production or accidental beam related background. The elasticity cut mentioned below effectively performs a more detailed comparison of tagged photon energy and total calorimeter energy.

In the offline analysis, we will apply the following basic event selection criteria for tagged photon

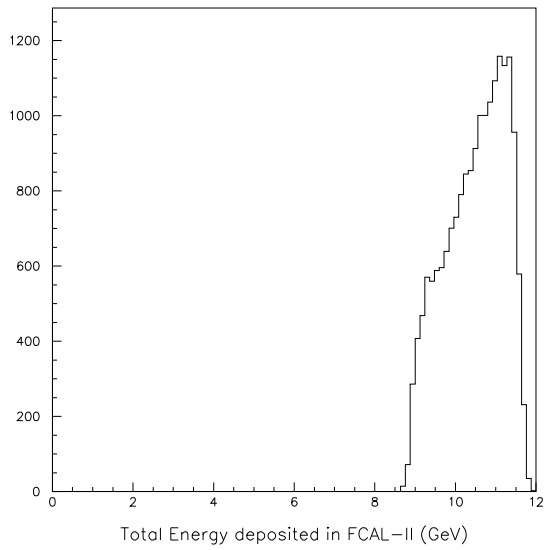


FIG. 25: Reconstructed total energy deposited in FCAL-II by $\eta \to \pi^0\gamma\gamma$. Nearly all events of interest deposit more than 8.5 GeV in the calorimeter (modulo the energy resolution, this is simply explained by the minimum photon beam energy of 9 GeV less the sum of the $\eta$ mass and proton recoil energy).

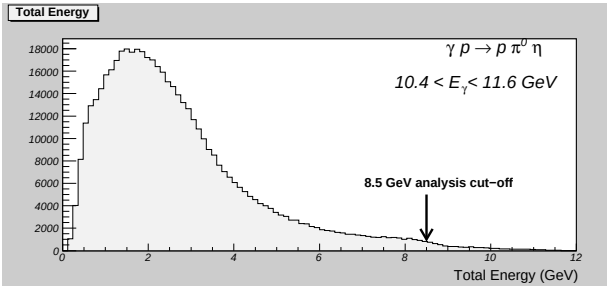


FIG. 26: Total energy deposited in FCAL-II by inelastic $\eta$ production through the $\gamma p \to \eta\pi^0 p$ reaction.

energies of 9-11.7 GeV: (0) single hit in the tagger for 9-11.7 GeV; (1) fiducial volume of FCAL-II for full shower containment (i.e., excluding the inner and outermost layers of crystals); (2) every shower in a candidate neutral meson must have good coincidence time with the tagger paddle that was hit (out of time showers must be dropped and the total energy recalculated); (3) there should be no significant missing energy based on the photon energy for this tagger paddle (the elasticity cut); (4) the invariant mass reconstructed from the decay photons in the principle shower must be consistent with the $\eta$ mass.

In this proposal, we only utilize exclusively produced $\eta$'s via the two-body $\gamma p \to \eta p$ reaction. Once an $\eta$ has passed our elasticity cut, the detection of the recoil proton is in principle redundant. However, simulations have shown it will increase our sensitivity to be able to over-determine the kinematics. While a small amount of continuum $\gamma p \to 2\pi^0 p$ will obviously pass the basic cuts, so

could an accidental coincidence between a tagged $\eta \rightarrow 2\gamma$ decay and $\pi^0$ production by an untagged low energy photon. Either of these backgrounds would be suppressed by additional cuts using proton information, hence: (5) there must be a single recoil proton, and (6) the recoil proton and $\eta$ must be co-planar.

As one can see from the top two panels of Figure 27, the recoil protons of interest have polar angles of 55-80 degrees and momenta of 0.2-1.4 GeV/c. Tracking is not possible for recoil protons from the smallest angle $\eta$'s because those protons either range out before reaching the CDC or don't produce enough hits in the CDC for reconstruction. From Figure 28, one sees the tracking efficiency is about 70% for recoil proton momenta above 0.325 GeV/c (55 MeV). These recoil protons account for over 80% of $\eta$'s reconstructed by FCAL-II for $3\gamma$ and $4\gamma$ final states. At lower proton momenta, reconstruction efficiency has dropped by half by 0.275 GeV/c (39 MeV) which is reasonably well understood in terms of the thickness of target and detector materials. (The range of a 39 MeV proton is about 1.3 $g/cm^2$ of $CH_2$-equivalent.)

Because recoil protons are ejected at similar, large angles for all neutral meson masses, there is much error magnification in reconstructing the neutral meson missing mass from proton information. Nevertheless, we tried this and were pleasantly surprised to get the result in Figure 29 with missing mass resolution of roughly 100 MeV which is sufficient to usually distinguish between $\pi^0$ and $\eta$ production. This would already be of some benefit to a likelihood distribution, but a more powerful proton cut variable appears to be the coplananarity cut (i.e., the difference of the azimuthal angles of the $\eta$ and the proton).

Once an $\eta$ decay has been identified, it will be sorted into categories: $\eta \rightarrow 2\gamma$ (normalization), $\eta \rightarrow$ "$3\gamma$", or $\eta \rightarrow$ "$4\gamma$". Although our $\eta \rightarrow$ "$4\gamma$" dataset will be dominated by $\pi^0 2\gamma$ plus a modest background, our physics goals require that we search for 3 signals: $\pi^0 2\gamma$, $2\pi^0$, and $4\gamma$ (only one $\pi^0$, two $\pi^0$'s, and no $\pi^0$'s). Since all 6 combinations of 2 photons must be tried, there are 6 opportunities for uncorrelated photons to mimic a $\pi^0$, thus the excellent resolution in $\pi^0$ invariant mass demonstrated in the previous section is important for high sensitivity.

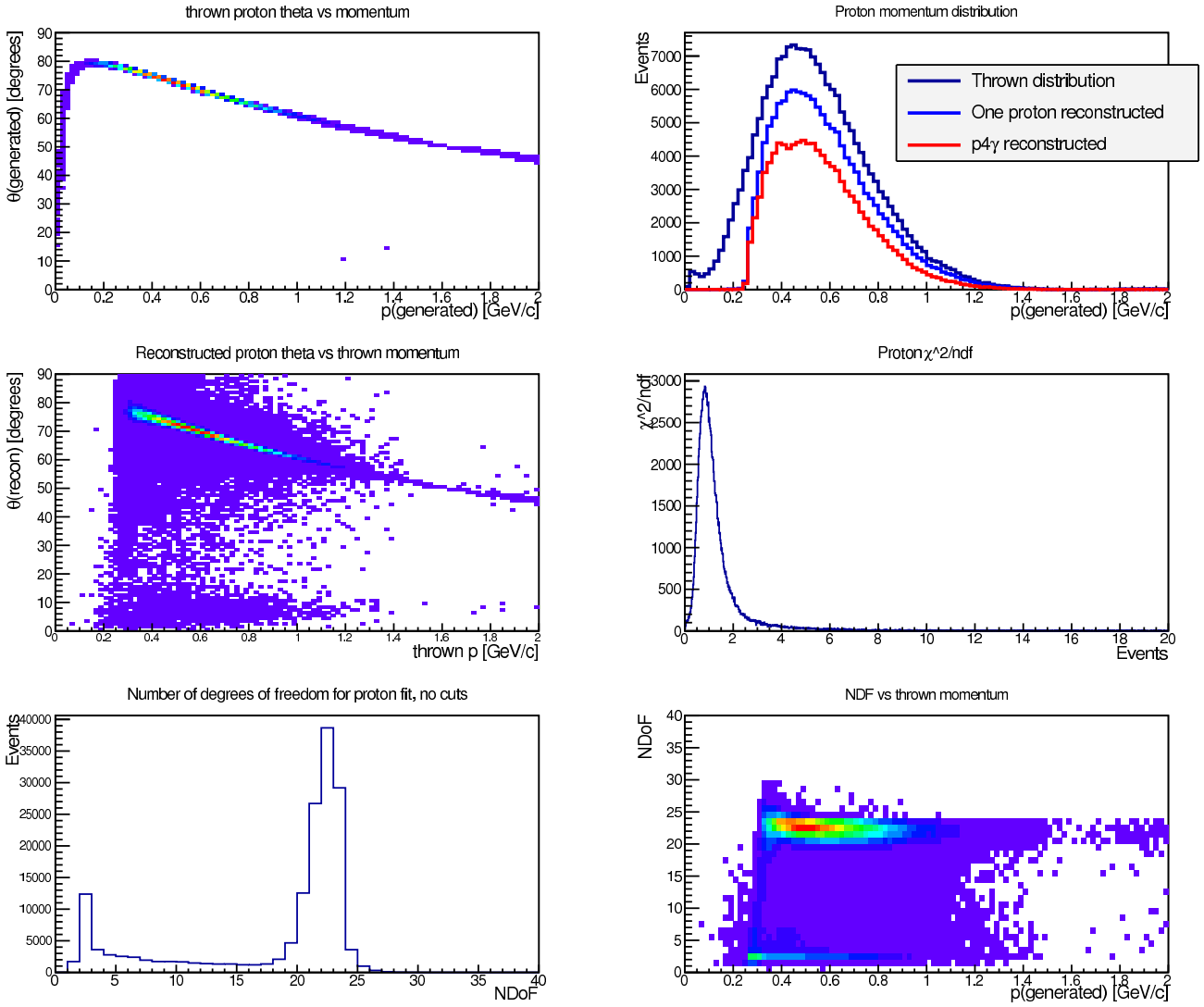


FIG. 27: Monte Carlo simulation for track reconstruction of recoil protons by GlueX detector. Top-left: polar angle vs proton momentum for the thrown distribution; The majority of recoil protons are ejected near 75 degrees, passing through several cm of $LH_2$ and the target walls, the start counter, and into the CDC. Top-right: momentum distribution of recoil protons; Middle-left: reconstructed polar angle vs proton momentum; Middle-right: Chi-squared per number of degrees of freedom (NDF) distribution; Bottom-left: NDF distribution; Bottom-right: NDF vs proton momentum.

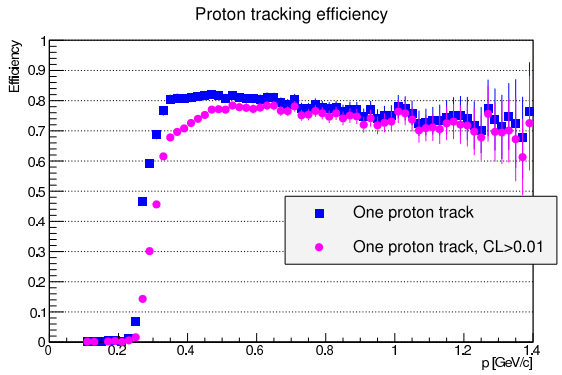


FIG. 28: The reconstruction efficiency for recoil protons. Above 0.325 GeV/c, the inefficiency is due to the reconstruction finding more than one track. Such events may be recoverable.

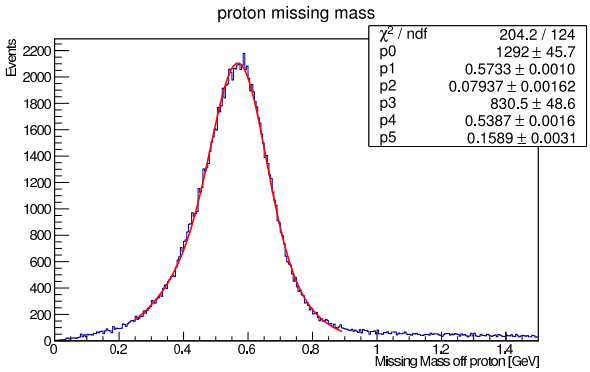


FIG. 29: Reconstructed missing mass using the recoil proton from the $\gamma p \to \eta p$ reaction.

## VII. MAJOR NEW EXPERIMENTAL EQUIPMENT (COST, MANPOWER AND FINANCIAL RESOURCES, AND COMMITMENTS)

Besides the Hall D base equipment, this proposal requires a major upgrade of the current FCAL to include high-resolution, high-granularity $PbWO_4$ crystals. An option which would preserve the large acceptance needed for the GlueX spectroscopy program, allow it to benefit from the better properties of lead tungstate, and minimize overhead in configuration changes, is to insert the $118 \times 118$ cm$^2$ $PbWO_4$ crystals into the present Pb glass FCAL. This would make it a hybrid calorimeter, similar to a larger version of the state-of-art, high-resolution PrimEx calorimeter (HyCal) used in Hall B. Several institutions on this proposal were major players in the design and construction of HyCal and would play a leading role in developing the future FCAL-II. Previously, we successfully obtained the resources necessary to develop and construct HyCal from the NSF Major Research Instrumentation (MRI) program while establishing collaborations with Chinese institutions. The same strategy would be applied to the FCAL-II development.

The estimated total cost for 3445 $PbWO_4$ modules, including the crystal, PMT/base, flash ADC and HV is \$2.7M-\$4.6M depending on the assumptions for recycling existing equipment (see attached document on "Response to PAC39 Issues and Recommendations" for details). Prof. X.

Chen, a co-spokesperson on this proposal, will lead several Chinese institutes in applying for funds($0.5M-$1.0M) from the Chinese National Science Foundation to cover the cost of the crystals. Prof. L. Gan (spokesperson of this proposal) will lead the US institutes in applying for a Major Research Instrumentation program (MRI) grant from the National Science Foundation ($1.0M-$3.5M) to cover the cost of PMT's, bases, possibly the Flash ADCs, plus small ancillary detectors. Two other co-spokespersons are JLab staff members and will help coordinate design and construction.

To characterize the calorimeter, we will need a stand with vertical and horizontal motion capability so that any point on the front face can be moved into the photon beam. Since the new calorimeter may be incorporated into Hall D base equipment at the disgression of Hall D management, we would like the power supplies, cabling, possibly the Flash ADCs, and other readout support to come from JLab. It is likely we will need design and engineering support for additional small detectors (e.g., cosmic tag, beam hole tag, etc.), as well as support from the Physics Division electronics group in designing low power PMT bases.

This experiment has the potential to add significant new manpower to the Hall-D effort, in particular from groups that have historically had little activity at Jefferson Lab. During the detector development and construction period, the Chinese team will be responsible for procuring and testing the $PbWO_4$ crystals. The US team will be responsible for the procuring and testing of the electronics. Several local universities near Jlab will play a major role in the detector assembly and testing.

## VIII. $\eta$ PRODUCTION RATE, SENSITIVITY, AND BEAM REQUEST

The sensitivity of the experiment depends on the number of exclusively produced $\eta$'s, the fraction of decays which are accepted by the calorimeter, and the efficiency including the live time and losses due to cuts. We will address each of these issues in turn in the following subsections.

## A. $\eta$ Production Rate by Forward $\gamma + p \rightarrow \eta + p$

We have chosen an electron beam current of 0.4 $\mu$A with a Au radiator of thickness $2 \times 10^{-4}$ radiation lengths to provide a luminosity comparable to the successful PrimEx program in Hall B.[8] Under these conditions, the so-called equivalent $\gamma$ rate over a wide range of energy is $\sim 5.0 \times 10^8$ Hz, or $\sim 50$ MHz/GeV, three times less than the tagger design limit of 150 MHz/GeV. All photons are transported in vacuum. Using a 5 mm diameter primary collimator, $\sim 30\%$ of the $\gamma$'s will reach the physics target, yielding a total $\gamma$ rate at that location of $1.5 \times 10^8$ Hz. In the 9.0–11.7 GeV photon energy range required for significant $\eta$ cross sections and boost, the tagger focal plane provides 100% efficiency for tagging these photons in 30 MeV wide energy bins [62]. The tagged $\gamma$ rate on the target will therefore be:

$$\begin{aligned} N_\gamma &= 1.5 \times 10^8 \times \ln(11.7 GeV / 9.0 GeV) \\ &\sim 4 \times 10^7 \text{ Hz} \end{aligned}$$

We will use the standard Hall D $LH_2$ target. It is 30 cm thick (3.46% R.L.), hence the number of proton's in the target is:

$$N_p = 1.28 \times 10^{24} \text{ protons/cm}^2$$

From reference [76], the average total cross section for $\gamma p \rightarrow \eta p$ in the 9 to 11.7 GeV photon energy range is $\sim 70$ nb. The total rate of exclusively produced $\eta$'s by the exclusive channel $\gamma + p \rightarrow \eta + p$ is therefore:

$$\begin{aligned} N_\eta &= N_\gamma \cdot N_p \cdot \sigma \\ &= 4 \times 10^7 \cdot 1.28 \times 10^{24} \cdot 70 \times 10^{-33} \\ &\sim 3.6 \text{ Hz (or } 3.1 \times 10^5 / day \text{ or } 3.1 \times 10^7 / 100 \text{ } days \text{ )} \end{aligned}$$

Anticipating the detector acceptance results from the next section, the number of *effective* $\eta$'s ($N_\eta \times Acceptance$) will still be O($10^7$) per year of JLab accelerator operations, several times the effective production rate of KLOE-I in its prime (using $\phi \rightarrow \eta + \gamma$), and an order of magnitude

[8] The Hall D dump can easily handle 2.2 $\mu$A.

better than BES-III (using $J/\psi \rightarrow \eta + \gamma$).[46] This is the basis for our calling Hall D with FCAL-II an "$\eta$ factory".

### B. Detection Rates, Errors, and Sensitivities

Our reference design assumes that the transverse dimension of FCAL-II are $118 \times 118$ cm$^2$ and that it is located at 6 m downstream of the target center. The detected rate of an $\eta$ decay depends on the number of $\gamma$'s in the final state. We will use copious $\eta \rightarrow \gamma\gamma$ decays to normalize all other rare $\eta$ decay channels (BR = $39.43 \pm 0.26\%$ [15]). The acceptance for this channel is $\sim 45\%$ thus the $\eta \rightarrow \gamma\gamma$ detection rate will be:

$$N_{\eta\rightarrow\gamma\gamma} = 3.1 \times 10^5/day \times 0.3943 \times 0.45$$
$$\sim 5.5 \times 10^4/day$$

providing a statistical error on the normalization of less than 1% per day.

#### *1.* $\eta \rightarrow \pi^0\gamma\gamma$

The rare decay $\eta \rightarrow \pi^0\gamma\gamma$ has a branching ratio of $2.7 \times 10^{-4}$ [15], bearing in mind that this is the average of several widely inconsistent measurements. Assuming the $4\gamma$ final state follows phase space, the experimental acceptance is $\sim 20\%$ hence the actual detection rate for $\eta \rightarrow \pi^0\gamma\gamma$ will be:

$$N_{\eta\rightarrow\pi^0\gamma\gamma} = 3.1 \times 10^5/day \times 2.7 \times 10^{-4} \times 0.20$$
$$\sim 16.7/\text{day or } 1670/100 \text{ days}$$

With this many events the error on the $\eta \rightarrow \pi^0 2\gamma$ branching ratio, including statistical and normalization errors, plus background subtraction will be less than 5%.

As for the differential branching ratio, $d\Gamma/dM_{2\gamma}$, the S/B ratio will be 3:1 as suggested by Figure 11 before additional cuts. The statistical error in each of 8 bins of $d\Gamma/dM_{\gamma\gamma}$ would be

$$\frac{\Delta S}{S} = \frac{\sqrt{S+2B}}{S} = \frac{\sqrt{209+2(209/3)}}{209} = 9\% \tag{11}$$

Note that, for a fixed number of signal events, larger backgrounds result in larger final errors. In our case, the expected error magnification from the naive relative error of $1/\sqrt{S}$ is only about 33%,

but in the Crystal Ball data in Figure 7 the error magnification must have been several hundred percent.

In Figure 30, our projected errors have been overlaid on a plot adapted from reference [22] based on the calculations by Ng and Peters.[80] Although the $\eta \to \pi^0 2\gamma$ branch requires that one pair of gammas have $M_{2\gamma} = M_\pi$, it is likely that we'll lose the bin corresponding to a second pair of gammas having $M_{2\gamma}$ near $M_\pi$ due to the $2\pi^0$ continuum background. This has been assumed in the figure. It is clear that the projected uncertainties would allow one to disentangle dynamical questions such as whether the dominant expected amplitudes interfere constructively or destructively. Even more clear is that there would be no more factor of 2 ambiguities in the total BR!

### *2.* $\eta \to \pi^0\pi^0$

The acceptance of the P and CP forbidden $\eta \to \pi^0\pi^0$ is $\sim 20\%$. Table IV contains nominal signal rates under various branching ratio assumptions. The rare decay $\pi^0 2\gamma$ is now a background in the $4\gamma$ final state but is suppressed by cutting all events that are not consistent with two $\pi^0$'s. At that point the remaining background will be dominated by the $2\pi^0$ continuum. According to our simulation, the background fraction in our $\eta$ invariant mass signal window is $\sim 4 \times 10^{-5}$. The estimated BR upper limit will be:

$$BR(\eta \to 2\pi^0) \leq 2 \times \sqrt{\frac{f_{bkg}}{N_\eta * Acceptance}} = 2 \times \sqrt{\frac{4 \times 10^{-5}}{3.1 \times 10^7 \times 0.2}} \sim 5 \times 10^{-6} \qquad (12)$$

This is more than 1.5 orders of magnitude better than the existing upper limit for the neutral channel $\eta \to 2\pi^0$, bringing the sensitivity in this channel down to the level of the KLOE $\eta \to \pi^+\pi-$ result.

### *3.* $\eta \to 3\gamma$

We haven't studied these backgrounds as carefully as the $4\gamma$ case, but can make inferences from a previous experiment. As discussed earlier in sub-section I C 3, the dominant background in the

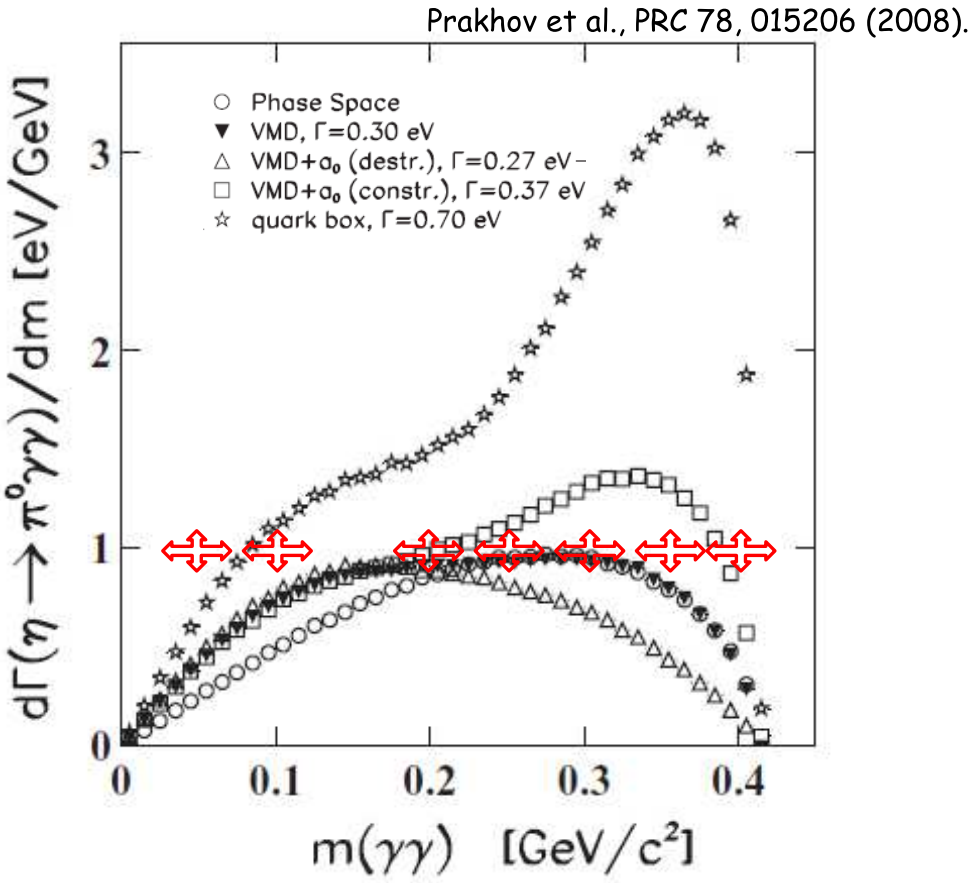


FIG. 30: Our error projections (red bars) for $\eta \to \pi^0 2\gamma$ compared to calculations by Ng and Peters.[80] The figure was adapted from reference [22].

Crystal Ball experiment at BNL was found to be continuum $2\pi^0$ production followed by the loss or merging of photons to yield an apparent "$3\gamma$" final state. In our setup, photon loss will not dominate for two reasons: First of all, our use of boosted $\eta$'s means that events with invariant mass $M_{2\pi^0} = M_\eta$ that lose a photon will fall out of the signal window for reconstructed invariant mass. Secondly, although events with invariant mass $M_{2\pi^0} > M_\eta$ could lose a photon and fall *into* the $\eta$ invariant mass window, these will be removed by the elasticity cut. We therefore expect our dominant background to arise from $2\pi^0$ continuum with $M_{2\pi^0} = M_\eta$ followed by photon merging.

To estimate this $3\gamma$ background, we need the number of continuum $2\pi^0$ events in the signal window

TABLE IV: The nominal signal rate for the P and CP forbidden $\eta \to \pi^0\pi^0$ with different branching ratio assumptions. The branching ratio in the first line is the present best upper limit[15].

| **Branching Ratio** | **Nominal Rate at BR (events/100 days)** |
|---|---|
| $3.5 \times 10^{-4}$ | 2200 |
| $10^{-5}$ | 62 |
| $10^{-6}$ | 6 |

and the probability that 4 showers will merge into 3. The first step in the analysis will be to remove all $\pi^0 2\gamma$ events by throwing out all events where a pair of photons reconstructs to a $\pi^0$. From the previous section we know this will leave us with a $2\pi^0$ "source term" of about 560 events without employing recoil proton cuts. The merging probability is very small as can be inferred from the peaking background in our $4\gamma$ study in Figure 8. That figure shows us that only $10^{-5}$ of $\eta \to 3\pi^0$ events will undergo 2 mergers yielding 4 reconstructed showers. An upper bound on the probability for a single merger in the $4\gamma \to 3\gamma$ case at hand is therefore $\sqrt{10^{-5}} = 0.3\%$. An upper bound on the $3\gamma$ background due to the merging of $2\pi^0$ continuum events is therefore 560 events x 0.003 = 2 events.

Other potential backgrounds arise from either photon splitting[9] or pile up of $\eta \to 2\gamma$ events. Obviously one can throw away all $3\gamma$ candidates with close pairs, or where one of the photons is very low energy and/or near the beam hole hence more likely to be piled up. These backgrounds are easily suppressed but the acceptance will be reduced. To make a somewhat conservative estimate of our sensitivity, we increase the number of background events from 2 to 10, while assuming the effective number of $\eta$'s is reduced an additional factor of 2 by cuts, giving

$$BR(\eta \to 3\gamma) \leq 2 \times \frac{\sqrt{N_{bkg}}}{N_\eta * Acceptance} = 2 \times \frac{\sqrt{10}}{3.1 \times 10^7/2 \times 0.3} = 1.4 \times 10^{-6} \qquad (13)$$

which would be an order of magnitude better than the existing best result, 1.6x10$^{-5}$. Table V has been made for the C forbidden $\eta \to 3\gamma$ processes.

[9] Photon splitting is where a shower is initiated by a single photon but reconstructs as a close pair.

| Branching Ratio | Nominal Rate at BR (events/100 days) |
|---|---|
| $10^{-4}$ | 900 |
| $10^{-5}$ | 90 |
| $10^{-6}$ | 9 |

TABLE V: The nominal signal rate for either C forbidden reaction leading to 3 photons in the final state for different assumptions about the branching ratio. The current BR upper limit for $\eta \to 3\gamma$ is $1.6 \times 10^{-4}$.

*4.* $\eta \to 3\pi^0$

Since $\eta \to 3\pi^0$ (BR = 32.6%) is the largest background channel for our rare decay measurements, the experimental configuration is not designed to optimize the acceptance for this channel. According to our simulation, however, we still have about 7.3% acceptance in the experiment. The event detection rate will be:

$$N_{\eta\to 3\pi^0} = 3.1 \times 10^5/day \times 33 \times 10^{-2} \times 0.073$$
$$\sim 7{,}468/\text{day or } 746{,}800/100 \text{ days}$$

### C. Beam Time Request

We request 100 days of beam time on the $LH_2$ target, plus commissioning and overhead as outlined below. This will provide about 1670 actual $\eta \to \pi^0\gamma\gamma$ events, sufficient statistics to precisely measure the Dalitz plot of the $2\gamma$ invariant mass. In addition, we'll improve the upper limit on several SM forbidden channels by 1-1.5 orders of magnitude depending on the channel.

A summary of the requested beam time, specified for each major activity, is shown in Table VI. To understand backgrounds from the target windows and beamline sources such as the collimators (quasi-elastic protons, high energy neutrons, etc.) we need 7 days for both empty target and target-out runs. We will measure the tagging efficency with the Total Absorption Counter and the pair-spectrometer several times. This will be interspersed with production and requires minimal

TABLE VI: Beam time request.

| | |
|---|---|
| $LH_2$ production | 100 days |
| Empty target and target-out runs | 7 days |
| Tagger efficiency, TAC runs | 3 days |
| FCAL-II commissioning, calibration, and checkout | 12 days |
| Luminosity optimization (pile-up, accidentals studies) | 14 days |
| Total | 136 days |

configuration changes, hence only 3 days are budgeted. Based on our experience from the first PrimEx experiment in Hall B, we need 12 days for commissioning, calibration, and general checkout of FCAL-II with beam. The majority of this time will be used for the gain calibration and trigger setup including threshold adjustment. To be able to achieve the greatest possible sensitivity in 100 days of production, we further require 14 days to find the luminosity that optimizes our figure of merit $N_\eta * Acceptance * Efficiency/\sqrt{N_{bkg}}$.

This request is for dedicated beam time. During the GlueX running period, we will parasitically take data in the beam energy range 9.0-11.7 GeV. It will provide a rich data set to study backgrounds such as $\gamma p \to \pi^0\pi^0 p$ at these high photon beam energies. The standard GlueX configuration however is incompatible with the background suppression required for $\eta$ rare decay decay measurements. The augmented GlueX configuration (ie, FCAL-II with a lead tungstate core) has modest incompatabilities such as photon tagging efficiency (30% in JEF vs. 15% in GlueX) and a different distance between the target and calorimeter (6m in JEF versus 5.6m in GlueX), but *major* incompatabilities in the form of the JEF trigger (8 GeV threshold in FCAL-II) as well as larger JEF event sizes for offline pile-up analysis.

## IX. SUMMARY

The availability of significantly boosted $\eta$'s in Hall D, and the planned lead tungstate calorimeter with flash ADC readout on every channel will improve the signal to background ratio for channels with 3-5 photons in the final state by up to 2 orders of magnitude. We therefore expect to make revolutionary improvements to the dataset for $\eta$ rare decays with 3-5 photons which have historically suffered from tremendous backgrounds. This includes our priority channels $\eta \to \pi^0 2\gamma, 2\pi^0, 3\gamma$ as well as our $\eta \to \pi^0\gamma$ control. In parallel, the large new dataset of $\eta \to 3\pi^0$ we obtain will not only constrain backgrounds for the rare decay channels, but may yield an important new extraction of the $m_d - m_u$ quark mass with different systematics than published results. Significant improvements can also be expected in ancillary channels such as the 4 photon $\eta \to 4\gamma$ (allowed but highly suppressed in the SM) and the 5 photon channel $\eta \to 2\pi^0\gamma$ (C violating). These measurements will allow us to address issues of chiral perturbation theory at high order while searching for new sources of C, P, and CP violation in the non-weak decays of the best meson candidate for such studies.

We estimate Hall D can produce $3\times10^7$ $\eta$'s in 100 days in the forward, exclusive channel $\gamma+p \to \eta+p$ alone. Folding in the calorimeter acceptance of about 0.25, the effective number of $\eta$'s meets or exceeds that of published datasets of the last decade by a factor of several.

## APPENDIX A: SELECTION RULES FOR ALL-NEUTRAL $\eta$ DECAYS

The relevant masses and quantum numbers are given in Table VII. The results for different numbers of $\gamma$'s and $\pi^0$'s in the final state are summarized in Table VIII. Because only neutral particles can be states of good C, any selection rules derived below assuming C conservation do not generally apply to $\pi^{\pm}$.

TABLE VII: Mass and quantum numbers for the $\eta$, $\pi^0$, and $\gamma$.

| Particle | Mass $(GeV/c)^2$ | I | G | J | P | C |
|---|---|---|---|---|---|---|
| $\eta$ | 547.9 | 0 | +1 | 0 | -1 | +1 |
| $\pi^0$ | 135.0 | 1 | -1 | 0 | -1 | +1 |
| $\gamma$ | 0.0 | 0,1 | – | 1 | -1 | -1 |

### 1. $\eta \to N\pi$

In this section we examine the selection rules for $\eta \to N\pi$ and explain why $\eta \to 3\pi$ is a major branch while the unobserved $\eta \to 2\pi$ would be both P and CP violating.

Momentum and energy conservation allow $\eta \to N\pi$ for N = 2, 3, and 4 only. Compared to the $\eta \to 2\pi^0$ case which has similar selection rules, the decay $\eta \to 4\pi^0$ is highly suppressed by phase space (the Q value would be only 7.9 MeV) and, with 8 $\gamma$'s in the final state, the detection efficiency is relatively low. Nefkens and Price[9] have nevertheless advocated the use of this channel due to relatively low backgrounds. While the $4\pi^0$ case will be one of the ancillary rare decay channels searched for in this experiment, we will not discuss it in detail because our initial background simulations were done for 3 and 4 photon final states.

G-parity, approximately conserved only by the strong interaction, would require that $G_\eta = G_{N\pi}$ or $+1 = (-1)^N$ which is true only for even N.

TABLE VIII: $\eta$ decays to $\pi^0$'s and $\gamma$'s. Branching ratios of observed states are given. Upper limits are quoted at 90% confidence level. Final states conserve C, P, and CP unless otherwise noted. (CV means "charge symmetry violating" while "PV" means "parity violating".) The $2\pi^0$ or $4\pi^0$ final states would conserve C but violate P, CP. Final states with odd numbers of $\gamma$'s would violate C, however, for $3\gamma$ both parity conserving and violating final states are possible.

| | $0\pi^0$ | $1\pi^0$ | $2\pi^0$ | $3\pi^0$ | $4\pi^0$ |
|---|---|---|---|---|---|
| $0\gamma$ | – | – | PV, CPV<br>$< 3.5 \cdot 10^{-4}$ | allowed<br>32.6% | PV, CPV<br>$< 6.9 \cdot 10^{-7}$ |
| $1\gamma$ | – | CV,CPV<br>$< 9 \cdot 10^{-5}$ | CV<br>$< 5 \cdot 10^{-4}$ | CV,CPV<br>$< 6 \cdot 10^{-5}$ | CV<br>unknown |
| $2\gamma$ | allowed<br>39.3% | allowed<br>$2.7 \cdot 10^{-4}$ | allowed<br>$< 1.2 \cdot 10^{-3}$ | allowed<br>unknown | allowed<br>unknown |
| $3\gamma$ | CV<br>$< 1.6 \cdot 10^{-5}$ | CV<br>unknown | CV<br>unknown | CV<br>unknown | CV<br>unknown |
| $4\gamma$ | allowed<br>$< 2.8 \cdot 10^{-4}$ | allowed<br>unknown | allowed<br>unknown | allowed<br>unknown | allowed<br>unknown |

Parity conservation, which in the Standard Model is generally assumed to be conserved by the strong and electromagnetic interactions and violated only by the weak interaction, would require that $P_\eta = P_{N\pi} = P_\pi^N(-1)^L$ or $-1 = (-1)^N(-1)^L$. Because the $\eta$ and $\pi^0$ are spinless, conservation of total J = L + S = 0 requires L = 0 in the final state hence $-1 = (-1)^N$ . Parity conservation therefore would allow $\eta \to 3\pi$ (the only odd number of pions consistent with energy and momentum conservation) while the $2\pi^0$ or $4\pi^0$ final states would violate parity.

The conservation of C parity, usually assumed to hold for all but the weak interaction, would require $C_\eta = C_{N\pi}$ or $+1 = (+1)^N$ hence is conserved for all N.

Observations show [43] the $\eta$ has a major decay branch to $3\pi^0$ (33%). Clearly, conservation of G parity contributes to the long lifetime of the $\eta$ by suppressing the strong interaction, but G parity is broken by isospin-violating strong interactions that conserve P. The $2\pi^0$ branch, which would violate P conservation but conserve C and thus be CP violating, has never been observed with an upper limit of $3.5 \times 10^{-4}$. Because C conservation plays no role in $\eta \to N\pi$ decays, the $\pi^+\pi^-$ branch would also be P and CP violating and, presumably due to larger backgrounds for all-neutral decays in KLOE, has a more tightly constrained upper limit of $1.5 \times 10^{-5}$.

### 2. $\eta \to M\gamma_{r,v}$

In this section we examine the selection rules for $\eta \to M\gamma$ and explain why $\eta \to 2\gamma$ is a major decay branch while $\eta \to 3\gamma$ would violate C (while leaving the conservation of CP ambiguous). The same selection rules can be applied to reactions with final state pairs of $e^+e^-$ or $\mu^+\mu^-$ provided they arise from the usual suspect, $\gamma_v \to l^+l^-$ (Dalitz decay).

Momentum and energy conservation allow $\eta \to M\gamma$ for all M greater than 1.

C parity requires that $C_\eta = C_{M\gamma}$ hence $+1 = (-1)^M$. Therefore, only even numbers of photons are allowed if C parity is conserved. Any odd number of photons implies a violation of C. This is an important and general rule which (anticipating the next section) holds for an arbitrary number of $\pi^0$'s in the final state because $C_{\pi^0} = +1$.

Briefly put, parity conservation effectively yields no constraints on the final number of photons. The rest of this paragraph contains the long version which you are welcome to skip: Parity conservation would require that $P_\eta = P_{M\gamma} = P_\gamma^M(-1)^L$ or $-1 = (-1)^M(-1)^L$. Taking as an example the two-photon final state: parity conservation for this case gives $-1 = (-1)^2(-1)^L = (-1)^L$. But what is L? Conservation of total angular momentum means $J_f = L + S$ has to be coupled to 0 in the final state. Since two spin one photons can be coupled to S = 0, 1, or 2, total $J_f = 0$ requires L = 0, 1, or 2, respectively. Because both even and odd values of L are available to the decay, a parity conserving reaction will select L = 1 while a parity violating interaction will select L = 0 or

2. The status of the conservation of parity would therefore be ambiguous. (A corollary is that a parity-conserving decay option always exists, but if a new source of C violation were observed, it could be CP conserving or violating.) Similar arguments can be made for the case of more than two photons.

Observations show [43] that the $\eta$ has a large branch to C-conserving $2\gamma$ (39%). The smaller branching ratios to $\gamma + e^+e^-$ ($7\times10^{-3}$) and $\gamma + \mu^+\mu^-$ ($3.1\times10^{-4}$) can be roughly quantitatively understood as the basic $2\gamma$ process times $\alpha$ and phase space factors. The fact that the $2\gamma$ and $3\pi^0$ branching ratios are comparable highlights the extent to which the strong interaction is suppressed in $\eta$ decays. This suppression allows rare $\eta$ decays to probe new sources of C, P, and CP violation above the (effectively zero) Standard Model floor. The C-violating $3\gamma$ branch, which is a priority channel for us, has never been observed and has an upper limit of $1.6\times10^{-5}$.

A comment about the C-allowed $4\gamma$ branch: it has never been seen with an upper limit of $2.8\times10^{-4}$ hence it does not pose a significant potential background for our precision $\pi^0 2\gamma$ measurement which has a branching ratio of $2.7\pm0.5 \times 10^{-4}$ (the PDG result combines several experiments). A significantly improved measurement or upper limit for the $4\gamma$ branch will be another ancillary product of our program.

### 3. $\eta \to N\pi^0 + M\gamma$

This section will only discuss cases *not* covered in the previous two sections (N,M each $\geq 1$). None of these branches is large, but some of them are important for tests of chiral perturbation theory at high order or have potential for tests of C conservation.

Momentum and energy conservation are satisfied for N = 1,2,3,4 and M = 1,2,... .

C parity conservation means $C_\eta = C_{N\pi}C_{M\gamma}$ or $+1 = (+1)^N(-1)^M = (-1)^M$. There are no restrictions on the number of pions N but C is conserved for even numbers of photons and violated for odd numbers of photons.

Parity conservation can be written $P_\eta = P_{N\pi} P_{M\gamma} (-1)^L$, or $-1 = (-1)^{N+M+L}$. Two cases need to be discussed:

i. Single $\gamma$ - Conservation of total angular momentum J requires the spin of the photon S and angular momentum L to couple to 0. The only possible value of L is 1 so $-1 = (-1)^{N+1+1} = (-1)^N$. Parity is therefore conserved for odd numbers of pions and violated for even numbers of pions. Although all single $\gamma$ states would violate C, the CP state would alternate with the number of pions: the $\pi^0\gamma$ state would violate CP, the $2\pi^0\gamma$ state would conserve CP, and so on. The status of CP is only unambiguous in this one photon case.

ii. Two or more $\gamma$'s - As we saw in the section on $\eta \to M\gamma$, if there is more than one photon in the final state then the reaction can always select a value of L that conserves parity, or a different value of L that violates parity. The existence of the final state is not constrained by a parity selection rule. If the C violating $3\gamma$ final state were observed, for example, the status of P conservation and therefore CP would be ambiguous without a study of the angular correlation to determine L.

What is observed? The only observed channel in this class is $\pi^0 2\gamma$ with branching ratio of $2.7 \pm 0.5 \times 10^{-4}$. This channel is a priority for us not only because it tests chiral perturbation theory at $O(p^6)$ but because it is a "gateway" channel important for understanding the SM backgrounds in new physics searches such as $\eta \to \pi^0 e^+ e^-$.

Another allowed channel is $2\pi^0 2\gamma$ which has a crude upper limit of $1.2 \times 10^{-3}$. This will be an ancillary rare decay channel in our experiment but the $6\gamma$ final state has large backgrounds due to the copious branch $\eta \to 3\pi^0$.

There are several channels, for which only upper limits exist, with odd numbers of photons which would violate C. The simplest, $\pi^0\gamma$, is absolutely forbidden by angular momentum selection rules and may therefore serve as an analysis control during the search for C violation in $\eta \to 3\gamma$. Ancillary channels searching for C violation include two yielding 5 photons in the final state ($2\pi^0\gamma$ and $\pi^0 3\gamma$) and two yielding 7 photons ($3\pi^0\gamma$ and $2\pi^0 3\gamma$). The 7 photon final states seem most promising since backgrounds from $\eta \to 3\pi^0$ followed by photon splitting can be efficiently suppressed by cutting events with close showers in the calorimeter.

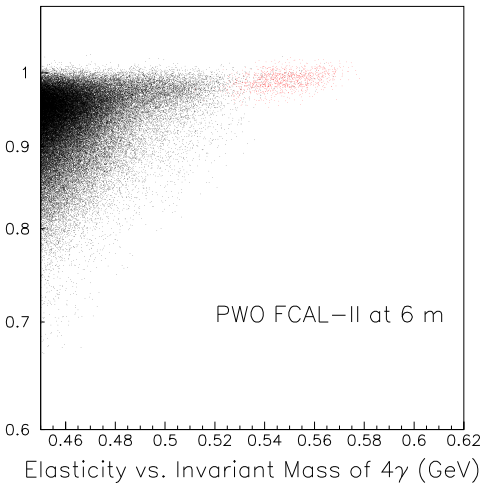


FIG. 31: Monte Carlo simulation assuming the $PbWO_4$ calorimeter in our reference design (FCAL-II). The vertical axis is the measured elasticity (a missing energy-like variable) while the horizontal axis is the reconstructed invariant mass, $M_{4\gamma}$. Signal events $\eta \to \pi^0\gamma\gamma$ appear as red dots while background $\eta \to 3\pi^0$ events are black.

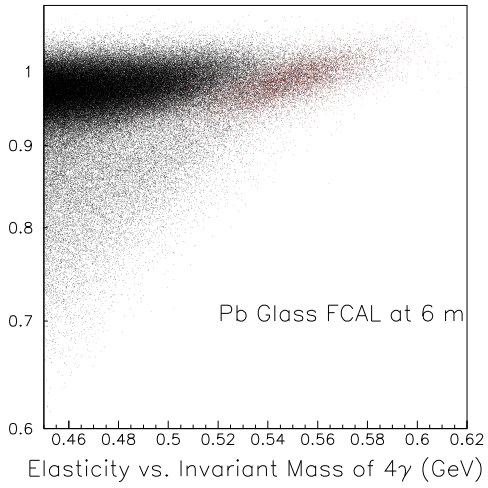


FIG. 32: Same conditions as the previous figure but using a current Hall D forward lead glass calorimeter (FCAL) at 6m.

## APPENDIX B: LEAD TUNGSTATE VS LEAD GLASS BOTH AT 6M

## APPENDIX C: ELECTROMAGNETIC BACKGROUND

Monte Carlo simulations were done using the standard GlueX *sim-recon* package to estimate the trigger and accidentals rates coming purely from electromagnetic background. The simulation used the standard GlueX geometry which included the FCAL lead-glass calorimeter at its nominal position and the Forward Drift Chambers (FDC) installed, also in the nominal position. The simulation consisted of searching for photons in FCAL arising from the full beam photon spectrum at a rate consistent with $4 \times 10^7$ tagged $\gamma$/s running. A 100ns time window was used. The results shown here therefore consist of events where a single beam photon contributed to the detector response as well as events where multiple beam photons contributed. Note that in the offline analysis, showers will only be accepted if they are coincident within a single 2 nsec RF beam bucket, so the offline event rate from electromagnetic background will be far smaller than the trigger rate from this background.

Used in the study were two candidates for the GlueX level-1 trigger. These are defined as:
**L1a** : $(E_{BCAL} + 4 * E_{FCAL}) > 2GeV \& (E_{BCAL} > 200MeV) \& (E_{FCAL} > 30MeV)$
and
**L1b** : $(E_{BCAL} + 4 * E_{FCAL}) > 2GeV \& (E_{BCAL} > 30MeV) \& (E_{FCAL} > 30MeV) \& (N_{SC} > 0)$
where $SC$ indicates the Start Counter, and $BCAL$ is for Barrel Calorimeter. The reconstruction software requires FCAL cluster energies to be greater than 0.5 GeV. No other cuts are applied. Neither of these potential GlueX triggers is a close match to the JEF trigger (which will require the total energy in FCAL to exceed 8 GeV), but this existing simulation tool provides insight into how the electromagnetic background decreases rapidly with increasing energy.

Figure 33 shows the number reconstructed photons per event in the FCAL for events passing the level-1 triggers described above. Since both level-1 triggers require energy in the FCAL, the bin at $N_{photons} = 0$ is empty. Figure 34 shows the total reconstructed energy in FCAL for 5 seconds of real time. Under the level-1 trigger condition, the trigger rate due to electromagnetic background would be approximately $4.2kHz$, but with an 8 GeV threshold it will be less than 1 Hz hence negligible.

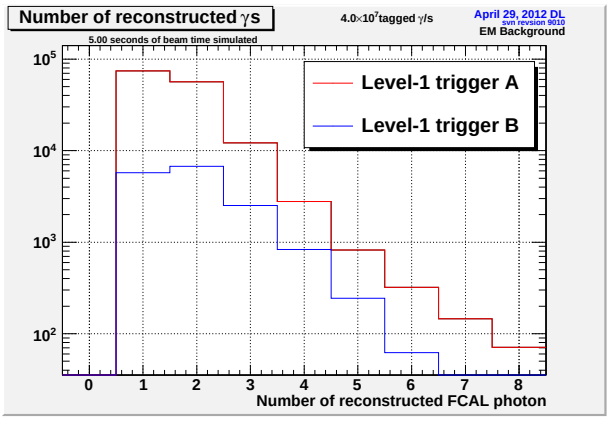


FIG. 33: Number of reconstructed photons in GlueX FCAL for events triggered by electromagnetic beam background.

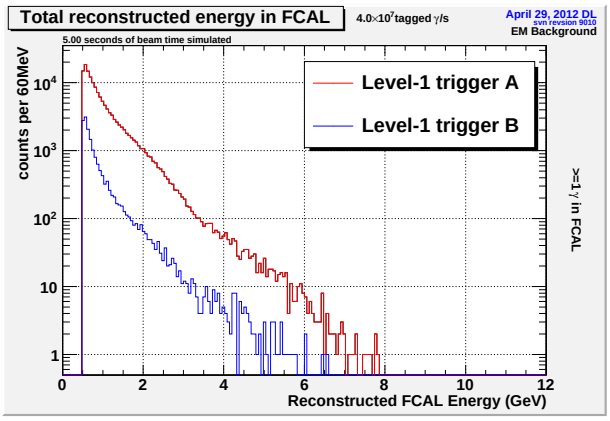


FIG. 34: Energy sum of all reconstructed photons in GlueX FCAL for events triggered by electromagnetic beam background.

Figure 35 shows the invariant mass of all reconstructed FCAL photons for events with at least 4 reconstructed photons. The histogram has been scaled by the 5 seconds of beam time simulated to make the y-axis in units of trigger rate per 2MeV of invariant mass. Extrapolating Figure 35 to the $\eta$ mass, the rate is about $6.7 \times 10^{-6}$ Hz, roughly two orders of magnitude smaller than the expected $\eta \to \pi^0\gamma\gamma$ signal rate ($2 \times 10^{-4}$ Hz). Taking into account that the offline coincident time window of 2 ns is much smaller than the 100 ns sampling window considered here, we conclude that beam related electromagnetic background plays no significant role in either the JEF online trigger rate or in the offline 4-photon accidentals background.

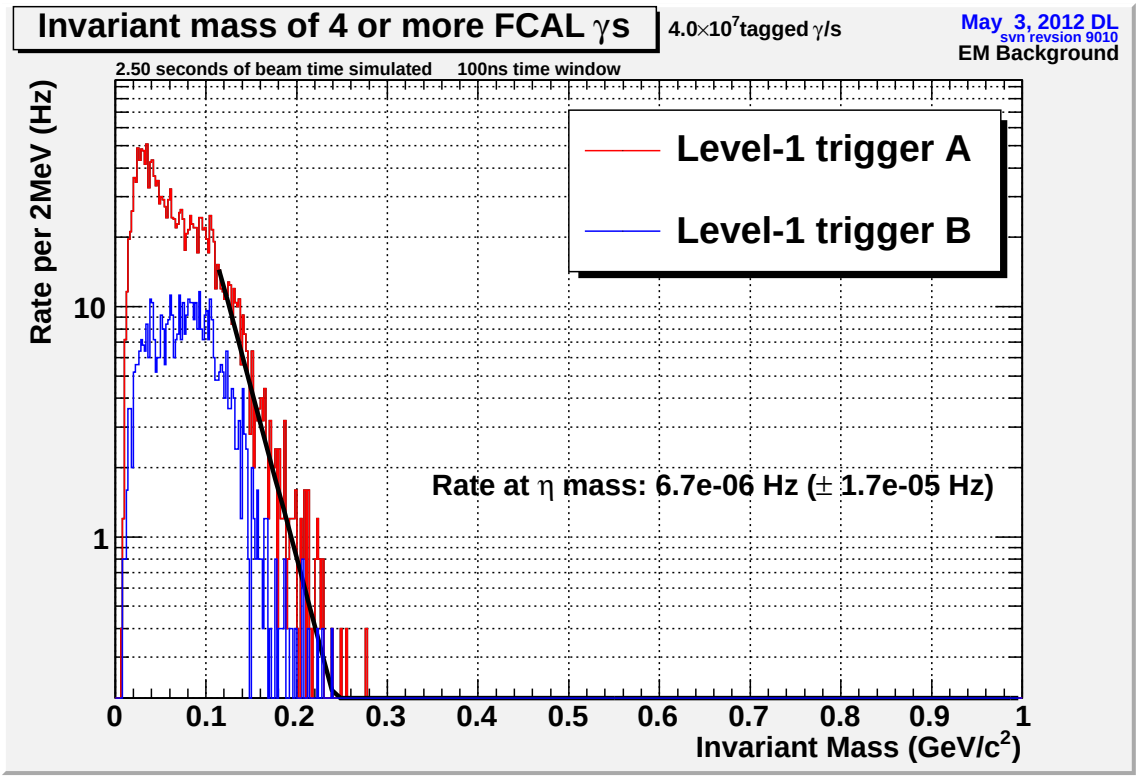


FIG. 35: Invariant mass of all reconstructed photons in GlueX FCAL for events triggered by electromagnetic beam background that have at least 4 reconstructed photons.

## APPENDIX D: PERFORMANCE OF THE PRIMEX $PbWO_4$ CALORIMETER (HYCAL)

### 1. Energy and Position Resolutions

During the PrimEx-I experiment in 2004, calibration of HyCal was performed using a low intensity tagged photon beam with energies of $E_\gamma = 0.5 - 5.5$ GeV. After the center of each detector module was irradiated, the calorimeter was moved to scan the photon beam continuously across the entire front face of the calorimeter, row by row. The measured energy and position resolutions *versus* initial incident photon energy are shown in Figure 36 and Figure 37 respectively. Excellent energy and position resolutions were achieved which was crucial to achieving the good resolution in $M_{\gamma\gamma}$ needed to isolate good $\pi^0$ events from background and to accurately determine the $\pi^0$ production

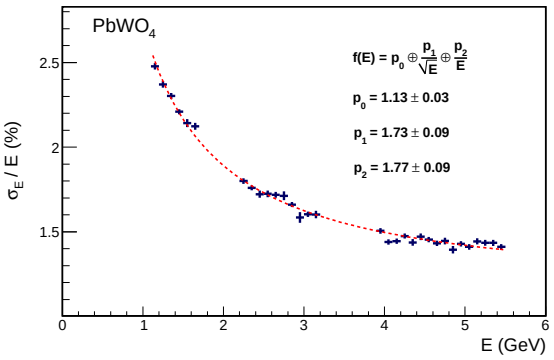


FIG. 36: Measured result for the $PbWO_4$ calorimeter energy resolution *versus* initial incident photon energy. (PrimEx-I calibration) Extrapolated to 10 GeV, the energy resolution will be 1.3% or 130 MeV.

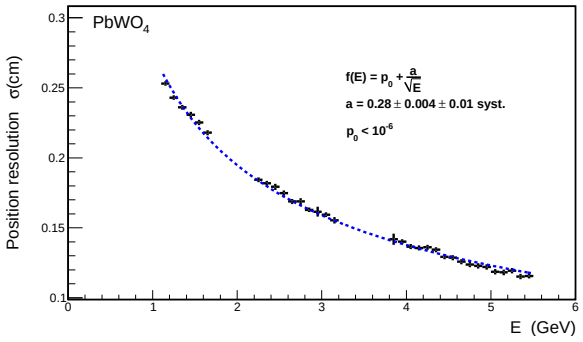


FIG. 37: Measured result for the $PbWO_4$ calorimeter position resolution *versus* initial incident photon energy. (PrimEx-I calibration) Extrapolated to 10 GeV, the position resolution will be 0.9mm.

angle used to identify the Primakoff peak. A 2.8% total uncertainty on the $\pi^0$ lifetime [74] was obtained in PrimEx-I, a factor of two and half more precise than the Particle Data Group average of several old experiments [75].

The PrimEx program proved the $PbWO_4$ material was highly radiation resistant. In terms of angle, the central beam hole in HyCal was more than 3x smaller than we plan for FCAL-II in Hall D ($4.1 \times 4.1$ cm$^2$ at 7 m for Hycal versus 12x12 cm$^2$ at 6m for FCAL-II). HyCal was in the beam for more than three months at $7 \times 10^7$ $\gamma$'s/sec on a 5% radiation length (R.L.) target during PrimEx-I and a 10% R.L. target in PrimEx-II. When calibration data were compared from the beginning and end of the program, the gain changes for $\sim$ 1200 channels were less than a few percent.

### 2. Pile-Up in the PrimEx $PbWO_4$

Another important issue in calorimetry is pile-up, the probability that any given event will appear in combination with clusters from a separate scattering event.

In our rare-decay experiment, pile-up could cause $\eta \to 2\gamma$ events to look like $\eta \to 3\gamma$ events, or it could push $\eta \to 3\pi^0$ events with lost photons back into the elasticity cut. During both PrimEx-I and PrimEx-II, clock trigger events were used to open a 100 nsec wide ADC gate with minimal bias. Figure 38 and Figure 39 show the energy-dependent occupancy seen by PrimEx-II which ran at twice the planned JEF luminosity. The probability of a 100 MeV background event occuring during a high energy shower of interest was reduced an additional factor of 50 through the use of TDCs. Although the analysis of the PrimEx-II dataset is still ongoing, the effect on the detection efficiency due to piled-up events was less than 0.5% in the published PrimEx-I result.

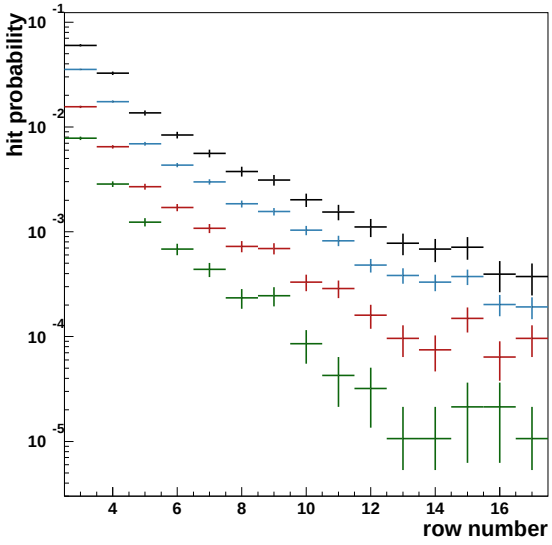


FIG. 38: Probability of a crystal module to register a hit in 100 nsec *versus* the distance from the beam axis in PrimEx-II (1 row = 2.05cm). Rows 1 and 2 are missing due to the beam hole. The black, blue, red and green data points are for the energy deposits in the counter greater than 10 MeV, 20 MeV, 50 MeV, and 100 MeV, respectively. The green points with 100 MeV threshold are most relevant. JEF will use a larger beam hole, effectively starting at row number 4, and run at half the PrimEx-II luminosity.

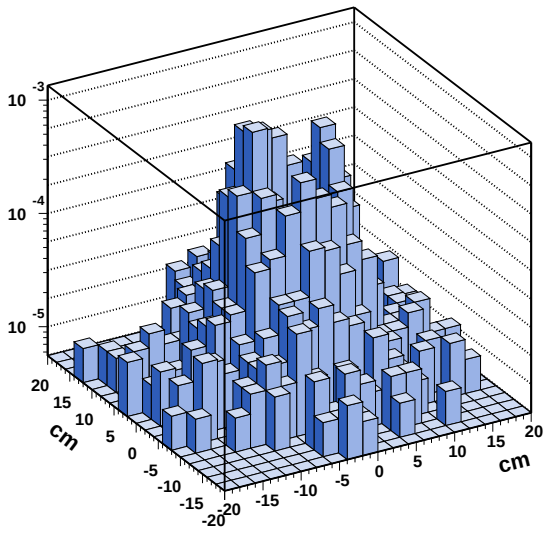


FIG. 39: The $\gamma$ occupancy probability distribution on the HYCAL measured in PrimEx-II.

### 3. Photon Merging in a Cluster Reconstruction Algorithm

Recently, collaborator I. Larin developed a so called "Island Algorithm" for cluster reconstruction in the calorimeter to improve the efficiency of shower reconstruction and minimize overlapping showers. We discuss it here because it is relevant to the background in the $4\gamma$ channel due to photon merging from the large branch $\eta \rightarrow 3\pi^0$.

The algorithm follows three steps: (1) identifying a crystal cell with the maximum energy deposition; (2) declaring all surrounding connected cells as an initial "raw" cluster; (3) splitting the "raw" cluster into many hits based on the transverse shower profile function. The transverse shower profile function for the $PbWO_4$ crystal was measured with a $6 \times 6$ matrix $PbWO_4$ prototype detector in a secondary electron beam. The $x$ and $y$ coordinate of incident beam were determined by a scintillating fiber detector located in front of the prototype calorimeter. The scintillating fiber detector consisted of two scintillating fiber arrays with a 0.6 mm resolution. Figure 40 shows the experimental result for a 2-dimensional shower profile, and Figure 41 shows the shower profile function extracted from the experimental data in Figure 40.

This newly developed cluster reconstruction algorithm was tested by mixing two hits from the PrimEx-II "snake scan" data. A 5 GeV hit was selected from the data as the stationary shower, while a second hit with energy of 1–5 GeV approached the stationary one. The "Island Algorithm" was applied to reconstruct the clusters. Any cases where the two hits were reconstructed as a single cluster were counted as inefficient.

Figure 42 and Figure 43 are the resulting two-cluster reconstruction efficiency *versus* the separation distance between two hits for the 2.05x2.05x18cm$^3$ $PbWO_4$ and 4x4x45cm$^3$ Pb glass, respectively. There is no merging of clusters in the $PbWO_4$ calorimeter when the showers are separated by at least 2.5cm, and the majority of close showers are identifiable as such even when their axes are as close as 1.25cm. In lead glass, showers begin to merge even when hits are separated by 6cm, although the majority of close showers can still be flagged as two hits when they are as close as 4.25cm. Using the separation at which 50% of two-cluster hits are reconstructed as a single hit, the use of

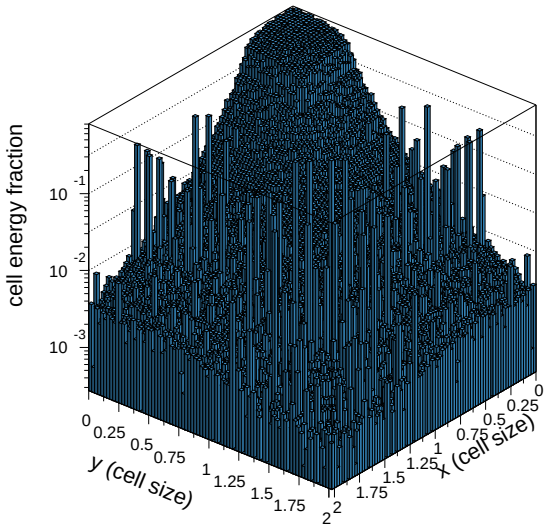


FIG. 40: The $PbWO_4$ calorimeter transverse shower profile measured from the PrimEx beam test.

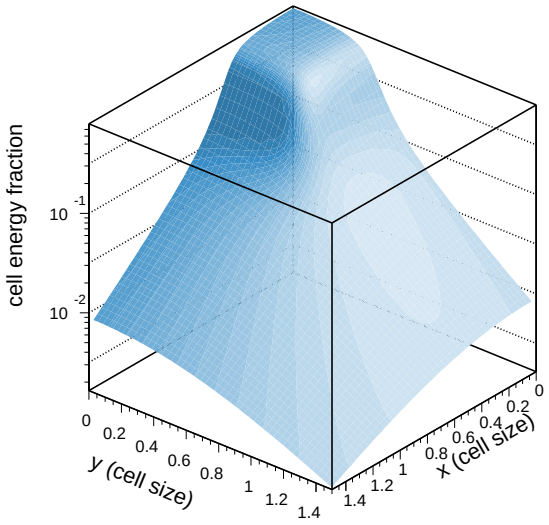


FIG. 41: The $PbWO_4$ calorimeter transverse shower profile distribution function extracted from the PrimEx beam test result shown in Figure 40.

lead tungstate can be expected to reduce merging probability by roughly $(4.25cm/1.25cm)^2$ $\sim$12.

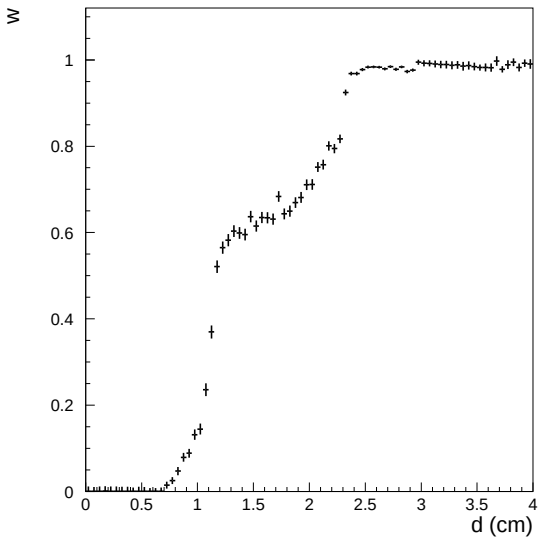


FIG. 42: The $PbWO_4$ calorimeter two-cluster reconstruction efficiency *versus* the separation distance between two showers.

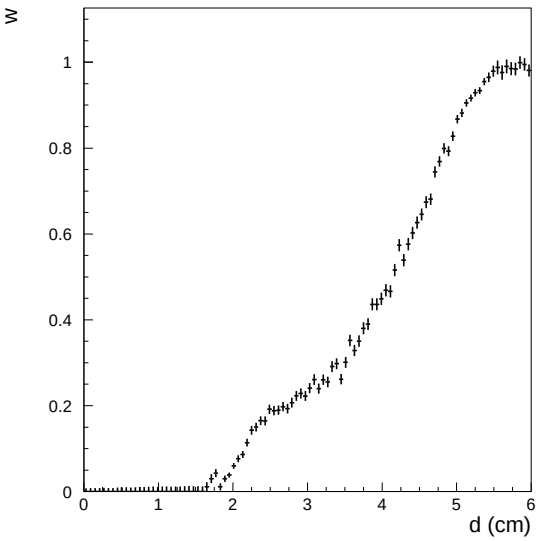


FIG. 43: The Pb glass calorimeter two-cluster reconstruction efficiency *versus* the separation distance between two showers.

[1] Proceeding for the 7th international workshop on chiral dynamics, Aug 6-10, 2012, Newport News, VA.

[2] J. Bijnens and K. Kampf, Nucl.Phys.Proc.Suppl., **207-208**, 220 (2010).

[3] S. Cohen, H. Lin, J. Dudek, R. Edwards, arXiv:0810.5550 [hep-lat].

[4] N.H. Christ, *et al.*, Phys.Rev.Lett., **105**, 241601 (2010).

[5] B.R. Holstein, Phys. Scri. T99, 55 (2002).

[6] Private discussions with B.R. Holstein and J. Goity.

[7] M. Reece and L.T. Wang, JHEP 07, 051 (2009).

[8] M. Gell-Mann, R. J. Oakes, and B. Renner. Phys. Rev. 175 (1968) 2195.

[9] B.M.K. Nefkens and J.W. Price, Phys. Scr. **T99** (2002) 114. This review is especially valuable for tying BR upper limits to model-independent constraints on C and CP violation in the strong and EM amplitudes.

[10] S. Kullander *et al.*, Acta Physica Polonica B, Vol. 29 (1998) 97-111. This is an easy reading and insightful

survey of the new physics potential of a broad, rare $\eta$ decay program.

[11] M. Unverzagt, Nucl. Phys. B (Proc. Suppl.) 198 (010) 174-181.

[12] A. Kupsc *et al.*, Nucl. Phys. B (Proc. Suppl.) 181-182 (2008) 221-225.

[13] M. Blanke, New Physics Sensitivity of Kaon Decays, Workshop on Fundamental Physics at the Intensity Frontier, Rockville, MD, Dec 2011.

[14] F. Mescia, C. Smith, and S. Trine, JHEP **08** (2006) 088.

[15] C. Amsler et al.(Particle Data Group), Phys. Lett., B667, 1 (2008).

[16] M.N. Achasov et al., Nucl. Phys. B600, 3 (2001).

[17] L. Ametller, J. Bijnens, A. Bramon and F. Cornet, Phys. Lett. B276, 185 (1992).

[18] E. Oset, J.R. Pelaez, L. Roca, Phys. Rev. D77, 073001 (2008).

[19] P. Ko, Phys. Lett. B349, 555 (1995); S. Bellucci and C. Bruno, Nucl. Phys. B452, 626 (1995); J. Bijnens, F. Fayyazuddin and J. Prades, Phys. Lett. B379, 209 (1996); J.N. Ng and D. J. Peters, Phys. Rev. D46, 5034 (1992); M. Jetter, Nucl. Phys. B459, 283 (1996); E. Oset, J.R. Relaez and L. Roca, Phys. Rev. D67, 073013 (2003).

[20] D. Alde et al., Yad. Fiz 40, 1447 (1984); D. Alde et al., Z. phys. C25, 225 (1984); L. G. Landsberg, phys. Rep., 128, 301 (1985).

[21] S. Prakhov et al., Phys. Rev. C72, 025201(2005).

[22] S. Prakhov et al., Phys. Rev. C78, 015206 (2008).

[23] S. Prakhov, Proceeding of the 11th International Conference on Meson-Nucleon Physics and the Structure of the Nucleon, Juelich, 2007, http://www.fz-juelich.de/ikp/menu2007/Program/ProgramSessions.shtml.

[24] B.Di Micco et al., Acta Phys. Slovaca 56, 403 (2006).

[25] T.D. Lee and C.N. Yang, Phys, Rev. 104, 254 (1956); Z.K. Silagadze, Phys. At. Nucl. 60, 272 (1997).

[26] C. Jarlskog and E. Shabalin, Phys. Rev. D52, 248 (1995)

[27] C. Jarlskog and E. Shabalin, Phys. Rev. D52, 6327 (1995).

[28] Particle Data Group, Phys. Rev., D66, (2002).

[29] G. Hooft, Phys.Rev.Lett. **37**, 8 (1976).

[30] V. Baluni, Phys.Rew., **D19**, 2227 (1979).

[31] R.J. Crewther, *et al.*, Phys.Lett., **88B**, 123 (1779).

[32] M.A. Shifman, *et al.*, Nucl.Phys. **B166**, 493 (1980).

[33] A. Pich and E. de Rafael, Nucl.Phys. **B367**, 313 (1991).

[34] I. Bigi, arxiv:hep-ph/9712475v1, 1997.

[35] M.S. Sozzi, "Discrete Symmetries and CP Violation", Oxford University Press, 2007.

[36] C.A. Baker, *et al.*, Phys.Rev.Lett., **97**, 131801 (2006).

[37] A. Abada, *et al.*, Phys.Lett., **B256**, 508 (1991).

[38] H.Y. Cheng, Phys.Rev., **D44**, 166 (1991).

[39] K. Ottnad, *et al.*, Phys.Lett., **B687**, 42 (2010).

[40] C. Jarlskog and E. Shabalin, Physica Scripta T99, 23 (2002).

[41] C.Q. Geng *et al.*, Modern Physics Letters A, Vol. 17, No. 23 (2002) 1489-1497; and Dao-Neng Gao, Modern Physics Letters A, Vol.17 No. 24 (2002) 1583-1588.

[42] E.L. Bratkovskaya *et al.*, Phys. Lett. B 359 (1995) 217-222.

[43] K. Nakamura et al. (Particle Data Group), JPG **37**, 075021 (2010) and partial 2011 update for the 2011 edition.

[44] K. Nakamura et al. (Particle Data Group), JPG **37**, 075021 (2010) and partial 2011 update for the 2011 edition. http://pdg.lbl.gov/2011/tables/rpp2011-conservation-laws.pdf

[45] R.R. Akhmetshin *et al.*, PLB 462 (1999) 380-388.

[46] M. Ablikim *et al.*, PRD **84**, 032006 (2011)

[47] A.M. Blik *et al.*, Physics of Atomic Nuclei, **70** (2007) 693-701.

[48] F. Ambrosino *et al.*, Phys. Lett. B 606 (2005) 276-280.

[49] D.A. Dicus, Phys. Rev. D 12 (1975) 2133-2136.

[50] J. McDonough et al, Phys. Rev. D 38 (1988) 2121.

[51] A. Aloisio et al., Physics Letters B 591 (2004) 49-54.

[52] B.M.K. Nefkens et al, Phys. Rev. C **72**, 035212 (2005).

[53] F. Ambrosino *et al.*, Phys.Lett. **B694**, 16 (2010).

[54] C. Adolph *et al.*, Phys.Lett. **B677**, 24 (2009).

[55] S. Prakhov *et al.*, Phys.Rev. **C79**, 035204 (2009).

[56] M. Bashkanov *et al.*, Phys.Rev. **C76**, 048201 (2007).

[57] S. Prakhov *et al.*, Phys. Rev., **C69**, 042202 (2004).

[58] T. Matsumura *et al.*, Nucl. Phys., **A721**, 723 (2003).

[59] Proposal for the Wide Angle Shower Apparatus (WASA) at COSY-Juelich "WASA at COSY", arXiv:nucl-ex/0411038v1 19 Nov 2004

[60] P. Gauzzi, KLOE Results on Light Meson Spectroscopy and Prospects for KLOE-2, talk in Meson Production at Intermediate and High Energies, Nov 10-11, Messina, Italy. Available online at http://newcleo.unime.it/workshop2011/talks.html .

[61] M. Unverzagt, Rare Meson Decays, talk in Meson Production at Intermediate and High Energies, Nov 10-11, Messina, Italy. Available online at http://newcleo.unime.it/workshop2011/talks.html .

[62] The Technical Design of the Hall-D Polarized Photon Beam at the Thomas Jefferson National Accelerator Facility, The GlueX Collaboration, Novermber 7, 2008.

[63] Jefferson Lab Hall D CDR, version 5.0.

[64] Silvia Niccolai, *Three-body photodisintegration of* $^3$*He measured with CLAS*, Ph.D. thesis, George Washington University, 2003, unpublished.

[65] R. Bradford and R.A. Schumacher, CLAS-NOTE 2002-003, unpublished.

[66] R.A. Schumacher, CLAS-NOTE 99-010, unpublished.

[67] Mapping the Spectrum of Light Quark Mesons and Gluonic Excitations with Linearly Polarized Photons, The GlueX Collaboration, gluex.org, July 2006.

[68] Overview of Hall D solenoid refurbishment and testing, G. Biallas et al., September 2010.

[69] Start Counter Update, W. U. Boeglin et al., Florida International University, February 2008.

[70] The GLUEX Central Drift Chamber: Design and Performance, Y. Van Haarlem et al., NIM A, 622 (2010) 142–156.

[71] Performance of the prototype module of the GlueX electromagnetic barrel calorimeter, B. D. Leverington et al., NIM A, 596 (2008) 327–337.

[72] Time of Flight Detector, Conceptual Design Report, The GlueX Collaboration, March 2008.

[73] J.V. Bennett, M. Kornicer, and M.R. Shepherd, Precision timing measurement of phototube pulses using a flash analog-to-digital converter, NIM A622, 225 (2010).

[74] I. Larin et al., Phys. Rev. Lett., 106, 162303 (2011).

[75] K. Nakamura et al. (Particle Data Group), J. Phys. G 37, 075021 (2010).

[76] J.M. Laget, Phys Rev. **C72**, 022202 (2005).

[77] H. Beck et al., Nucl. Instr. Meth., A269, 568 (1988).

[78] Jlab proposal "A Precision Measurement of the $\eta$ Radiative Decay Width"(E-10-011), 2010.

[79] Jlab 12 GeV upgrade white paper "The Science Driving the 12 GeV Upgrade of CEBAF".

[80] J.N. Ng and D.J. Peters, Phys. Rev. D **47**, 4939 (1993).

# Response to PAC39
# Issues and Recommendations
# for PR12-12-003,
# the Jlab Eta Factory Experiment

May 5, 2013

# Issue Slide I

"The experiment requires a major upgrade of the standard Hall D equipment including the replacement of the lead glass forward calorimeter (FCAL) with a new high resolution PbWO calorimeter with flash ADC readout on every crystal. The PAC has concerns about costs and people-power. The cost of such a calorimeter is expected to be on a scale of several millions and will need considerable manpower to operate and maintain it."

Our proposal falls under the category of Major New Experimental Equipment. Last year, our cost range was $2.7M-4.6M depending on what equipment would be borrowed in various calorimeter scenarios. We update that estimate toward the end of these slides.

For a project of this size, we believe a combination of NSF MRI, Jlab Physics Division, and foreign funding sources is a viable solution. We request PAC approval so U.S. and foreign collaborators can start that process.

This experiment has the potential to add significant new manpower to the Hall-D effort, in particular from groups that have historically had little activity at Jefferson Lab.
(see following slide)

Calorimeters are low-maintenance detectors. Furthermore, the manpower needed to operate and maintain our proposed FCAL-II (3445 channels) is not much larger than that needed for the existing FCAL-I (2800 channels).

# JEF Considerably Augments Hall D Manpower

Symmetry Tests of Rare Eta Decays to All-Neutral Final States:
The JLab Eta Factory (JEF) Experiment

(The GlueX Collaboration and Other Participants)

M. Dugger,1 B. Ritchie,1 E. Anassontzis,2 P. Ioannou,2 C. Kourkoumeli,2 G. Voulgaris,2
N. Jarvis,3 W. Levine,3 P. Mattione,3 C. A. Meyer,3 R. Schumacher,3 P. Collins,4 F. Klein,4
D. Sober,4 D. Doughty,5 A. Barnes,6 R. Jones,6 J. McIntyre,6 F. Mokaya,6 B. Pratt,6
I. Senderovich,6 W. Boeglin,7 L. Guo,7 P. Khetarpal,7 E. Pooser,7 J. Reinhold,7 H. Al
Ghoul,8 V. Crede,8 P. Eugenio,8 A. Ostrovidov,8 N. Sparks,8 A. Tsaris,8 D. Ireland,9
K. Livingston,9 D. Bennett,10 J. Bennett,10 J. Frye,10 J. Leckey,10 R. Mitchell,10 K. Moriya,10
M. R. Shepherd,10 A. Szczepaniak,10 R. Miskimen,11 M. Williams,12 P. Ambrozewicz,13
S. Danagoulian,13, ∗ A. Gasparian,13 R. Pedroni,13 T. Black,14 L. Gan (Spokesperson),14
S. Denisov,15 G. Huber,16 S. Katsaganis,16 D. Kolybaba,16 G. Lolos,16 Z. Papandreou,16
A. Semenov,16 I. Semenova,16 M. Tahani,16 W. Brooks,17 S. Kuleshov,17 A. Toro,17
F. Barbosa,18 E. Chudakov,18 H. Egiyan,18 M. Ito,18 D. Lawrence,18 L. Pentchev,18 Y. Qiang,18
E. S. Smith,18 A. Somov (Co-Spokesperson),18 S. Taylor,18 T. Whitlatch,18 E. Wolin,18 B. Zihlmann,18
J. Benesch,18, ∗ J. Goity,18, ∗ D. Mack (Co-Spokesperson),18, ∗ X. Chen (Co-Spokesperson),19, ∗
P. Zhang,19, ∗ J. He,19, ∗ D. Chen,19, ∗ H. Yang,19, ∗ R. Wang,19, ∗ D. Armstrong,20, ∗ W. Deconinck,20,
∗ W. Briscoe,21, ∗ A. Opper,21, ∗N. Semicevic,22, ∗ S. Wells,22, ∗ J. Dunne,23, ∗ D. Dutta,23, ∗ P. King,24, ∗
J. Roche,24, ∗ K.E. Myers,25, ∗ M. Dalton,26, ∗ A. Asratyan,27, ∗ A. Dolgolenko,27, ∗ V. Goryachev,27, ∗
I. Larin,27, ∗ V. Matveev,27, ∗ V. Tarasov,27, ∗ A. Sitnikov,27, ∗ V. Vishnyakov,27, ∗
S. Gevorkyan,28, ∗ L. Roca,29, ∗ S. Fang,30, ∗ H. Lui,30, ∗ X.Z. Bai,31, ∗ H.X. He,31, ∗ J. Feng,31, ∗
S.Y. Hu,31, ∗ S. Y. Jian,31, ∗ X.M. Li,31, ∗ C. Shan,31, ∗ H.H. Xia,31, ∗ L. Ye,31, ∗ J. Yuan,31, ∗
J. Zhou,31, ∗ S.H. Zhou,31, ∗ B. Hu,32, ∗ Y. Zhang,32, ∗ L. Ma,32, ∗ V. Berdnikov,33, ∗
A.Pognosov,33, ∗ G. Nigmatkulov,33, ∗ D Romanov,33, ∗ S. Somov,33, ∗ and I. Tolstukhin33, ∗

# Issue Slide II

"The PAC also felt that the physics case for this large instrument could be strengthened. On one side, the flagship physics case —testing the standard model —would be sharpened by removing focus from the more model-dependent results and concentrating on the cleanest standard model tests.

On the other side, the PAC would like to see more exploration of the broader, secondary physics program that the new calorimeter could support, e.g. what could be learned from the angular distributions of other (non-forbidden) all-neutral final states as measured by this high-resolution device? "

We too felt the physics case could be strengthened and have attempted to do so in our update to PAC40. However, we greatly benefit from the synergies between $\eta \rightarrow \pi^0 2\gamma$ and our 2 SM test channels.

- Firstly, since all these decays involve 3-4 photon final states, the allowed $\eta \rightarrow \pi^0 2\gamma$ channel is itself a potential background.
- Secondly, our thorough simulations of $\eta \rightarrow \pi^0 2\gamma$ predicting unprecedented Signal/Bkg are a nice visual way to suggest our sensitivity for the SM channels (where there is in principle no peak).
- Finally, the fact that $\eta \rightarrow \pi^0 2\gamma$ is one of our 3 priority channels has been helpful in recruitment. For some of us, the flagship physics case is indeed testing the SM. For others, it is, "Can we understand the combination of nearly forbidden strong and EM processes which allow this rare decay to occur?"

There is some tension between the issue at the top left and the issue at the bottom left (originally from the same paragraph):

- From the GlueX proposal, neglecting the recoil nucleon, interesting final states for exotics searches are $3\pi$, $2\pi\omega$, and $2\pi\eta$. Since both the $\eta$ and $\omega$ have significant branches to final states yielding photons, indeed all-neutral final states are relevant and will benefit from the improved resolution of the new calorimeter.
- As for $\eta \rightarrow 2\gamma$, the approved PrimEx in Hall D will measure this and would benefit from the higher resolution of the new calorimeter.
- As for $\eta \rightarrow 3\pi^0$, although this is not a rare decay, we will acquire a large data sample with very low background using the new calorimeter.

# Issue Slide III

"The PAC's present charge defines "approval" of an experiment as placing it in the "top half of the priority list for the first 5 years of 12 GeV running". This promising but ambitious project did not make a convincing case that it would be able to run that quickly. The proposed JEF and GlueX itself are unique in the world; with no competition envisioned, this new undertaking seems suited for a later phase of Hall D running than that covered by PAC39's charge. "

The "first 5 years" language has been removed from the charge for PAC40. Since it was never an issue in our case, it's worth mentioning a few points that may not be widely appreciated (see next slide for time-line):

- After approval of the original PrimEx experiment in Hall B, it took their small group only 4 years to fund and build their 1200 channel Lead Tungstate calorimeter. Our new effort has access to more manpower.
- Hall D has 120+79 = 199 days of approved experiments. Using the usual 50% scheduling efficiency and ~30 weeks per year, this corresponds to only about 2 calendar years of approved program in Hall D. The Hall will potentially run out of approved program in mid- to late CY2017.
- If approved at PAC40, and assuming a year of commissioning in Hall D before its formal physics program begins, JEF could begin installation in Q3 CY2017.

(see next slide)

# Straw Man Schedule for JEF

(unofficial working schedule for JEF internal planning, version April 2013)

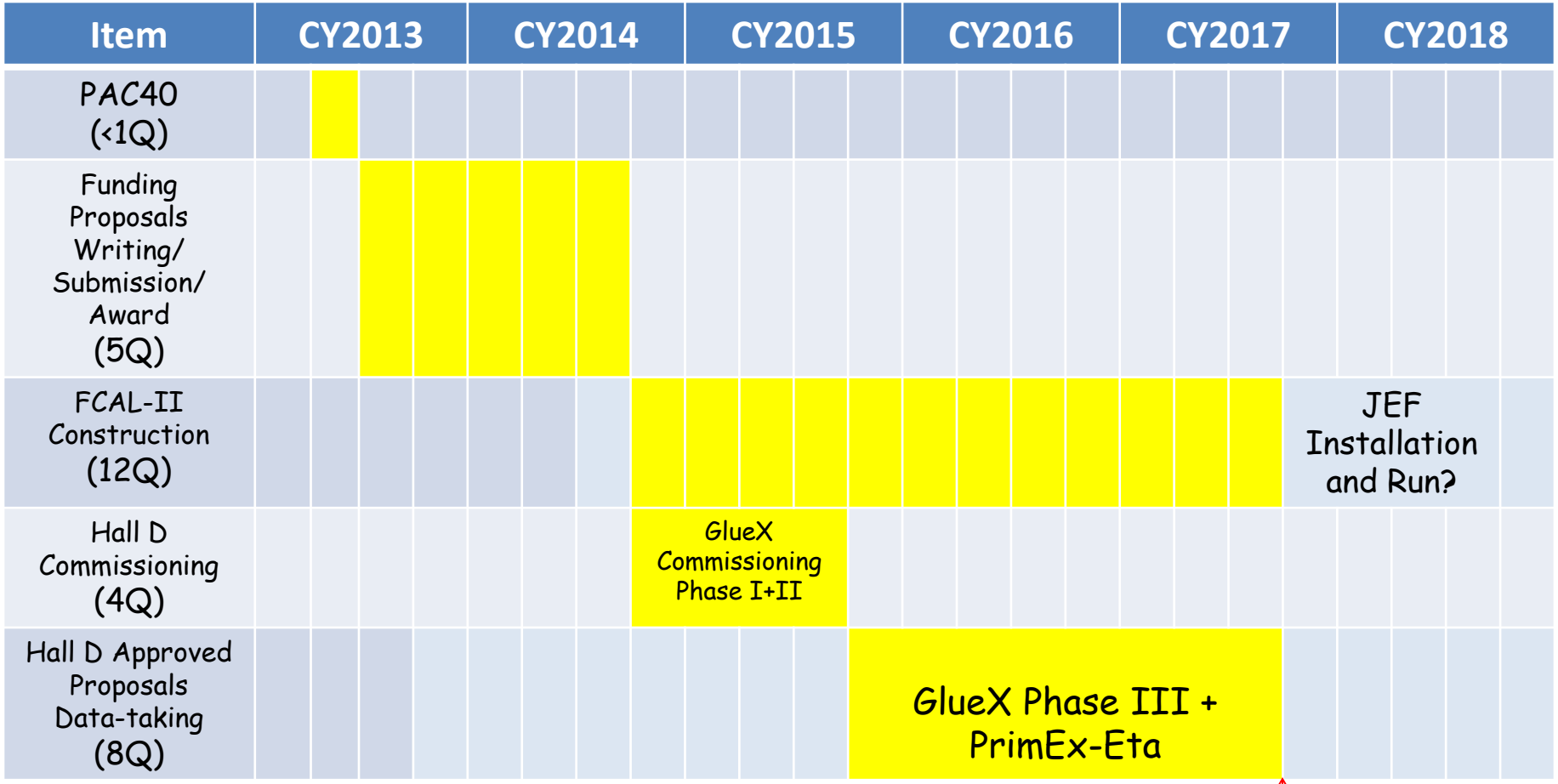

# Recommendations Slide I

"We encourage the proponents to carry out a more detailed study of the cost and required people-power for the new PbWO calorimeter. "

On an earlier slide we generated a range of costs from $2.7M - $4.6M depending on the calorimeter configuration which has to be agreed upon by GlueX, the rare eta decay program, and Jlab management. Once a scenario is chosen, the cost estimates become quite firm because our PrimEx collaborators previously built a large PbWO4 calorimeter, and because Flash ADCs are being delivered now to Jlab under firm contracts.

*The scenario which seems to appeal to most stake-holders in Hall D would be to permanently integrate new PbWO4 crystals into the central region of a lead glass calorimeter renamed FCAL-II.*

In the FCAL-II scenario, which is not the cheapest since no PrimEx crystals and relatively few Flash ADCs can be borrowed, the total estimated cost is about $4.5M .

(see next slide)

# Estimated Cost for FCAL-II*

(hybrid PbWO4-Lead Glass version replacing FCAL-I, as of April 2013)

| Item | Channels | Cost/Channel | Cost | Nominal Responsibility |
|---|---|---|---|---|
| Crystal | 3445 | $250 | $0.86M | China |
| PMT+base+ magshield | 3445 | $450* | $1.55M | U.S. |
| Flash ADC | 3445 – 861** = 2584 | $378 | $0.98M | |
| HV | 3445 | $300 | $1.03M | |
| | | | ---------- | |
| **Total** | | | **$4.4M** | |

*Increase per channel of $50 wrt April 2012 estiate reflects recent Hamamatsu quote of $350/pmt.

** 861 is the approximate number of 4cmx4cm lead glass modules displaced by the new 2cmx2cm PbWO4 modules at small angles.

Neglects infrastructure costs like the support structure ($250K), cables and patch panels ($345K assuming $100/channel).

# Recommendations Slide II

We also encourage them to include the new device in the ongoing design studies for upgrading GlueX's forward particle identification (Threshold Cerenkov counter vs RICH). All experiments in Hall D will likely benefit from the availability of an improved forward particle identification system.

The question of FCAL-I vs FCAL-II should not impact $\pi^{+-}/k^{+-}$ separation with the new PID detector under design in Hall D.

Detailed simulations will certainly be carried out before a final decision to integrate new PbWO4 blocks into the Hall D forward calorimeter. However, the rare η decay program can run with a stand-alone PbWO4 calorimeter if necessary.

# Extras

# Estimated Lead Tungstate Calorimeter Cost at PAC39*

(118x118cm$^2$ , as of April 2012)

| Item | Channels | Cost/Channel | Cost |
|---|---|---|---|
| Crystal | 3445 | $250 | $0.86M |
| PMT+base | 3445 | $400 | $1.38M |
| Flash ADC | 3445 | $378 | $1.30M |
| HV | 3445 | $300 | $1.03M |
| | | | ---------- |
| **Total** | | | **$4.57M** |
| Including possible cost offsets from equipment loans: | | | |
| PrimEx | 1200 | $650 (xtal+pmt+base) | $-0.78M |
| FCAL-I | 2800 | $378 (Flash ADC) | $-1.06M |
| **Revised Total** | | | **$2.73M to $4.57M** |

For the 118x118 cm$^2$ FCAL-II, the total cost is $2.7M to $4.6M.

This is within the $4M range of an NSF MRI assuming a small equipment loan or foreign funds or Physics Division support for ADCs or HV.

* This cost neglected infrastructure like the stand, cables, and patch panels.